Yukon Geological Survey

BULLETIN 15

Bedrock geology compilation of the Anvil District (parts of NTS 105K/2, 3, 5, 6, 7 and 11), central Yukon

by
Lee C. Pigage[1]
with contributions from F. Cordey, J.K. Mortensen,
M.J. Orchard and M. Villeneuve

[1]lee.pigage@gov.yk.ca, Yukon Geological Survey, Whitehorse, Yukon

2004

Published under the authority of the Minister of Energy, Mines and Resources, Yukon Government

http://www.emr.gov.yk.ca

Printed in Whitehorse, Yukon, 2004.

ISBN 1-55362-205-7

This, and other Yukon Geological Survey publications, may be obtained from:
Geoscience and Information Sales
c/o Whitehorse Mining Recorder
102-300 Main Street
Box 2703 (K102)
Whitehorse, Yukon, Canada Y1A 2C6
phone (867) 667-5200, fax (867) 667-5150
e-mail geosales@gov.yk.ca

Visit the Yukon Geological Survey web site at www.geology.gov.yk.ca

In referring to this publication, please use the following citation:
Pigage, L., 2004. Bedrock geology compilation of the Anvil District (parts of NTS 105K/2, 3, 5, 6, 7 and 11), central Yukon. Yukon Geological Survey, Bulletin 15, 103 p.

Production by K-L Services, Whitehorse, Yukon.

Cover photo. *Shows D_1 and D_2 minor folds in outcrop southeast of the Grum deposit. Small-scale fold pattern has same appearance as large-scale folding patterns visible in the Grum cross-section (smaller image). This vertical cross-section 80W of the Grum deposit is oriented southwest-northeast and looking northwest. Note steep to vertical D_1 folds refolded by gently dipping, near-horizontal D_2 folds.*

Preface

The Anvil Zinc-Lead District has been a mainstay of the Yukon's economy for more than 25 years. Exploration in the Camp lasted for more than 40 years, from the discovery of the Vangorda massive sulphide deposit in 1953, through the subsequent discoveries of the Faro, Grum, Dy and Swim deposits, and into the waning stages of the mine's life. This project was initiated in 1998 to compile and interpret the most important parts of this legacy of knowledge and information so that the significant remaining exploration potential of the District will eventually be realized.

Lee Pigage was responsible for many exploration programs in the area and has made some of the most important contributions to our understanding of the geology and origin of the Anvil District. This study integrates the results of past government studies and company exploration with new mapping carried out by Lee. It includes a detailed geological report and 17 associated bedrock geology maps.

Préface

Le district minier de plomb et de zinc d'Anvil a été le principal soutien de l'économie du Yukon depuis plus de 25 ans. L'exploration dans le camp a duré plus de 40 ans, depuis la découverte du gisement Vangorda de sulfures massifs en 1953, les découvertes subséquentes des gisements Faro, Grum, Dy et Swim, jusqu'aux dernières étapes de la vie de la mine. Le présent projet a été entrepris en 1998 dans le but de compiler et d'interpréter les parties les plus importantes de cet héritage de connaissances et d'information, afin que le reste de l'important potentiel d'exploration du district puisse éventuellement être réalisé.

Lee Pigage a été responsable de nombreux programmes d'exploration dans la région et a apporté certaines des contributions les plus importantes pour la compréhension de la géologie et de l'origine du district minier d'Anvil. La présente étude intègre les résultats d'anciennes études du gouvernement et de l'exploration minière réalisée par l'entreprise, auxquelles s'ajoute une nouvelle cartographie exécutée par Lee Pigage. L'étude comprend un rapport géologique détaillé accompagné de 17 cartes géologiques du substratum rocheux.

Grant Abbott

Chief Geologist — Géologue en chef
Yukon Geological Survey — Commission géologique du Yukon
Energy, Mines and Resources — Departement de l'énergie, des mines et des ressources
Yukon Government — Gouvernement du Yukon

Acknowledgements

Dave Jennings and Gregg Jilson first introduced me to the complexities of Anvil District geology. Through the many discussions of the geology they always had another outcrop which helped elucidate the understanding of the District. Maurice Colpron and Don Murphy provided interest and discussions concerning relations between Yukon-Tanana and Slide Mountain rocks in the Faro area and Yukon-Tanana and Slide Mountain rocks in the Finlayson Lake area. This bulletin was reviewed by Gregg Jilson and Jim Mortensen.

Jason Adams, Dylan MacGregor, and Justin Pigage provided interested and able assistance in the field. Helicopter support was provided by Trans North Helicopters based out of Ross River.

Abstract

The Anvil Mining District contains the most westerly exposures of the off-shelf basinal facies (Selwyn Basin) of the Cordilleran miogeocline, a prism of sedimentary rocks of Precambrian to Jurassic age deposited along the relatively stable, passive continental margin of western North America. Anvil District is immediately northeast of the Slide Mountain and Yukon-Tanana Terranes, the most easterly of the allochthonous suspect terranes which were amalgamated with North America starting in Jurassic time.

The total interpreted stratigraphic thickness of the metasedimentary rocks of North American affinity is greater than 7400 m, ranging in age from latest Precambrian or earliest Cambrian through Devonian. These metasedimentary rocks consist predominantly of fine clastic sediments deposited in an off-shelf marine basin with local occurrence of euxinic carbonaceous shales and coarser sandstones and conglomerates. Extensive Ordovician within-plate basaltic submarine volcanic rocks and associated epiclastic breccias are indicative of localized rifting along the continental margin.

Rocks of Yukon-Tanana and Slide Mountain terranes are thrust northeastward over the Selwyn Basin rocks in the Anvil District along the Inconnu thrust. These overthrust rocks consist of two disparate successions separated by the extensional Vangorda fault. The most southwesterly Yukon-Tanana succession consists of Paleozoic micaceous quartzite and phyllite, unconformably overlain by fine- to coarse-grained Triassic clastic rocks. The micaceous quartzite is tentatively correlated with the Grass Lakes succession of Yukon-Tanana Terrane mapped further to the southeast. This assemblage contains a belt of Permian eclogite occurrences along its northeast margin. Coarse, proximal clastic rocks of the Triassic Faro Peak formation indicate submarine fan deposition, possibly related to developing fault scarps.

Northeast of Vangorda fault, the Slide Mountain succession is dominated by argillites and bedded cherts with intervals of sandstone and chert-pebble conglomerate in the lower part of the succession. Conglomerates and sandstones contain clasts of shale, monocrystalline quartz, monocrystalline K-feldspar and chert, indicating a provenance containing either eroding intrusive or felsic volcanic rocks. The sequence is capped by Permian Campbell Range formation basalts and associated bedded cherts, and minor epiclastic rocks which have a N- (normal) or BAB- (back-arc basin) MORB (mid-ocean ridge basalt) geochemical signature. Basalts and associated bedded cherts are intruded by Permian (?) ultramafic magmas.

All sequences have been intruded by felsic magmas during Cretaceous and Eocene. The oldest felsic intrusive rocks are of the Anvil plutonic suite (109 Ma) consisting of biotite-muscovite granite with S-type geochemical and petrologic affinities. The dominant body is the Anvil Batholith which cores the northwest-trending Anvil Arch in the central part of the District. The Tay River plutonic suite (97 Ma) consists of biotite±hornblende granodiorite to granite. It forms the large Orchay Batholith at the southeast margin of the District, as well as numerous dykes and sills throughout the District. The suite has petrologic and geochemical I-type affinities; the geochemical signature and age of the plutonic suite indicates it is the subvolcanic equivalent of the South Fork volcanics which outcrop immediately to the northeast. The youngest intrusives in the District consist of quartz-feldspar porphyry bodies (55 Ma). These Eocene intrusions occur as elongate dykes or circular plugs scattered throughout the District. Locally, they have flow-banding textures indicating near-surface intrusion.

Rocks in the Anvil District are complexly polydeformed and polymetamorphosed. The first two deformation phases (D_1 and D_2) are the most important in that they are regionally developed and accompanied by regional structural fabrics. The two deformations are coaxial, trending southeast. D_1 deformation is delineated by steep, tight, northeast-verging minor folds. D_1 structural fabric is present in Triassic Faro Peak formation; therefore D_1 deformation post-dates Triassic time and pre-dates the subsequent D_2 deformation

and associated structural fabric. TwoPete and Inconnu thrust faults are considered to have been active during D_1 deformation. D_1 deformation marks the general convergence of Yukon-Tanana Terrane with ancestral North America.

D_2 deformation is delineated by a gently dipping axial-planar crenulation cleavage and associated open to tight minor folds. S_2 fabrics and folds are most strongly developed and tightest over the Anvil Batholith and decrease in intensity both to the northeast and southwest. Vergence of folds also reverses over the Anvil Batholith with southwest-verging structures occurring southwest of the batholith and northeast-verging structures occurring northeast of the batholith. The Anvil plutonic suite contains D_2 structural fabric, and the Tay River plutonic suite is unfoliated. D_2 deformation is therefore restricted to the time interval between 109-96 Ma. Major compressive stress is near vertically oriented and most intense over Anvil Batholith, suggesting the D_2 deformation is kinematically linked to buoyant intrusion of the Anvil plutonic suite. The latest stage of D_2 deformation consists of extensional faults locally developed along the southwest margin of Anvil Batholith and overlying metasedimentary rocks. Extensional faults have proven displacements of over 1 km locally. They probably represent the collapse of the deformation edifice created by intrusion of the Anvil plutonic suite.

D_2 deformation is accompanied by pervasive M_2 metamorphism. Metamorphic isograds are concentric around Anvil Batholith. Metamorphic assemblages range from lower greenschist facies to sillimanite-muscovite zone in the amphibolite facies. Maximum temperatures and pressures during metamorphism are approximately 620°C and 4 kilobars. This corresponds to a depth of burial of up to 12 km during metamorphism. M_2 metamorphism has totally overprinted earlier M_1 metamorphism associated with D_1 deformation.

The Anvil District contains significant sedimentary-exhalative (SEDEX) zinc-lead-silver-barite mineralization. Exploration in the District has discovered an estimated 225 million tones of sulphide mineral-bearing rock (Jennings and Jilson, 1986) distributed in 5 base metal deposits occurring within a 150-metre stratigraphic interval straddling the Mount Mye-Vangorda contact in the ancestral North American succession. Mining in the District began in 1969 and continued with interruptions until 1997. Known deposits occur along a curvilinear trend which has been postulated to be a syngenetic fault structure during deposit formation. Despite exploration efforts for over 45 years in the District, substantial areas of the Mount Mye-Vangorda geological contact remain untested for undiscovered, deeply buried massive sulphide mineralization.

Yukon MINFILE occurrences within the District document mineralized showings and prospects for sediment-hosted barite, intrusion-related polymetallic veins, and volcanic-hosted sulphide mineral deposit models. Only recently have exploration efforts within the District been directed towards these other exploration targets. As with SEDEX mineralization, exploration potential for these additional deposit models has not been fully tested to date.

Résumé

Le district minier d'Anvil renferme les affleurements les plus occidentaux du faciès de bassin (bassin de Selwyn) du miogéoclinal de la Cordillère, un prisme de roches sédimentaires datant du Précambrien au Jurassique déposé le long de la marge continentale de l'ouest de l'Amérique du Nord. Le district minier d'Anvil est situé immédiatement au nord-est des terranes de Slide Mountain et de Yukon-Tanana, les plus orientaux des terranes suspects allochtones qui se sont amalgamés à l'Amérique du Nord à partir du Jurassique.

L'épaisseur stratigraphique totale interprétée des roches métasédimentaires d'affinité nord-américaine est supérieure à 7400 m, et l'âge de ces roches varie du Précambrien tardif ou du Cambrien précoce jusqu'au Dévonien. Ces roches métasédimentaires présentent une prédominance de sédiments clastiques fins déposés dans un bassin océanique avec, par endroits, des schistes carbonés euxiniques, ainsi que des grès grossiers et des conglomérats. Des roches volcaniques basaltiques sous-marines et des brèches épiclastiques d'affinité intraplaque, datant de l'Ordovicien, indiquent un milieu de rift localisée le long de la marge continentale.

Les roches des terranes de Yukon-Tanana et de Slide Mountain chevauchent vers le nord-est les roches du bassin de Selwyn dans le district minier d'Anvil, le long de la faille de chevauchement Inconnu. Ces roches chevauchantes comprennent deux successions disparates séparées par la faille d'extension de Vangorda. La succession de Yukon-Tanana au sud-ouest se compose de quartzite et de phyllade micacés, recouverts en discordance par des roches clastiques triasiques à grains fins à grossiers. Le quartzite micacé est provisoirement corrélé avec la suite de Grass Lakes du terrane de Yukon-Tanana vers le sud-est. Cet assemblage contient des occurrences d'éclogite datant du Permien, le long de sa bordure nord-est. Des roches clastiques grossières proximales de la formation de Faro Peak datant du Trias indiquent une sédimentation de cônes sous-marins, peut-être reliée à la formation d'escarpements de failles.

Au nord-est de la faille de Vangorda, la succession de Slide Mountain est dominée par des argilites et des cherts lités avec des intervalles de grès et de conglomérats à cailloux de chert dans la partie inférieure de la succession. Les conglomérats et les grès renferment des clastes de schiste argileux, de quartz monocristallin, de feldspath potassique monocristallin et de chert, indiquant l'érosion d'une source de roches intrusives ou de roches volcaniques felsiques. La séquence est recouverte de basaltes de la formation de Campbell Range, datant du Permien, et des cherts lités associés, ainsi que de quantités mineures de roches épiclastiques, qui ont une signature géochimique N- (normale) ou BAB- (bassin marginal) MORB (basalte de la dorsale médio-océanique). Des magmas ultramafiques du Permien (?) ont pénétré par intrusion dans les basaltes et les cherts lités associés.

Des intrusions de magmas felsiques, qui se sont produites au cours du Crétacé et de l'Éocène, recoupent toutes les séquences. La roche intrusive felsique la plus ancienne est la suite plutonique d'Anvil (109 Ma), composée de granite à muscovite et biotite avec des affinités géochimiques et pétrologiques de type S. Le massif dominant est le Batholite d'Anvil qui forme le cœur de l'arche d'Anvil d'orientation nord-ouest, dans la partie centrale du district minier. La suite plutonique de Tay River (97 Ma) est composée de granodiorite et de granite à biotite±hornblende. Elle forme le vaste Batholite d'Orchay à la bordure sud-est du district minier, ainsi que de nombreux dykes et filons-couches dans l'ensemble du district. La suite a des affinités pétrologiques et géochimiques de type I; la signature géochimique et l'âge de la suite plutonique indiquent qu'il s'agit de l'équivalent subvolcanique des volcanites de South Fork qui affleurent immédiatement au nord-est. Les roches intrusives les plus récentes du district minier sont composées de massifs de porphyre à quartz et à feldspath (55 Ma). Ces intrusions de l'Éocène se présentent comme des dykes allongés ou des culots circulaires sporadiques dans tout le district minier. Par endroits, ces intrusions ont des textures à litage de flux indiquant qu'il s'agit d'intrusions près de la surface.

Les roches du district minier d'Anvil présentent des polydéformations et des polymétamorphismes complexes. Les deux premiers épisodes de déformation (D_1 et D_2) sont les plus importants puisqu'ils se sont produits à l'échelle régionale et sont accompagnés de fabriques structurales régionales. Les deux déformations sont coaxiales et d'orientation sud-est. La déformation D_1 est délimitée

par des plis mineurs abrupts et serrés, avec une vergence nord-est. La fabrique structurale D_1 est présente dans la formation de Faro Peak du Trias; par conséquent, la déformation D_1 est postérieure au Trias et antérieure à la déformation D_2 subséquente et à la fabrique structurale associée. On estime que les failles chevauchantes TwoPete et Inconnu ont été actives pendant la déformation D_1. Celle-ci marque la convergence générale du terrane de Yukon-Tanana avec l'ancienne Amérique du Nord.

La déformation D_2 est délimitée par une schistosité de crénulation de plan axial à pendage faible et associée à des plis mineurs qui varient d'ouverts à fermés. Les fabriques S_2 et les plis sont plus accentués et plus serrés au-dessus du Batholite d'Anvil et diminuent en intensité à la fois vers le nord-est et le sud-ouest. De plus, la vergence des plis est renversée sur le Batholite d'Anvil avec des structures de vergence sud-ouest présentes au sud-ouest du batholite et des structures de vergence nord-est présentes au nord-est du batholite. La suite plutonique d'Anvil présente une fabrique structurale D_2, tandis que la suite plutonique Tay River n'est pas foliée. Par conséquent, la déformation D_2 se limiterait à l'intervalle de 109 à 96 Ma. La contrainte de compression est près de la verticale et est la plus intense au-dessus du Batholite d'Anvil, indiquant que la déformation D_2 a un lien cinématique avec l'intrusion moins dense de la suite plutonique d'Anvil. La phase la plus récente de la déformation D_2 est caractérisée par la formation, par endroits, de failles d'extension le long de la bordure sud-ouest du Batholite d'Anvil et des roches métasédimentaires susjacentes. On a constaté que les rejets le long des failles d'extension atteignent plus de 1 km par endroits. Ils représentent probablement l'effondrement de l'édifice de la déformation causé par l'intrusion de la suite plutonique d'Anvil.

La déformation D_2 est accompagnée d'un métamorphisme M_2 pénétratif. Les isogrades de métamorphisme sont concentriques autour du Batholite d'Anvil. Les assemblages métamorphiques varient du faciès des schistes verts inférieur à la zone à sillimanite-muscovite du faciès des amphibolites. Les températures et pressions maximales atteintes durant le métamorphisme sont approximativement de 620°C et de 4 kilobars. Cela correspond à une profondeur d'enfouissement pouvant atteindre 12 km pendant le phénomène de métamorphisme. Le métamorphisme M_2 s'est entièrement surimposé au métamorphisme M_1 plus ancien, associé à la déformation D_1.

Le district minier d'Anvil renferme d'importantes minéralisations sédimentaires exhalatives (SEDEX) en zinc-plomb-argent-barityne. L'exploration dans le district minier a permis de découvrir, selon les estimations, 225 millions de tonnes de roches sulfurées minéralisées (Jennings et Jilson, 1986) réparties en 5 gisements de métaux communs présents dans un intervalle stratigraphique de 150 mètres au contact Mount Mye-Vangorda dans l'ancienne succession nord-américaine. Dans le district, l'exploitation minière a commencé en 1969 et s'est poursuivie sans interruption jusqu'en 1997. Les gisements connus se présentent suivant une orientation curvilinéaire que l'on interprète comme une structure faillée syngénétique à la sédimentation. En dépit des efforts déployés pendant 45 ans d'exploration du district minier, d'importantes régions le long du contact géologique Mount Mye-Vangorda doivent encore être vérifier pour la présence de minéralisations de sulfures massifs non découvertes et profondément enfouies.

L'inventaire MINFILE du Yukon pour le district minier d'Anvil contient aussi la documentation d'indices minéraux de barytine dans les roches sédimentaires, de veines polymétalliques associées à des intrusions, et de minéraux sulfurés dans des roches volcaniques. Ce n'est que récemment que les efforts d'exploration dans le district minier ont été dirigés vers ces autres cibles d'exploration. Comme pour les minéralisations SEDEX, le potentiel d'exploration pour ces autres modèles de gisements n'a pas encore été mis à l'épreuve jusqu'à maintenant.

Contents

Preface/Préface i

Acknowledgements ii

Abstract iii

Résumé v

Introduction
- Location and access 1
- Physiography 1
- Glacial history 3
- Previous work 3
- Regional setting 3

Stratigraphy
- Introduction 5
- North American stratigraphy 5
  - Mount Mye formation 6
  - Vangorda formation 8
  - Menzie Creek formation 12
  - Road River Group 17
  - Platy siltstone 20
  - Quartz sandstone and dolostone 20
  - Earn Group 21
- Yukon-Tanana Terrane stratigraphy 21
  - Micaceous quartzite 21
  - Faro Peak formation (new) 24
- Slide Mountain stratigraphy 27
  - Mount Aho formation (new) 28
  - Rose Mountain formation (new) 31
  - Campbell Range formation 33

Intrusive rocks
- Introduction 37
- Instrusive suites 37
  - Ordovician-Silurian gabbro and pyroxenite 37
  - Permian(?) mafic and ultramafic intrusions 39
  - Anvil plutonic suite (revised) 39
  - Tay River plutonic suite 41
  - Eocene quartz-feldspar porphyry 43

Structure
- Introduction 45
- D_1 deformation (folding) 45
- D_1 deformation (thrust faults) 46
- D_2 deformation (folding) 48
- D_2 deformation (normal faults) 49

Metamorphism 51

Age of deformation and metamorphism
- D_1 deformation and M_1 metamorphism 53
- D_2 deformation and M_2 metamorphism 54
- D_3-D_5 deformation and metamorphism 54
- Normal and strike slip faults 54
- Vangorda fault 54
- Tintina Fault 55
- Cooling, uplift and erosion 55

Economic geology
- Introduction 57
- Sedimentary-exhalative (SEDEX) zinc-lead-silver-barite massive sulphide deposits 57
- Sediment-hosted barite deposits 58
- Polymetallic intrusion-related quartz veins 58
- Volcanic-hosted massive sulphide mineralization 59

Summary 61

Recommendations for further work 63

Selected references 65

APPENDICES

Appendix I: Whole rock geochemical analyses 75

Appendix II: Fossil identification 85

Appendix III: Isotopic age dating 99

Figures

p. x Sulphide mineral blast in Faro mine open pit

p.2 Figure 1. Anvil District location map

p.2 Figure 2. View looking northeast from Robert Campbell Highway in Tintina Trench.

p.4 Figure 3. Schematic stratigraphic columns, North American succession.

p.6 Figure 4. Mount Mye formation phyllite

p.6 Figure 5. Mount Mye formation phyllite, NQ size core.

p.6 Figure 6. Mount Mye formation phyllite with andalusite prisms pseudomorphed by chlorite

p.7 Figure 7. Mount Mye formation, NQ size core. Biotite-andalusite clusters and clots

p.7 Figure 8. Mount Mye formation schist. Staurolite-garnet-biotite-muscovite-quartz schist

p.7 Figure 9. Mount Mye formation, carbonaceous phyllite

p.9 Figure 10. Mount Mye formation marble

p.9 Figure 11. Mount Mye formation marble with calc-silicate boudins

p.9 Figure 12. Mount Mye formation calc-silicate rock, NQ size core.

p.9 Figure 13. Mount Mye formation calc-silicate rock

p.10 Figure 14. Vangorda formation phyllite

p.10 Figure 15. Vangorda formation phyllite NQ size core

p.10 Figure 16. Vangorda formation phyllite, thin limestone interbeds in phyllite

p.10 Figure 17. Vangorda formation calc-silicate rock

p.11 Figure 18. Vangorda formation calc-silicate rock, NQ size core

p.11 Figure 19. Vangorda formation basal carbonaceous phyllite member

p.11 Figure 20. Vangorda formation basal carbonaceous phyllite member, NQ size core

p.12 Figure 21. Vangorda formation, contact metamorphosed phyllite

p.13 Figure 22. Menzie Creek formation pillow basalt flow

p.13 Figure 23. Menzie Creek formation pillow basalt flow, isolated pillows

p.13 Figure 24. Menzie Creek formation basalt breccia, isolated pillows

p.14 Figure 25. Menzie Creek formation basalt breccia

p.14 Figure 26. Menzie Creek formation basalt breccia

p.14 Figure 27. Menzie Creek formation epiclastic volcanic sandstone

p.15 Figure 28. Menzie Creek formation, extrusive rocks discriminant and multi-element diagrams

p.16 Figure 29. Menzie Creek formation, extrusive rocks tectonic discriminant diagrams

p.18 Figure 30. Duo Lake Formation carbonaceous shale overlain by Menzie Creek formation

p.18 Figure 31. Duo Lake Formation carbonaceous phyllite

p.19 Figure 32. Duo Lake Formation altered and hornfelsed carbonaceous phyllite

p.22 Figure 33. Yukon-Tanana Terrane eclogite and greenstone discriminant and multi-element diagrams

p.23 Figure 34. Yukon-Tanana Terrane eclogite and greenstone tectonic discriminant diagrams

p.26 Figure 35. Faro Peak formation basalt discriminant and multi-element diagrams

p.27 Figure 36. Faro Peak formation basalt tectonic discriminant diagrams

p.28 Figure 37. Mount Aho formation pale green argillite

p.28 Figure 38. Mount Aho formation maroon chert and siliceous argillite

p.29 Figure 39. Mount Aho formation pale green argillite and chert-pebble conglomerate

p.29 Figure 40. Mount Aho formation black chert and dark grey limestone

p.29 Figure 41. Mount Aho formation black chert-pebble conglomerate

p.30 Figure 42. Mount Aho formation interbedded barite and tan chert

p.30 Figure 43. Mount Aho formation bedded barite

p.31 Figure 44. Rose Mountain formation pale cream phyllitic chert

p.32 Figure 45. Rose Mountain formation red chert

p.33 Figure 46. Campbell Range formation basalt

p.33 Figure 47. Campbell Range formation green chert interbedded with basalt

p.34 Figure 48. Campbell Range formation basalt discriminant and multi-element diagrams

p.35 Figure 49. Campbell Range formation basalt tectonic discriminant diagrams

p.37 Figure 50. Ordovician-Silurian gabbro sill in Vangorda formation, BQ size core

p.37 Figure 51. Quartz-carbonate altered Ordovician-Silurian gabbro sill, BQ size core

p.38 Figure 52. Ordovician-Silurian gabbro and pyroxenite discriminant and multi-element diagrams

p.39 Figure 53. Ordovician-Silurian gabbro and pyroxenite tectonic discriminant diagrams

p.40 Figure 54. Anvil plutonic suite granite

p.40 Figure 55. Anvil plutonic suite, granite contact with Vangorda formation calc-silicate rock

p.41 Figure 56. Tay River plutonic suite intrusive

p.43 Figure 57. Eocene quartz-feldspar porphyry with flow-banding

p.43 Figure 58. Eocene quartz-feldspar porphyry with smoky quartz phenocrysts

p.45 Figure 59. D_1 fold in Vangorda formation refolded by D_2 minor fold

p.45 Figure 60. D_1 fold in Vangorda formation refolded by D_2 minor fold, NQ-size core

p.46 Figure 61. D_1 fold in Vangorda formation refolded by D_2 minor fold
p.46 Figure 62. D_1 fold in Mount Aho formation
p.47 Figure 63. Comparison of structural and stratigraphic interpretations for Rose Mountain area
p.48 Figure 64. D_2 fold in Vangorda formation, BQ-size core
p.49 Figure 65. D_2 fold in micaceous quartzite of Yukon-Tanana Terrane
p.49 Figure 66. Extensional fault rock, Vangorda Plateau, NQ-size core
p.49 Figure 67. S-C banding Anvil Batholith, Anvil plutonic suite
p.52 Figure 68. Metamorphic Pressure-Temperature diagram Anvil District
p.53 Figure 69. Ar-Ar plot for stepwise heating of Mount Aho formation phyllite and Vangorda formation phyllite
p.57 Figure 70. Discovery showing on Vangorda Creek, Vangorda SEDEX deposit
p.58 Figure 71. Float boulder of sulphide breccia in Anvil plutonic suite, JRV property
p.103 Figure 72. Concordia diagrams for samples from the Anvil District
p.103 Figure 73. Concordia diagrams for Eocene porphyry samples, Anvil District

Tables

p.17 Table 1. Fossil localities, Menzie Creek formation
p.19 Table 2. Fossil localities, Duo Lake Formation
p.24 Table 3. Isotopic dates for metamorphic minerals in Yukon-Tanana Terrane eclogites
p.25 Table 4. Fossil localities, Faro Peak formation
p.30 Table 5. Fossil localities, Mount Aho formation
p.32 Table 6. Fossil localities, Rose Mountain formation
p.41 Table 7. Isotopic age dates, Anvil plutonic suite (Mount Mye phase)
p.42 Table 8. Isotopic age dates, Tay River plutonic suite
p.42 Table 9. Isotopic age dates, Eocene quartz-feldspar porphyry
p.57 Table 10. Discovery dates for SEDEX deposits, Anvil District
p.76 Table I-1. Geochemistry of volcanic rocks, Menzie Creek formation
p.78 Table I-2. Geochemistry of Ordovician-Silurian gabbro
p.80 Table I-3. Geochemistry of eclogites, Yukon-Tanana Terrane
p.81 Table I-4. Geochemistry of volcanic rocks, Faro Peak formation
p.82 Table I-5. Geochemistry of volcanic rocks, Campbell Range formation
p.84 Table I-6. Geochemistry of Permian mafic and ultramafic intrusive rocks
p.102 Table III-1. U-Pb analytical data for plutonic rocks from the Anvil District

Plates

Plate 1. Geoscience Map 2004-1 Intrusive suites and major stratigraphic-tectonic successions (1:100 000 scale)
Plate 2. Geoscience Map 2004-2 Geological map of Anvil District (1:100 000 scale)
Plate 3. Geoscience Map 2004-3 Geological map of Rose Mountain (NTS 105K/5 NW) (1:25 000 scale)
Plate 4. Geoscience Map 2004-4 Geological map of Rose Mountain (NTS 105K/5 NE) (1:25 000 scale)
Plate 5. Geoscience Map 2004-5 Geological map of Rose Mountain (NTS 105K/5 SE) (1:25 000 scale)
Plate 6. Geoscience Map 2004-6 Geological map of Mount Mye (NTS 105K/6 NW) (1:25 000 scale)
Plate 7. Geoscience Map 2004-7 Geological map of Mount Mye (NTS 105K/6 W) (1:25 000 scale)
Plate 8. Geoscience Map 2004-8 Geological map of Faro (NTS 105K/3 NW) & Mount Mye (NTS 105K/6 SW) (1:25 000 scale)
Plate 9. Geoscience Map 2004-9 Geological map of Mount Mye (NTS 105K/6 NE) & Barwell Lake (NTS 105K/11 SE) (1:25 000 scale)
Plate 10. Geoscience Map 2004-10 Geological map of Mount Mye (NTS 105K/6 E) (1:25 000 scale)
Plate 11. Geoscience Map 2004-11 Geological map of Faro (NTS 105K/3 NE) & Mount Mye (NTS 105K/6 SE) (1:25 000 scale)
Plate 12. Geoscience Map 2004-12 Geological map of Blind Creek (NTS 105K/7 NW) (1:25 000 scale)
Plate 13. Geoscience Map 2004-13 Geological map of Blind Creek (NTS 105K/7 SW) (1:25 000 scale)
Plate 14. Geoscience Map 2004-14 Geological map of Swim Lakes (NTS 105K/2 W) (1:25 000 scale)
Plate 15. Geoscience Map 2004-15 Geological map of Blind Creek (NTS 105K/7 SE) (1:25 000 scale)
Plate 16. Geoscience Map 2004-16 Geological map of Swim Lakes (NTS 105K/2 NE) (1:25 000 scale)
Plate 17. Geoscience Map 2004-17 Geological map of Swim Lakes (NTS 105K/2 SE) (1:25 000 scale)

Sulphide mineral blast in Faro mine open pit, June 1979. Mill and office complex on left side of photo.

INTRODUCTION

The Anvil District in central Yukon contains the only lead-zinc mines developed in Selwyn Basin, a major lead-zinc province in western Canada. The District contains 5 known pyritic massive sulphide deposits with a total mineral inventory of 120.1 million tonnes averaging 9.3% combined lead and zinc (Jennings and Jilson, 1986). The deposits were discovered between 1953 and 1976. Three of the deposits have been mined or partly mined, and two remain undeveloped. With the bankruptcy of Anvil Range Mining Corporation in 1997, exploration and development in the District has been in a hiatus period.

Exploration potential in the District remains high. The Yukon Geology Program (precursor to the Yukon Geological Survey) initiated an integrated multidisciplinary geoscience study in 1998 to provide a unified geology framework for the area to assist future exploration. Projects within this integrated study included bedrock geology mapping and compilation (Pigage, this report), surficial geology mapping and basal till sampling (Bond, 2001), detailed lithogeochemistry of the immediate host rocks to the massive sulphide deposits (Stanley, in preparation), and a seismic geophysics line over the Grizzly/Dy deposit (Power, 1998).

This report summarizes the results of the bedrock mapping and compilation project. The goal of this project was to harmonize the detailed property geology mapping completed by exploration companies within the last 49 years of exploration with the regional geology mapping completed by the Geological Survey of Canada and that done during the course of this study. Primary data sources for the geology compilation were the Cyprus Anvil Mining Corporation detailed and regional maps (Jennings et al., 1978a, b), and the 1:50 000-scale maps completed by Gordey (1990a,b,c). Two field seasons were spent completing spot checks in selected areas. Samples of volcanic rocks were collected for research geochemical analysis. Selected samples were collected for isotopic age determinations and fossil conodont age determinations. Portions of the project have been previously reported (Pigage, 1999a, 2000a). The fifteen 1:25 000-scale bedrock geology maps encompassing the study were released over a period of three years as Open File maps (Pigage, 1999b,c,d, 2000b,c,d,e,f,g,h,i, 2001a,b,c,d,e). The bedrock geology maps contained in this report are second-generation maps; known errors and inconsistencies within the previously published Open File maps have been corrected. These geology maps are published separately as Geoscience Maps and are available in this report as plates in the envelope, and as PDF files and Autocad drawing files on the enclosed CD-ROM. All coordinate information in this report is presented in Universal Transverse Mercator format using the NAD83 datum (zone 8).

LOCATION AND ACCESS

Anvil District is located near the town of Faro in central Yukon (Fig. 1), approximately 200 km northeast of Whitehorse. The District encompasses portions of 50 000-scale NTS map sheets 105K/2, 105K/3, 105K/5, 105K/6, 105K/7 and 105K/11 with an overall area of approximately 2000 km^2. The Robert Campbell highway, Mitchell road, mine access road, Blind Creek road and Swim Lake road provide access to Faro and the southwest margin of the area (Plate 1). Numerous overgrown exploration and mining roads, passable by four wheel drive or all-terrain vehicles, provide limited access to the southwest part of the District. Exploration roads on the northeast portion of the District are largely overgrown and are passable only by all-terrain vehicles. Rapid access is best obtained using helicopter. Helicopter access for fieldwork during completion of this project was provided by contract helicopter service based in Ross River.

PHYSIOGRAPHY

The District is located within the Yukon Plateau physiographic province (Bostock, 1948), consisting of a dissected plateau surface that constitutes much of central Yukon. It is bound by the Tintina Trench on the southwest and the Tay River on the north. The Anvil Range forms the core of the District with summit elevations rising above 1800 m (5900 ft). Elevations range from 620 m (2030 ft) on the Pelly River to 2060 m (6763 ft) marking the summit of Mount Mye (Fig. 2). Treeline occurs at an elevation of 1370 m (4500 ft). Above treeline, cliffs are dominantly represented by north- and northeast-facing cirques caused by valley glaciers. Cliff areas at lower elevations are mainly stream cuts. The major upland plateaus in the area are dissected by broad southwest-trending preglacial valleys and narrower, northwest-trending glacial valleys (Jackson, 1994).

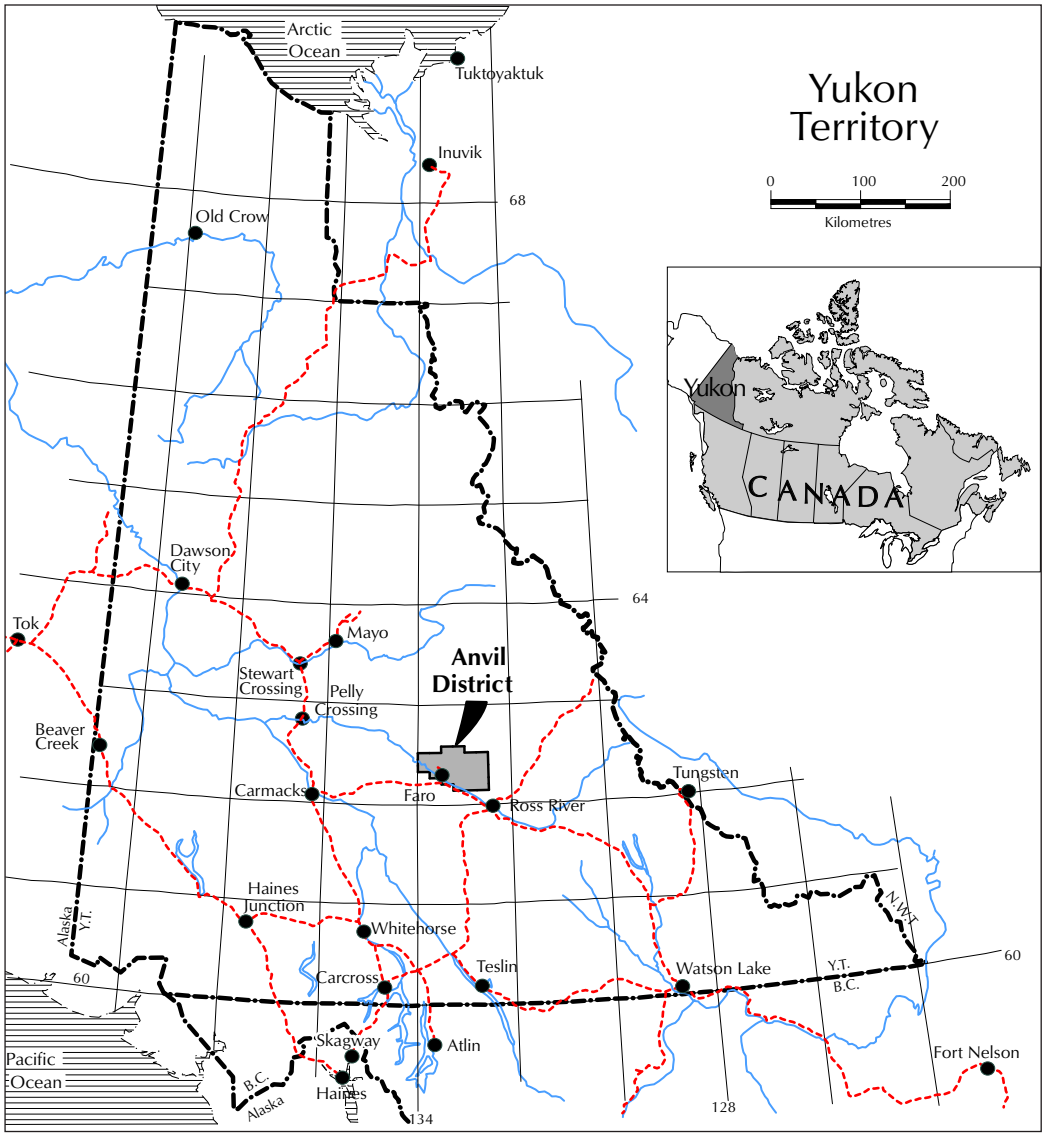

Figure 1. *Location of Anvil District, Yukon Territory.*

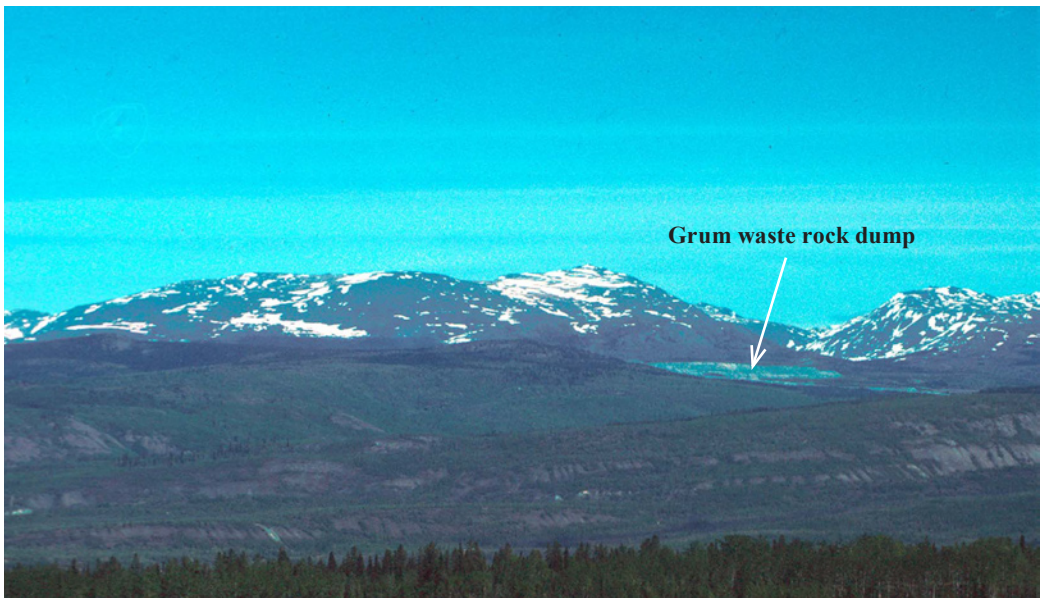

Figure 2. *Looking northeast from Robert Campbell Highway in 1995. Tintina Trench is in foreground. The south edge of the town of Faro is visible on left edge of photograph. The central area is Vangorda Plateau. Rock waste dumps from mining of Grum deposit are in the centre of the Vangorda Plateau. The Anvil Range forms mountains in background.*

GLACIAL HISTORY

Yukon has undergone a series of glacial and interglacial cycles that dates to the beginning of the Quaternary period, approximately 2.5 million years ago (Froese et al., 2000; Duk-Rodkin et al., 1996). The glacial history of the Anvil District is dominated by deposits of the late Wisconsinan McConnell glaciation, approximately 25 000 to 15 000 years ago. Jackson (1994) completed a regional study of the surficial geology of the area. An excellent detailed study of the glaciation, including 11 1:25 000-scale surficial geology maps of the Anvil District and geochemical studies of the till deposits is given by Bond (2001). Surficial geology maps in Bond's report have been coordinated so that they coincide with and can be superimposed on the bedrock geology maps presented in this report. They are also included on the CD-ROM.

During the McConnell glaciation the Anvil District was covered by ice that flowed west and northwest from the Selwyn Mountains, by ice that flowed east and northwest from the Pelly Mountains, and by local glaciers that developed in the Anvil Range itself. These different sources coalesced to form the Cordilleran regional ice sheet with dominant iceflow directed west to northwest along the Tintina Trench. The highest elevation of erratics mapped on Mount Mye is 1951 m, indicating that nunataks were present in the Anvil Range during the height of the glaciation (Bond, 2001). Glacial sediment cover, consisting dominantly of till with local glaciofluvial deposits, becomes increasingly abundant below 1460 m (Bond, 2001). Glacial deposits confirm a re-advance of the regional Cordilleran ice sheet during McConnell deglaciation.

Upon retreat of the ice sheet southeast, a glacial lake informally termed glacial lake Pelly (Bond, 2001) formed in the Tintina Trench. Thick deposits of glaciolacustrine silts, glaciofluvial sediments and till were deposited in the Trench during the melting and retreat of the Cordilleran ice sheet. Glacial overburden in the District varies greatly from less than 1 m to greater than 100 m. Generally, valley bottoms have more extensive glacial cover. In some instances glacial cover infills and 'hides' preglacial channels up to 100 m deep on the plateau uplands (e.g., immediately southeast of Grum deposit on Vangorda plateau).

PREVIOUS WORK

Regional bedrock geology for Tay River map area (105K) was completed at 1:253 440 scale by Roddick and Green (1961) and at 1:250 000 scale by Gordey and Irwin (1987). More detailed studies by Tempelman-Kluit (1972) at 1:125 000 scale and Gordey (1990a,b,c) at 1:50 000 scale were completed because of increased interest due to the discovery of several massive sulphide deposits in the area.

The discovery of five lead-zinc massive sulphide deposits between 1953 and 1976 resulted in the completion of extensive detailed property geology throughout the District by a large number of mining and exploration companies. Consolidation of much of the District under the control of one company, Cyprus Anvil Mining Corporation (CAMC) occurred by 1979.

CAMC completed a regional mapping program during the period 1971-1983. The results of this regional program were published internally with regional maps at 1:50 000 and 1:12 000 scales (Jennings et al., 1978a,b) scales, and summarized in Jennings and Jilson (1986). After 1979, CAMC exploration geologists began remapping areas of primary deposit potential at a scale of 1:5000. This detailed remapping program was continued by subsequent mine owners Curragh Resources Inc. and Anvil Range Mining Corporation Ltd. This work was discussed by Pigage (1990), but only published internally as a series of maps and as assessment reports.

REGIONAL SETTING

The Anvil District contains the most westerly off-shelf basinal facies of the Cordilleran miogeocline, a prism of sedimentary rocks of Precambrian to Jurassic age deposited along the relatively stable continental margin of western North America. Cordilleran miogeocline stratigraphy is presented in Abbott et al. (1986). More detailed discussion of the stratigraphy and structure of the Anvil District is given in Jennings and Jilson (1986) and Pigage (1990).

The District is part of Selwyn Basin, a large area of central Yukon in which deep water clastic rocks, chert, and minor carbonate accumulated along the ancient North American continental margin during Neoproterozoic and early Paleozoic time (Gabrielse, 1967). Northeast of the basin, a shallow carbonate platform (Mackenzie Platform) formed the near-shore facies of ancient North America (Abbott et al., 1986).

Anvil District lies immediately northeast of the Slide Mountain and Yukon-Tanana Terranes, the most easterly of the allochthonous terranes (Coney et al., 1980). Yukon-Tanana Terrane has been interpreted as a middle to late Paleozoic continental margin volcanic arc assemblage related to east-dipping subduction beneath distal North America (Mortensen and Jilson, 1985; Creaser et al., 1999;

Piercey et al., 2002). Slide Mountain Terrane consists of oceanic basalt and bedded cherts interpreted as a late Paleozoic back-arc or marginal ocean basin (Anvil or Slide Mountain Ocean) formed by rifting and westward migration of Yukon-Tanana Terrane relative to North America (Tempelman-Kluit, 1979a,b; Creaser et al., 1999). Tempelman-Kluit (1979a,b) and Gordey (1990a,b,c) interpreted the allochthonous terranes as being thrust northeastward over the North American rocks. Mortensen and Jilson (1985) interpreted the contact as a transpressive suture. More recently, crustal-scale seismic studies as part of Lithoprobe have confirmed the Yukon-Tanana and Slide Mountains terranes are a thin crustal veneer of arc-related and oceanic metasedimentary and metavolcanic rocks thrust over a westward-dipping wedge of North American sedimentary rocks resting on continental basement (Snyder et al., 2002).

Deformation and metamorphism associated with accretion of the allochthonous terranes was inititated in Jurassic and culminated in the Cretaceous (Tempelman-Kluit, 1979b). More recently, strike-slip faulting along the Tintina fault zone resulted in approximately 425 km of right lateral displacement during Early Tertiary time (Roddick, 1967; Murphy and Mortensen, 2003).

STRATIGRAPHY

INTRODUCTION

Stratigraphic units in the area encompassed by this report range from Neoproterozoic or Early Cambrian to Triassic in age. All units are strongly transposed and recrystallized with development of at least one structural fabric. In spite of the strong deformation and metamorphism, however, stratigraphic units are coherent and can be readily traced along strike. Primary depositional structures are still readily visible at lower metamorphic grades. All thicknesses in this report are structural thicknesses and may differ substantially from primary depositional thicknesses. The units form three stratigraphic successions with differing depositional environments and regional terrane associations. Plate 1 indicates the areal extent of each of the stratigraphic/tectonic successions. Stratigraphic units making up these different successions will be discussed in the following sections.

NORTH AMERICAN STRATIGRAPHY

Early to Middle Paleozoic metasedimentary rocks, with an aggregate thickness of greater than 7400 m, form the most southwesterly extent of the ancient North American miogeocline and constitute Anvil District (and most of the area encompassed by this report). In the Anvil District, this succession consists dominantly of fine-grained clastic rocks with lesser carbonate rocks and local coarse-grained clastic rocks. Extensive Ordovician basaltic volcanic and epiclastic rocks denote local rifting along the continental margin. Eight formations constituting this succession are described in this report. Figure 3 presents schematic stratigraphic columns for the North American succession southwest and northeast of the Anvil Batholith.

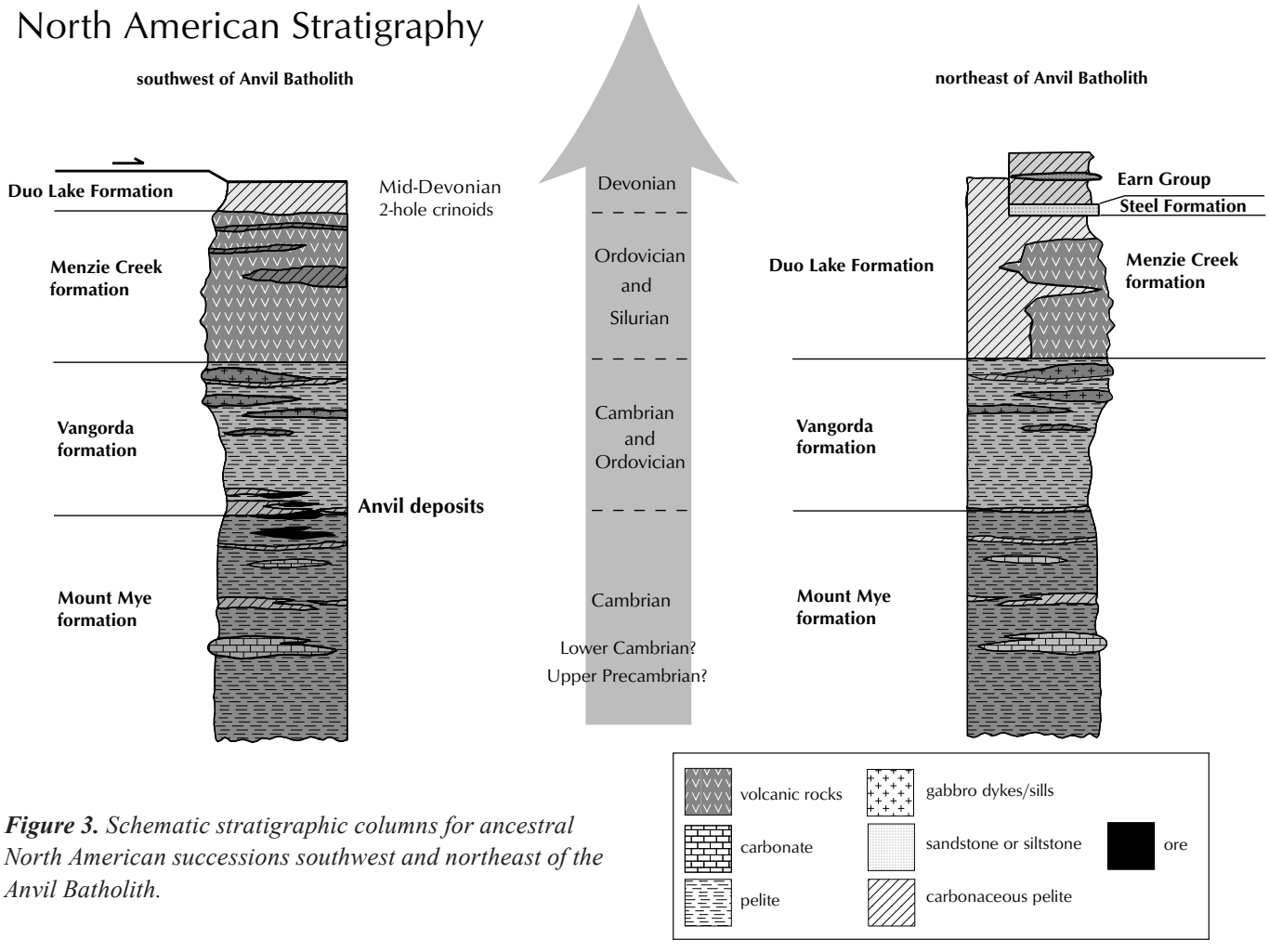

Figure 3. *Schematic stratigraphic columns for ancestral North American successions southwest and northeast of the Anvil Batholith.*

Mount Mye formation

The Mount Mye formation (Jennings and Jilson, 1986) is the oldest unit exposed in Anvil District. It is extensively exposed on the lower slopes of both the north and south sides of Mount Mye. The most complete section is on the north side of Mount Mye and extends from 601 280 E, 6 914 880 N to 602 810 E, 6 918 090 N (Plate 10). Excellent accessible exposures occur along the mine access road near the former fresh water reservoir and on the Blind Creek road immediately west of Van Gorder Creek. Cross sections on the north side of Mount Mye indicate a minimum present-day thickness of approximately 2000 m.

This unit is the immediate host rock for at least some stratiform massive and quartzose sulphide deposits in the District (Vangorda, Faro, Grum, Dy, Swim). It also contains the iron-sulphide showings constituting the SB, Sea, and Ace occurrences.

The dominant lithologies are biotite-muscovite-quartz-plagioclase±andalusite±garnet±staurolite±fibrolite schist at amphibolite facies metamorphic grade and muscovite-chlorite-quartz-plagioclase phyllite at greenschist facies metamorphic grade. Minor amounts of pyrite and/or pyrrhotite occur as irregular disseminated grains. The average bulk composition of 18 samples collected from Mount Mye formation are close in composition to average shale (Jennings and Jilson, 1986). Interbands of marble, calc-silicate rock, carbonaceous schist or phyllite, and chloritic phyllite or hornblende amphibolite occur in lesser amounts.

Figure 5. *Mount Mye formation phyllite. BQ-size core. Core breaks on finely spaced crenulation cleavage which forms the dominant foliation. Note minor colour variations are transposed subparallel to dominant foliation. Drill hole CNR76-01, 426 ft – 449 ft (130 m – 137 m).*

Typical Mount Mye phyllite is a medium to dark grey, noncalcareous, moderately soft to soft, fine-grained, micaceous phyllite (Figs. 4 and 5). Locally, foliation surfaces contain compositional bands 1 to 10 cm thick, in shades of light and dark grey. The phyllite weathers to a rusty brown, and foliation surfaces typically have an irregular, thin, patchy brown weathering coat. The dominant structural fabric is a closely spaced crenulation cleavage. Close to the Cretaceous felsic intrusions, the crenulation cleavage becomes a pervasive fabric with rarely preserved microlithons visible only in thin section.

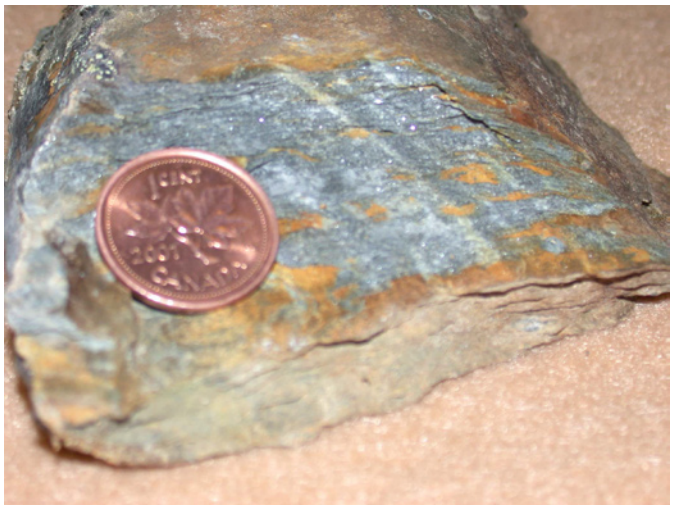

Figure 4. *Mount Mye formation phyllite. Weathering consists of a brownish coating. Bedding is visible progressing from top to bottom of photo near the centre. Canadian penny is 1.9 cm across.*

Figure 6. *Mount Mye formation phyllite transitional to schist with andalusite prisms pseudomorphed by dark green chlorite. Pencil is 14 cm long. Southwest wall of Faro open pit.*

Figure 7. *Mount Mye formation. NQ-size core. Biotite-andalusite clots and clusters within matrix of biotite-muscovite phyllite transitional to schist. Dominant foliation is closely spaced crenulation cleavage. Drill hole 84F-28.*

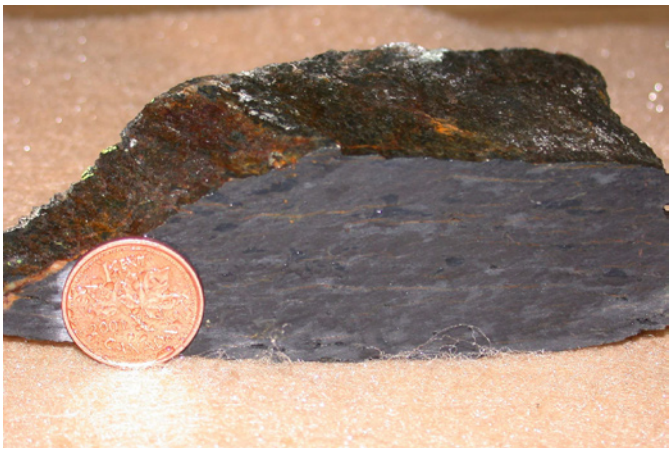

Figure 9. *Carbonaceous phyllite within Mount Mye formation. Penny is 1.9 cm across. Field station 98LP171.*

With increasing metamorphic grade, the muscovite-chlorite phyllite develops 1- to 20-cm-long, prismatic, andalusite porphyroblasts that are randomly oriented on the crenulation cleavage foliation surface (Figs. 6 and 7). Commonly, these porphyroblasts are pseudomorphed by dark green chlorite. At higher metamorphic grades, muscovite and biotite increase in grain size, and the phyllite becomes schist. At these higher metamorphic grades, the schist has a purplish brown weathering sheen, although the irregular patchy brown weathering coat is still present. Staurolite and garnet porphyroblasts are locally common in the schist (Fig. 8). Fibrolite is intergrown with biotite at highest metamorphic grades adjacent to the granitic intrusions.

Dark grey to black, carbonaceous, siliceous phyllites and schists are interlayered with the less carbonaceous metapelites. These darker coloured units comprise only about 10% of the formation (Jennings and Jilson, 1986), but are useful geological and geophysical marker horizons. Locally, they are calcareous with lenses and bands of dark grey marble. North of Mount Mye, a prominent carbonaceous horizon (locally calcareous) is 80 to 100 m thick and occurs approximately 800 to 1000 m below the top of the formation (Fig. 9). Near the Vangorda deposit, a 110-m-thick carbonaceous phyllite occurs 180 m below the top of the formation, and in the vicinity of the Swim deposit, a carbonaceous horizon up to 20 m thick occurs 100 m below the upper contact of the Mount Mye formation.

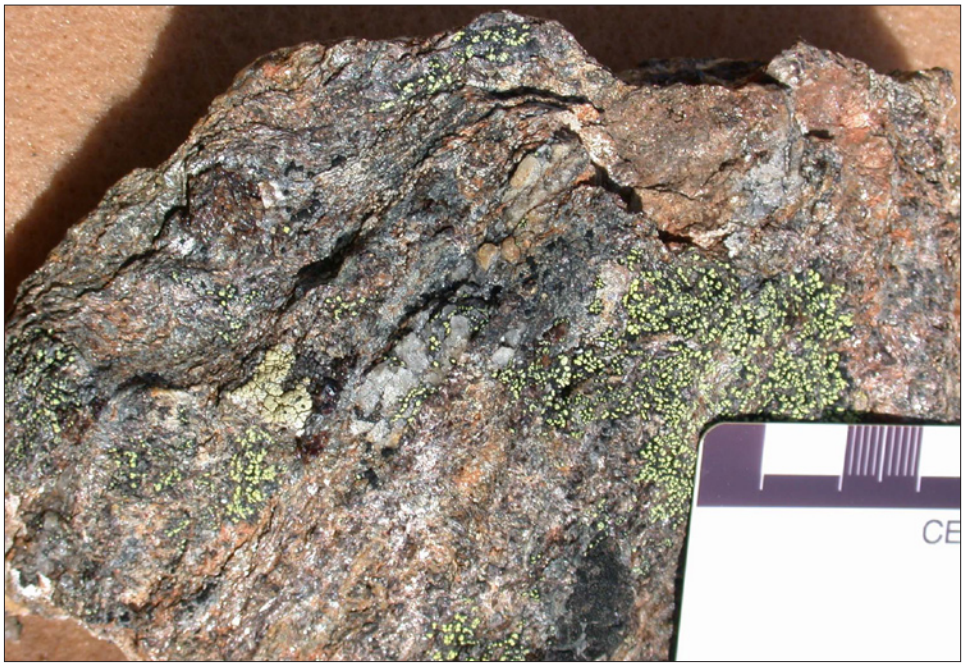

Figure 8. *Mount Mye formation. Staurolite-garnet-biotite-muscovite-quartz schist. Dominant foliation is a closely spaced crenulation cleavage. Major division of scale is 1 cm. Field station 98LP138.*

Marble and calc-silicate rocks are interlayered with the Mount Mye schists and phyllites, and constitute about 10% of the formation (Jennings and Jilson, 1986). The marble is white to medium grey to black, medium crystalline calcite, with abundant boudins and bands of biotite schist and calc-silicate rock (Figs. 10 and 11). Marble bands are interlayered with calc-silicate bands. Calc-silicate rock typically consists of thinly banded light green, cream and brown quartz-tremolite-biotite±diopside±garnet±calcite± epidote. Banding is irregular and typically on a scale of 1 to 20 cm (Figs. 12 and 13). Calc-silicate rocks are generally finer grained than the surrounding pelite schists. Lesser intervals of calc-silicate rock are carbonaceous and have a dark grey to black colour. North of Mount Mye, a prominent calc-silicate interval with minor limestone interbeds is approximately 200 m thick and occurs 1300 m below the top of the formation. The same unit farther to the northwest occurs only 540 m below the top of the formation and is approximately 300 m thick. South of Mount Mye, calc-silicate rock horizons range from 240 to 440 m below the top of the formation and are 120 to 200 m thick.

Chloritic phyllite (greenschist facies metamorphism) or amphibolite (amphibolite facies metamorphism) occur in small amounts in the Mount Mye formation. These rocks are generally strongly foliated, dark to pale green, and lack relict igneous texture. They are only a few metres to tens of metres thick and have small to moderate lateral dimensions. These units are chemically identical to the Ordovician-Silurian Menzie Creek formation and have been interpreted as subvolcanic feeder dykes and sills for the Menzie Creek basalts. They will be discussed further in the section on intrusive rocks.

The upper contact of the Mount Mye formation with the Vangorda formation is gradational, with limited interbanding of calcareous and noncalcareous lithologies. The contact is defined as the top of the uppermost substantial noncalcareous phyllite or schist. This constitutes a useful level because it coincides locally with the base of a thick carbonaceous, siliceous phyllite or schist, and corresponds to the general stratigraphic interval of the massive sulphide deposits in the Anvil District. The lower stratigraphic contact of the Mount Mye formation is not exposed as lowermost exposures of Mount Mye formation in Anvil district are intruded by mid-Cretaceous plutons.

Fine-grained pelites of the Mount Mye formation indicate a deep-water, quiet depositional environment. This is consistent with accumulation in an off-shelf setting.

Mount Mye formation corresponds to the noncal–careous schists and phyllites of unit 2 and the lower member of unit 3, as mapped by Tempelman-Kluit (1972). Gordey and Irwin (1987) correlated it with Gull Lake Formation (Gordey and Anderson, 1993) as defined in the Nahanni area (105I). Mount Mye formation does not contain any fossils. In the Nahanni area, archeocyathids in the lowermost member of the Gull Lake Formation indicate a lower age limit of Early Cambrian for Gull Lake Formation and suggests a similar lower age limit for Mount Mye formation. The Late Cambrian to late Middle Ordovician Rabbitkettle Formation (Gordey and Anderson, 1993) unconformably overlies the Gull Lake Formation in the Nahanni area and imposes an upper age limit of Late Cambrian for the Gull Lake Formation (and by lithologic correlation, the Mount Mye formation). Jennings and Jilson (1986) suggested that the lower part of the Mount Mye formation may be Hadrynian in age because of its quartzofeldspathic nature.

Vangorda formation

Pale silvery grey, calcareous, recessive phyllite constitutes the Vangorda formation (Jennings and Jilson, 1986) in much of the Anvil District. At higher metamorphic grade, the Vangorda formation consists of thinly banded, resistant, pale cream and dark brown calc-silicate rock. Lesser interbedded rock types include limestone/marble, carbonaceous phyllite/schist, dolomitic siltstone, and chloritic phyllite/amphibolite. The base of the formation locally contains a mappable carbonaceous phyllite/schist member. The unit is exposed both north and south of intrusions that make up the Anvil Batholith. A type section for the formation was not defined by Jennings and Jilson (1986), partly because of lack of suitable exposures for the entire unit. One ridge with scattered outcrop from the lower contact (573 900 E, 6 920 600 N) to the upper contact (570 500 E, 6 919 300 N) occurs 12 km northwest of the Faro deposit (Plate 4); this section includes examples of both calc-silicate rock and phyllite (the two dominant rock types of the formation). Accessible exposures of Vangorda formation phyllite occur on the Blind Creek road in the Grizzly/Dy deposit area south of Mount Mye. Excellent exposures of Vangorda formation calc-silicate rock occur in the southwest wall of the Faro deposit open pit and along the southwest margin of the former freshwater reservoir on the mine access road. Exposures of the basal carbonaceous member can be seen in the Faro pit, at the northwest end of the Vangorda pit, on the road to Swim Lake, and on top of the Old Ski Hill.

Figure 10. *Marble interval in Mount Mye formation. Banding delineated by schist and calc-silicate bands and boudins in marble. Clipboard is 25.5 cm wide. Field station 87LP024.*

Figure 11. *Closeup view of marble interval in Mount Mye formation. Abundant siliceous bands and boudins in a marble matrix. Pencil is 14 cm long. Siliceous bands parallel dominant foliation. Foliation is locally cross-cut by later shear bands. Field station 98LP015, in immediate hanging wall of extensional Tie fault.*

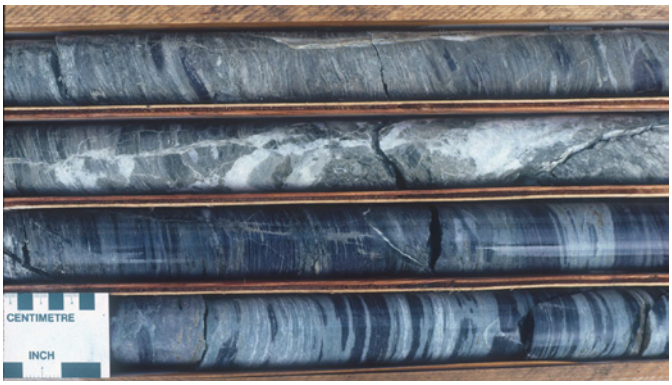

Figure 12. *Calc-silicate rock in Mount Mye formation. Drill hole 79F-01, 258 feet – 264 feet (78.6 m to 80.5 m). NQ-size core. Dark bands are biotite-rich pelite and light bands are calc-silicate rock.*

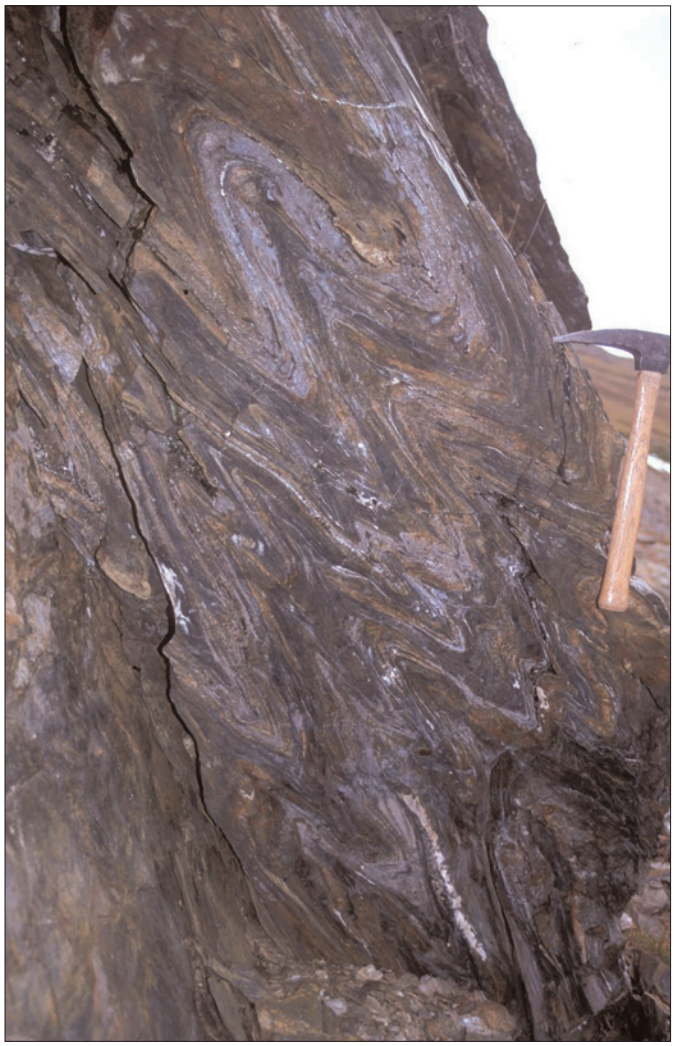

Figure 13. *Calc-silicate rock in Mount Mye formation. Thinly interbedded pale greenish calc-silicate rock and dark brown biotite schist. Outcrop strongly folded. Axial planar foliation is crenulation cleavage which forms dominant foliation in the outcrop. Field station 98LP142.*

Figure 14. *Vangorda formation phyllite. Light grey to white quartz-calcite siltstone interbeds in silvery grey, noncalcareous to slightly calcareous muscovite-chlorite phyllite. Coin is 2.7 cm wide.*

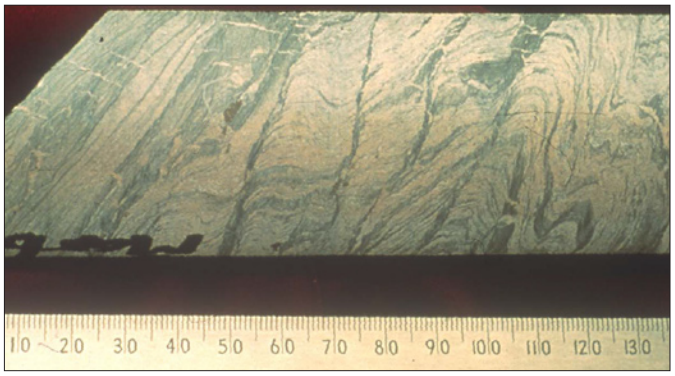

Figure 15. *Vangorda formation phyllite. NQ-size core. Pelitic bands are silvery grey. Siltstone interbands are pale cream and have a grainy texture. Dominant cleavage going across core is S_2 axial planar crenulation cleavage. Note microfolds between S_2 cleavages. Smallest division on scale is 1 mm.*

Figure 16. *Vangorda formation phyllite. Thin limestone interbeds in phyllite. Slaty cleavage is subhorizontal. Field station 99LP302. Solid division on scale is 1 cm.*

Figure 17. *Vangorda formation. Calc-silicate rock outcrop in southwest wall of Faro deposit open pit. Pale green calc-silicate rock bands and lenses, interbedded with dark purplish brown to grey biotite-rich bands and lenses. Pencil on right side of photo is 14.5 cm long.*

Thickness estimates for the Vangorda formation from cross-sections range from 700 to 2200 m. Jennings and Jilson (1986) suggested an average thickness of 1000 m, but acknowledged problems because of structural complications.

At lower metamorphic grades, the Vangorda formation is characterized by medium grey phyllite, very thinly interlayered with light grey calcite±quartz siltstone (Figs. 14 and 15) or marble bands (Fig. 16). Phyllitic bands are up to 1 cm thick, and siltstone and marble bands are up to 15 cm thick. Phyllites are thinly laminated on a 1- to 2-mm scale, with laminae being marked by dark grey striping within a light grey matrix. Siltstone interbands are commonly parallel-laminated with grading occurring rarely. This thin interbanding of lithologies is intricately folded on a hand-sample scale, with an axial planar crenulation cleavage forming the dominant structural foliation surface. Outcrops commonly have a drusy, opaque white calcite surface coating. Colour variations for the phyllite range from pale green to very dark grey to black. The phyllite typically weathers recessively to silvery grey scree slopes of phyllite chips. Mineralogically, the phyllite consists dominantly of quartz-muscovite-chlorite-calcite with local replacement of calcite by dolomite. Scattered subhedral grains of pyrite or anhedral grains of pyrrhotite are common.

At higher metamorphic grades, this calcareous phyllite is transformed into a thinly and discontinuously banded, green, cream and purplish brown calc-silicate rock (Figs. 17 and 18). The typical mineral assemblage

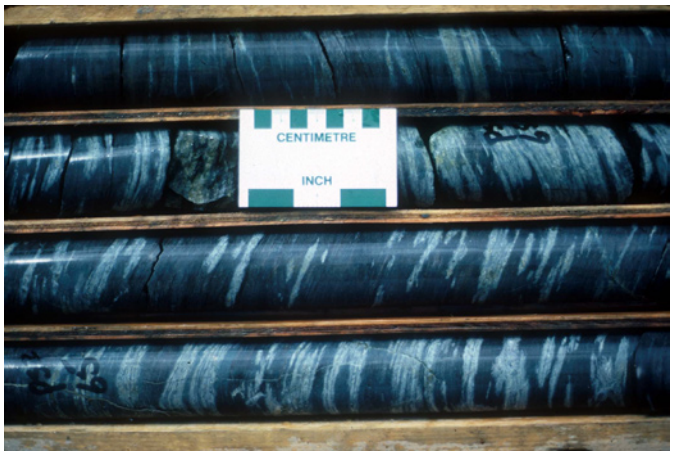

Figure 18. *Vanagorda formation. NQ-sized core. Calc-silicate rock from diamond drill hole 84F-09, 89 m-95 m.*

Figure 19. *Basal carbonaceous phyllite member of Vangorda formation. Outcrop located on the edge of the Swim Lake road, field station 98LP024. Fractures have orange-weathering surface coating.*

is quartz-tremolite-plagioclase-biotite±diopside±calcite ±epidote. The dark brown biotite schist intervals are the higher metamorphic-grade equivalents of the silvery grey phyllitic bands, and the pale cream and green-coloured calc-silicate rich bands are the higher metamorphic-grade equivalents of the calcareous quartz silty bands in the phyllite. Outcrops weather as blocky, resistant cliffs with a patchy, drusy, opaque white calcite coating. The dramatic difference in appearance and hardness of the calc-silicate rock and the calcareous phyllite resulted in the calc-silicate rock being initially mapped as an older, different stratigraphic unit than the calcareous phyllites. This misconception went on for at least 20 years after initial discovery of the massive sulphide deposits in the area.

Carbonaceous, dark grey to black phyllite and schist horizons occur throughout the Vangorda formation. Lateral and vertical dimensions of these carbonaceous horizons are poorly documented. Overall they constitute 10 to 15% of the formation. A homogeneous, variably siliceous, fine-grained, black phyllite to schist, with minor disseminated pyrite or pyrrhotite, occurs locally at the base of the Vangorda formation (Figs. 19 and 20). This carbonaceous unit was differentiated as a member of the Vangorda formation by Jennings and Jilson (1986) because of its close association with, and great thickness adjacent to, some of the massive sulphide ore deposits. It ranges up to 360 m thick and appears laterally equivalent to black, sulphide mineral-bearing, ribbon-banded, quartzite ore facies in the deposits (Jennings and Jilson, 1986).

North of Mount Mye (604 355 E, 6 920 865 N – Plate 12), a 50-m-thick horizon of dark grey- to tan-weathering, finely laminated, dolomitic siltstone occurs in the uppermost part of the formation. This particular unit

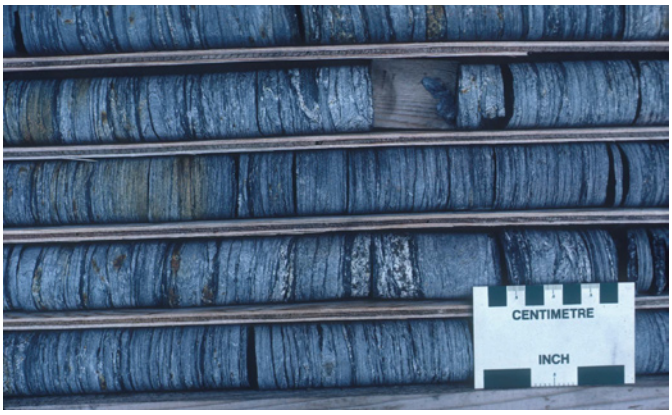

Figure 20. *Basal carbonaceous phyllite member of Vangorda formation. BQ-sized drill core from diamond drill hole CNR76-02, 304 m to 312 m. Disseminated pyrite cubes form rusty splotches in core.*

was not noted elsewhere. Thin interbedded marble units constitute a small part of the Vangorda formation. Marbles are white to medium grey, medium to coarsely crystalline, and commonly contain discontinuous bands and lenses of quartz and/or calc-silicate rock. Northwest of the Faro deposit, marble bands commonly have coarsely crystalline garnet, giving outcrops a skarned appearance. Marble interbands are typically a few metres to tens of metres thick.

The Vangorda formation also contains poorly foliated, fine- to medium-grained, dark green to olive green, chloritic phyllite (greenschist facies) or amphibolite (amphibolite facies) lens-shaped bodies ranging up to 100 m thick and locally extending along strike for up to several kilometres. These metabasites constitute about 15

to 20% of the formation (Jennings and Jilson, 1986) but are typically very conspicuous because they weather as resistant knobs and ridges. They are especially prevalent near the top of the formation. These bodies are interpreted as subvolcanic sill and dyke feeders to the basalts of the Menzie Creek formation, and they will be discussed further in the section on intrusive rocks.

Locally, adjacent to the metabasites, the dominant lithology of the Vangorda formation is a strikingly thinly laminated, green and white, commonly cherty and hard, generally calcareous phyllite (Fig. 21). In many cases these phyllites grade outward into green or greenish grey, texturally normal Vangorda formation phyllites. Mineralogically, these laminated phyllites are identical to normal Vangorda phyllites. In early mapping (Jennings et al., 1978b), they were interpreted as bedded tuffs, suggesting that the metabasites were extrusive flows. It is suggested herein that these laminated phyllites are actually contact metamorphosed Vangorda phyllites adjacent to an intrusive metabasite. The strikingly laminated nature of the phyllite is because primary textures and bedding are better preserved in the pressure shadow adjacent to the massive metabasite lenses.

The lower contact of the Vangorda formation with the underlying Mount Mye formation is conformable with interbedding of lithologies over a short stratigraphic interval. The upper contact with the Menzie Creek formation is also transitional with local interbedding of volcanic rocks and phyllites over a 10 to 30 metre interval. The fine-grained nature of the phyllites, and the thinly interbedded siltstones and marbles, suggest deposition in relatively deep water with a regular influx of carbonate and siltstone material by turbidity currents (Jennings and Jilson, 1986).

Figure 21. *Contact hornfelsed Vangorda formation phyllite adjacent to massive greenstone lens. Light bands are quartz-calcite siltstone and dark bands are greenish muscovite-quartz-chlorite phyllite. Field station 98LP026 on Swim Lake road.*

The Vangorda formation is a widespread unit in the Anvil District. It was mapped by Tempelman-Kluit as the upper member of unit 3. The portion of his unit 2 northwest of the Faro deposit corresponds to the calc-silicate rock metamorphic facies of the Vangorda formation. Gordey and Irwin (1987) mapped it as Rabbitkettle Formation (Gabrielse et al., 1973).

The Vangorda formation does not contain any fossils. A suggested maximum age limit of Early Cambrian is provided by the possible Cambrian age of the underlying Mount Mye Formation. The conformably overlying Menzie Creek formation contains Early to Middle Ordovician fossils and thereby restricts the Vangorda formation to a minimum age of Early Ordovician. Conodont collections from the Rabbitkettle Formation in the Nahanni map area (105I) have an age range of probable Late Cambrian to late Middle Ordovician (Gordey and Anderson, 1993), which is consistent with its correlation to the Vangorda formation. Basinal Cambrian-Ordovician carbonates are common in the northern Cordillera.

Menzie Creek formation

A thick, resistant, grey-weathering, basaltic volcanic unit, informally named the Menzie Creek formation (Jennings and Jilson, 1986), conformably overlies the Vangorda formation. Massive and pillowed, locally amygdaloidal flows are interbedded with volcaniclastic rocks which consist dominantly of monolithic basalt breccia with lesser conglomerate, sandstone and siltstone. These different lithologies vary dramatically in thickness laterally. Minor intercalated black phyllite, bedded black chert, calcareous phyllite, limestone and dolostone occur locally throughout the unit.

Menzie Creek formation outcrops both north and south of Mount Mye. The most accessible exposures are along the mine access road or the Blind Creek road. The best exposures are north of Mount Mye and are most easily accessed by helicopter. Two ridge traverses north of Mount Mye delineate the different Menzie Creek lithologies with readily visible primary textures. The first (from 605 300 E, 6 923 300 N to 603 600 E, 6 926 100 N – Plate 12) poorly exposes the lower contact with the Vangorda formation and does not expose the upper contact. The second (from 599 900 E, 6 929 000 N to 593 400 E, 6 927 900 N – Plate 9) provides excellent internal exposures but does not expose the upper and lower contacts of the formation.

Figure 22. *Menzie Creek formation. Pillow basalt flow. Field station 99LP258A.*

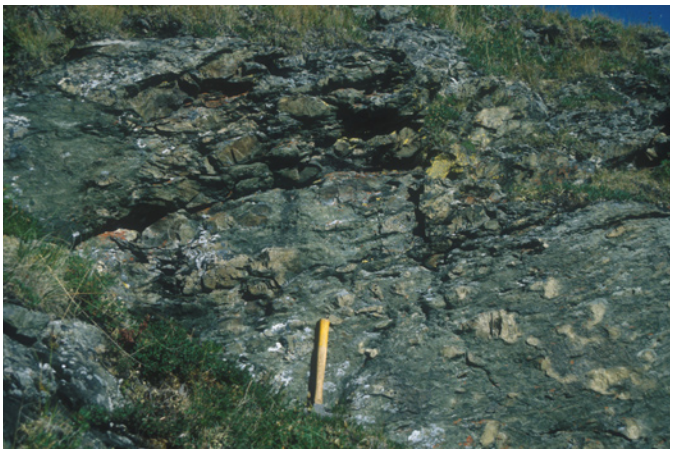

Figure 23. *Menzie Creek formation. Isolated pillows in chloritic matrix, pillow basalt flow. Field station 99LP209.*

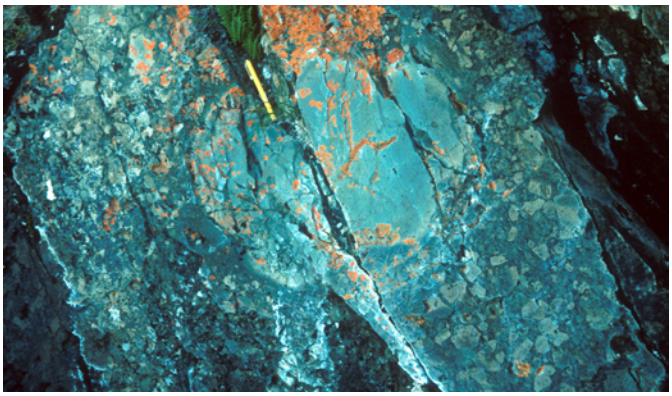

Figure 24. *Menzie Creek formation. Isolated pillow in monolithic basalt breccia. Pencil magnet is 12.5 cm long. Field station 99LP214.*

Both upper and lower contacts of the Menzie Creek formation are gradational over a short distance with interbedding of volcanic rocks with metasedimentary phyllites. Thickness of the formation varies considerably throughout the District. In the southeast corner near Swim Lake, an overall thickness of 140 m is estimated from cross sections. In contrast, north of Mount Mye an interpreted thickness of greater than 2800 m is possible.

South of the Anvil Batholith, the Menzie Creek formation consists of a medium green, pervasively foliated, noncalcareous to slightly calcareous chloritic phyllite (Pigage, 1999a). The phyllite commonly contains pale tan to white calcite amygdules up to 1 cm across. Dark green streaks are locally visible on the primary foliation surface. Deformation has obscured primary depositional textures such as pillows and breccia fragments and made them difficult to recognize.

North of the Anvil Batholith, primary depositional textures are well preserved in chloritic phyllites of the Menzie Creek formation. Massive and pillowed basalt flows form cliff outcrops consisting of black, dark brownish green, bluish green, or bluish olive-green, aphanitic to porphyritic basalt. Porphyritic varieties contain minor fine white feldspar and/or dark green mafic phenocrysts up to 5 mm across. The basalts display a porphyritic texture with microphenocrysts of plagioclase and clinopyroxene in a felted matrix of plagioclase microlites with secondary interstitial chlorite, titanite, opaque minerals and calcite. Many of the basalts are amygdaloidal, with vesicles up to 1 cm across infilled with white calcite, white quartz, dark green chlorite or white calcite rimmed by chlorite. Individual flows are not readily visible in outcrop. Pillow lavas contain varying proportions of pillows, ranging from flows consisting dominantly of pillows (Fig. 22), to those with isolated pillows in a dark green chloritic matrix (Fig. 23). Pillows range up to 1.5 m across, although diameters less than 0.5 m are more common. Pale green rinds up to 2 cm thick are locally visible on the pillow margins.

Monolithic basalt breccias consist of angular basalt fragments, typically up to 50 cm across within a dark green chloritic matrix. Some fragments display pillow-margin rinds. Locally, breccias contain a small proportion of nearly complete pillows among the clasts (Fig. 24). Breccias range from clast-supported (Fig. 25) to matrix-supported (Fig. 26), are generally nonstratified, and do not display primary bedding. In one locality, the breccias form an unstratified unit over 200 m thick. These textural characteristics are most similar to those of hyaloclastites (McPhie et al., 1993.)

Epiclastic volcanic conglomerates, sandstones and siltstones are locally interbedded with basalt flows

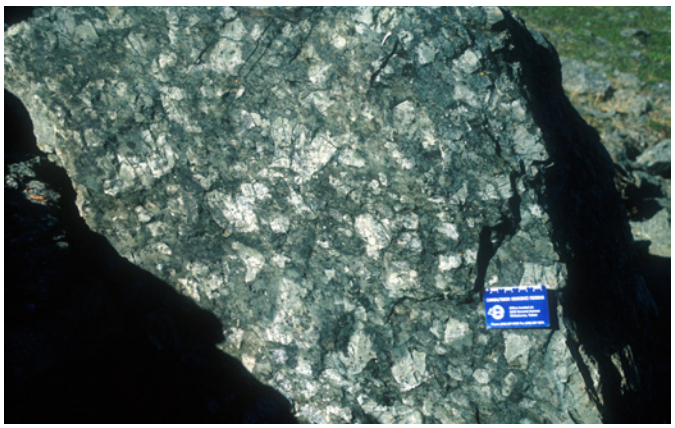

Figure 25. *Menzie Creek formation, clast supported, monolithic, basalt breccia. Field station 99LP220.*

Figure 26. *Menzie Creek formation, matrix supported, monolithic, basalt breccia. Field station 98LP181.*

and monolithic breccias in minor amounts (Fig. 27). These lithologies are generally only a few metres thick although rarely they range up to 20 m in thickness. Localized graded beds indicate that the volcanic section is stratigraphically upright. Coarse clasts are predominantly volcanic rock fragments. Rare dark grey to black silty phyllite, black bedded chert, pale grey limestone, and tan- to orange-weathering dolostone occur as 1- to 10-m-thick intervals at different stratigraphic levels within the volcanic sequence.

Locally, the basalts exhibit extensive quartz-carbonate alteration. With increasing alteration, the dark green rock becomes a rusty weathering, light tan, quartz-carbonate-muscovite rock which locally contains minor amounts of a bright green layer silicate resembling fuchsite. Modene (1982) identified this mineral as most probably being a Ni-bearing serpentine. These heavily carbonate-altered rocks resemble quartz-carbonate altered mafic and ultramafic igneous rocks described worldwide.

The geochemistry of basalt and basalt breccia samples from the Menzie Creek formation are given in Table I-1 (see Appendix I). Figures 28 and 29 are discriminant and multi-element diagrams for the samples. Most samples plot in the alkaline basalt field on the Zr/TiO_2 – Nb/Y discriminant diagram (Fig. 28a, Winchester and Floyd, 1977; as modified by Pearce, 1996). In the tectonic discriminant diagrams shown in Figure 29, the samples indicate a within-plate tectonic setting (Pearce, 1996). Figures 28c and d are multi-element diagrams normalized to primitive mantle and normal mid-oceanic ridge basalt (NMORB) using immobile elements suggested by Jenner (1996). Multi-element normalized patterns for oceanic island (OIB), enriched mid-oceanic ridge (EMORB) and normal mid-oceanic ridge (NMORB) basalt compositions are shown in Figures 28e and f for comparison (Sun and

Figure 27. *Menzie Creek formation. Epiclastic volcanic sandstone. Field station 99LP218.*

McDonough, 1989). Incompatible elements and light rare earth elements (REE) are strongly enriched in the multi-element pattern and most closely resemble the OIB pattern

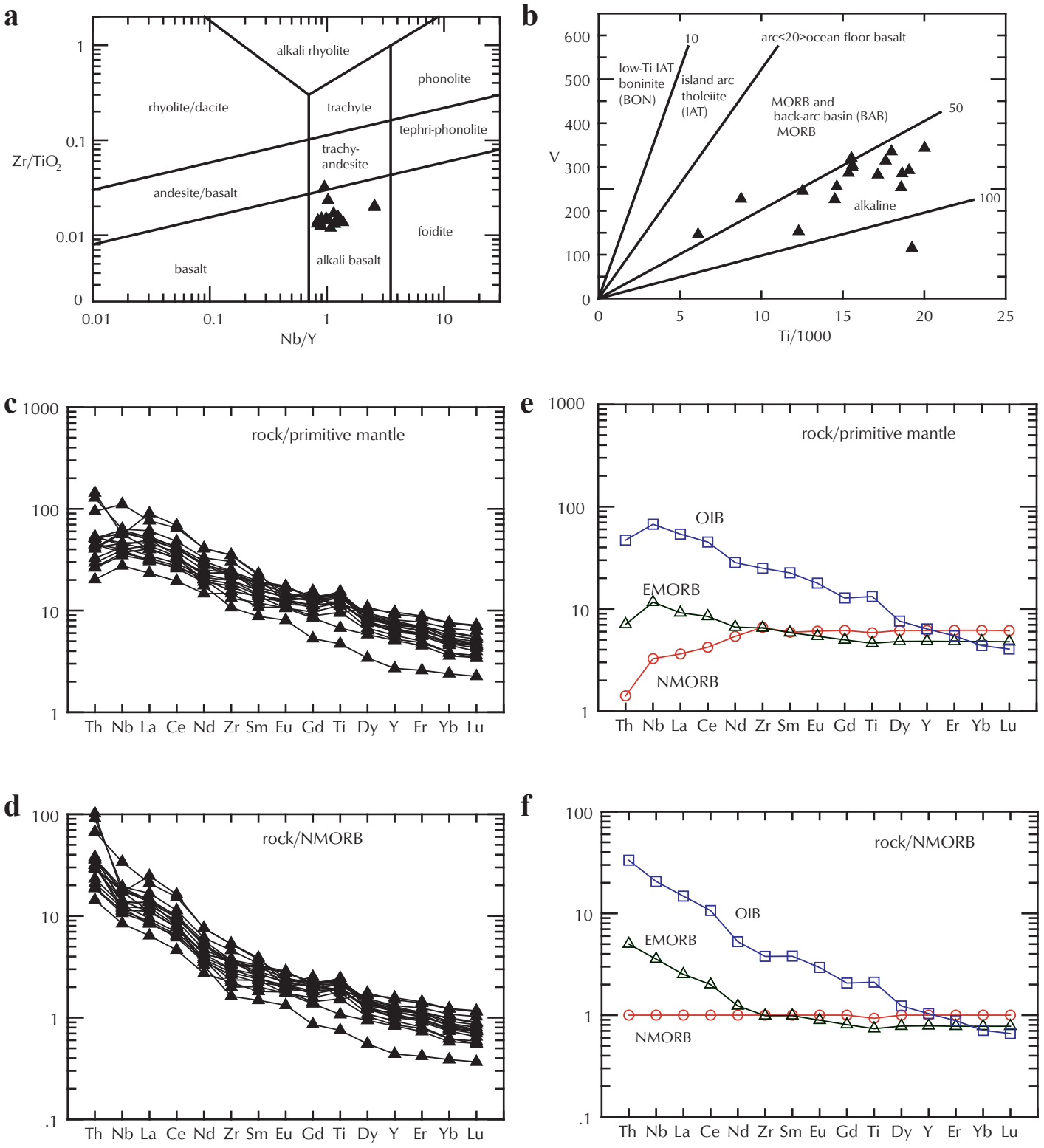

Figure 28. *Discriminant and multi-element diagrams for extrusive rocks of the Menzie Creek formation.* ***(a)*** *Zr/TiO_2-Nb/Y diagram of Winchester and Floyd (1977) as modified by Pearce (1996);* ***(b)*** *Ti-V diagram of Shervais (1982);* ***(c)*** *primitive mantle normalized multi-element diagram;* ***(d)*** *NMORB normalized multi-element diagram;* ***(e)*** *primitive mantle normalized multi-element diagram for oceanic island basalt (OIB), enriched mid-occeanic ridge basalt (EMORB), and normal mid-oceanic ridge basalt (NMORB);* ***(f)*** *NMORB normalized multi-element diagram for OIB, EMORB and NMORB.* ***(c-f)*** *Primitive mantle and NMORB values from Sun and McDonough (1989).*

in form and element ratios. This enrichment pattern is again similar to that of alkaline, within-plate basalt.

Primary depositional textures within the flow units indicate submarine volcanism. Epiclastic volcanic

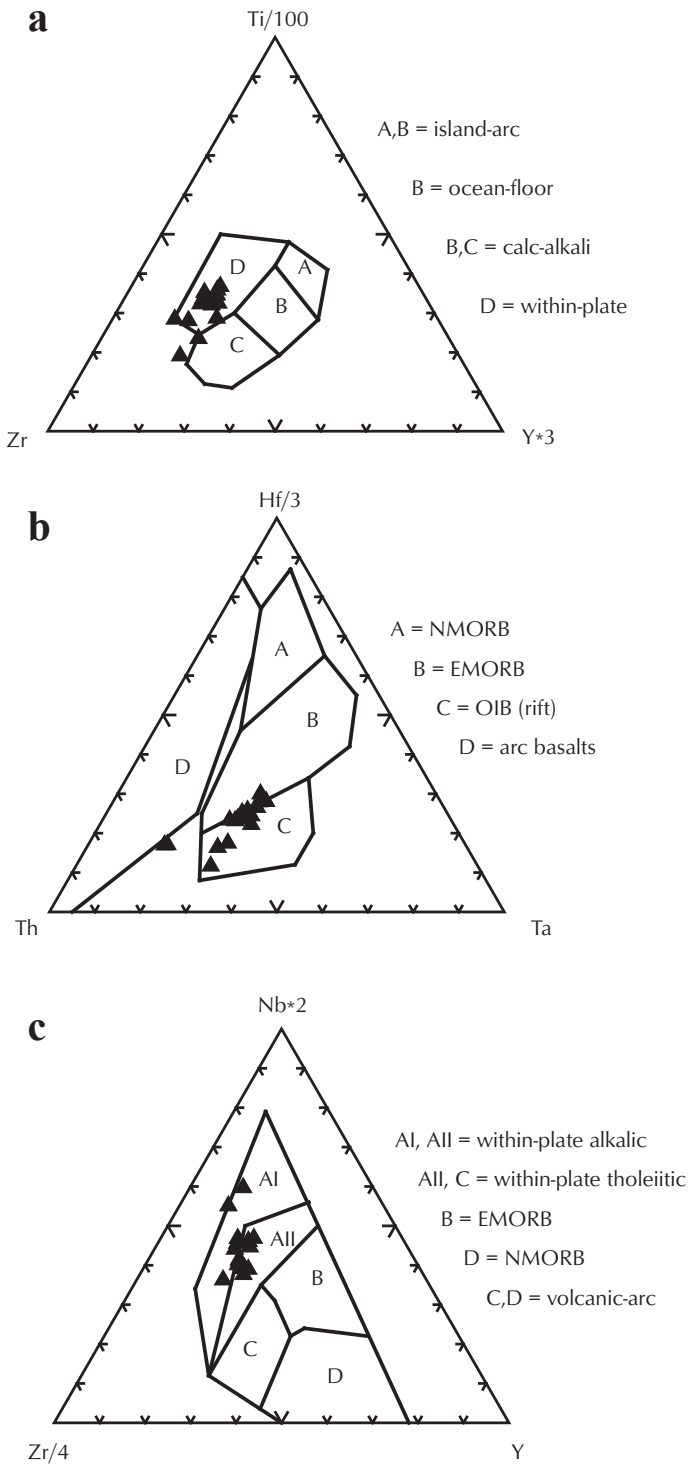

Figure 29. *Tectonic discriminant diagrams for extrusive basalts of the Menzie Creek formation.* ***(a)*** *Zr-Ti-Y diagram of Pearce and Cann (1973);* ***(b)*** *Th-Hf-Ta diagram of Wood (1980);* ***(c)*** *Zr-Nb-Y diagram of Meschede (1986).*

sedimentary rocks and intercalated shales, limestones and dolostones also suggest a subaqueous depositional environment. Jennings and Jilson (1986) suggested that limestone and dolostone lithologies in the upper part of the formation might be interpreted as indicating shoaling of the volcanic sequence with time. Menzie Creek formation represents a thick volcanic succession within the Anvil District area. The unit thins rapidly in all directions. Pigage (2000a) suggested that the northeast margin of the map area represented a possible edge to volcanic deposition with a probable syndepositional growth fault providing a conduit for volcanism. Basalt flows form the dominant Menzie Creek formation lithology closest to the proposed trace of the growth fault. Increasing amounts of basaltic breccias occur within the formation toward the northwest away from the eastern edge of the map area.

The Menzie Creek formation is the oldest unit in Anvil District with fossil age control. All fossil localities in the Menzie Creek formation occur northeast of the Anvil Batholith. Table 1 lists fossil localities from within the Menzie Creek formation. Conodonts and graptolites from the lower to middle portion of the Menzie Creek formation result in an overlapping age of Early Ordovician. Graptolite fossil ages from the mainly overlying Duo Lake Formation are Middle Ordovician.

North of Mount Mye, a 300-m-thick horizon of black silty phyllites of the Duo Lake Formation is underlain and overlain by basalts of the Menzie Creek formation. Gordey (1983, 1990a,b,c) interpreted the upper Menzie Creek formation as being thrust over the black phyllites along the Faro fault. More recently Pigage (2000a) suggested that this succession is conformable, and the Menzie Creek formation is intercalated with, and partly laterally equivalent to, the Duo Lake Formation. This tongue of Duo Lake Formation contains graptolites with a Middle Ordovician age. If the Menzie Creek formation is structurally emplaced on top of this unit, then a minimum age of Middle Ordovician is established for the volcanic rocks. If the units are interstratified, then the minimum age of the volcanic rocks is younger than Middle Ordovician. The total age range from fossil control is Early to Middle Ordovician. The age of the upper part of the Menzie Creek formation is not constrained by fossils. The overlying and interbedded Duo Lake Formation contains fossils ranging up to Middle Devonian in age. In the northeast part of the District, the Duo Lake Formation is conformably overlain by the Silurian Steel Formation. Given these poor constraints, it seems reasonable to infer a possible minimum age of Silurian for the Menzie Creek formation.

Table 1. *Fossil localities, Menzie Creek formation.*

Locality no.	UTM E*	UTM N*	Material	Age range	Reference
C-102596	599 193	6 929 979	conodont	Ordovician, Tremadoc	Orchard (1992a)
C-304783	597 428	6 924 392	conodont	Indeterminate-barren	Orchard (2000)
C-304790	601 177	6 926 701	conodont	Indeterminate-barren	Orchard (2000)
C-304791	597 809	6 928 877	conodont	Early Ordovician	Orchard (2000)
C-304792	597 809	6 928 877	conodont	Ordovician	Orchard (2000)
C-049977	602 331	6 925 883	graptolite	Early Ordovician	Norford (1977)

*NAD83 UTM coordinates, zone 8

Tempelman-Kluit (1972) correlated Menzie Creek formation with his Anvil Range Group (unit 8b) and considered it to be Permian in age. This necessitated a major unconformity beneath the unit 8b volcanic rocks because of the extensive age range of stratigraphic units immediately underlying unit 8b. Gordey (1983) recognized two volcanic suites within Tempelman-Kluit's unit 8b and differentiated Cambro-Ordovician (Menzie Creek) volcanic rocks as distinct from the Permian Anvil Range Group. Early Paleozoic mafic volcanism has been recognized in several localities along the strike length of the northern Canadian Cordilleran miogeocline (Goodfellow et al., 1995). Chemically, the Menzie Creek formation is most similar to the Group IV basalts as described by Goodfellow et al. (1995).

Road River Group

Early Paleozoic argillaceous limestones and carbonaceous phyllites that comprise the Road River Formation were first described in northern Yukon (Jackson and Lenz, 1962). The Road River Formation in that area consists of two members, a lower limestone unit and an upper shale and chert unit. In southeastern Yukon and southwestern Northwest Territories, Gabrielse et al. (1973) restricted the Road River Formation to include only the upper recessive carbonaceous shale portion of the original formation; the lower limestone unit was separated out and assigned to the Rabbitkettle Formation. Fossil control indicated an age range for the revised Road River lithologies from Caradocian (late Middle to early Late Ordovician) to Early Devonian. More recently, Gordey and Anderson (1993), using the same stratigraphic restriction as Gabrielse et al. (1973), elevated the Road River Formation to group status with two members, the lower Duo Lake Formation (Cecile, 1982) and the overlying Steel Formation. This report follows the definitions proposed by Gordey and Anderson (1993) but extends the upper range of the Duo Lake Formation in the Anvil District area. More extensive discussion concerning the current status and usage of Road River may be found in Morrow (1999).

The northeast and southwest margins of the Anvil map area are underlain by dark grey to black, noncalcareous phyllite, tan-weathering, bioturbated, dolomitic siltstone, minor massive to argillaceous limestone, and minor massive quartz sandstone and dolostone. Regionally these lithologies are correlated with the Road River Group (Gordey and Anderson, 1993). The Road River Group can be divided into two formations, the lower Duo Lake Formation (Cecile, 1982) and the upper Steel Formation (Gordey and Anderson, 1993). Descriptions of these two units are presented in Pigage (2000a) and below.

Duo Lake Formation

In northern Anvil District, the Duo Lake Formation appears in recessive stream cuts and scree slopes as dark grey to black, noncalcareous, silty shale with a slightly irregular slaty cleavage. Although a good reference section has not been identified, a series of scattered outcrops and scree slopes (Plate 12) extend from 603 600 E, 6 925 000 N (lower contact) to 604 500 E, 6 928 000 N (upper contact). Pieces of float in scree slopes commonly display a strong pencil rodding resulting from the intersection of bedding with the slaty cleavage. Typically the shale weathers pale grey to white with faint bluish, reddish, or pinkish hues. Thin interbeds of dark grey, tan-weathering, sandstone, siltstone, or silty dolostone are up to 5 cm thick. Minor disseminated pyrite commonly weathers as small yellow holes in exposed outcrops. In one outcrop, a 0.5-m-thick black, fine-grained limestone occurs as an interbed within the shale.

Recessive, black, carbonaceous, silty argillites with subordinate siltstones, sandstones and limestones form a continuous unit overlying the Menzie Creek formation northeast of the Tintina Trench on the southwest side of Anvil Batholith. Although it is generally poorly exposed,

Figure 30. *Altered and hornfelsed Duo Lake Formation carbonaceous phyllite. Field station 99LP280.*

Figure 31. *Carbonaceous shale of Duo Lake Formation conformably overlain by pillow basalt of Menzie Creek formation. Primary bedding dips gently to the left. Slaty cleavage dips about 45 degrees to the left. Field station 99LP238.*

the Duo Lake Formation has significant continuity along strike and is readily delineated by the recent airborne EM survey over parts of the District (Woolham, 1996). The best exposures occur as a 300-m interval (Plate 11) of stream cuts in a tributary stream draining into Blind Creek (599 800 E, 6 898 200 N). Subcrops also occur along the Swim Lake road as the road curves northward into the Swim Lake area. The argillites are indistinctly bedded on a scale of 15 to 30 cm (Fig. 30). Locally weathered surfaces have a slight bluish grey tinge; more typically, the argillite weathers with a patchy deep orange-brown surface coating. Interbeds of medium grey, tan-weathering, noncalcareous siltstone to fine sandstone are centimetres to tens of metres thick. Locally, the siltstones contain a fine millimetre-scale pinstriping between light and dark grey.

The lower contact of the Duo Lake Formation with Menzie Creek formation appears conformable with interbedding of carbonaceous argillites and basalt flows (Fig. 31). The Menzie Creek formation is absent in the southeast corner of the map area (near the Orchay Batholith), and in that area the Duo Lake Formation conformably lies on Vangorda formation. At the Ace High Creek locality northeast of Mount Mye, the Duo Lake Formation is inferred to overlie either the Menzie Creek formation (northwest exposures) or the platy siltstone unit Ssp (southeast exposures). The contact with Menzie Creek formation consists of interbedded carbonaceous silty shale and Menzie Creek basalt over a 7-m thickness. The contact with the underlying platy siltstone unit is not exposed.

Immediately northeast of Tintina Trench, the upper contact is the Inconnu thrust fault. Northeast of Mount Mye, the Duo Lake Formation is conformably overlain by the Silurian Steel Formation. The Steel Formation is absent in other parts of the District, and the upper contact of the Duo Lake Formation has been removed by erosion. Interpreted thickness of the unit ranges from approximately 100 m to at least 700 m. Pigage (1999a) estimated a thickness of 440 m near Rose Mountain. A tongue of Duo Lake Formation shales that extends westward between Menzie Creek formation volcanic rocks (see discussion above) is approximately 300 m thick. Previously, Gordey and Irwin (1987) interpreted this sequence as being faulted with Menzie Creek volcanic rocks being thrust over Duo Lake Formation along the Faro thrust. More recently, Pigage (2000a) suggested the entire sequence is conformable, with Menzie Creek volcanics being intercalated with Duo Lake Formation.

The dark shales are intercalated with lesser amounts of coarsely recrystallized, dark grey to grey to white, massive and argillaceous limestone, black bedded chert and medium grey, noncalcareous, finely laminated siltstone (Pigage, 2000a). These different lithologies are locally up to 50 m thick. Two massive quartz sandstone and dolostone units are described in more detail below (see section on Quartz sandstone and dolostone).

Along the east margin of the Anvil map area, shales of the Duo Lake Formation are strongly hornfelsed, with development of extensive disseminated pyrrhotite, a conchoidal fracture, and an irregular bleaching of the original dark grey shales (Fig. 32). Petrography of the bleached shales indicates extensive development of calc-silicate (epidote?) minerals, carbonate and quartz as irregular pods and fracture-controlled veinlets. Locally, the bleached phyllites have a faint purplish colour, possibly related to growth of fine-grained hornfels biotite.

Table 2 lists fossil localities within the Duo Lake Formation in the Anvil District. Fossil ages in the north part of the District range from Arenigian (late Early Ordovician) to Llandovery (early Early Silurian; Tempelman-Kluit, 1972; Gordey, 1983). Samples O-080030 and O-080031 were collected from approximately the same stratigraphic horizon; therefore the more restricted range of Arenigian (late Early Ordovician) to Caradoc (Middle Ordovician) is more appropriate for the age range of these fossil occurrences. In several localities southwest of Anvil Batholith, interbedded limestones contain one-hole and two-hole crinoids. Tempelman-Kluit (1972) assigned a Middle Devonian age to the fossiliferous limestones on the basis of the two-hole crinoids. A recent conodont collection from one of the limestones confirms this age assignment

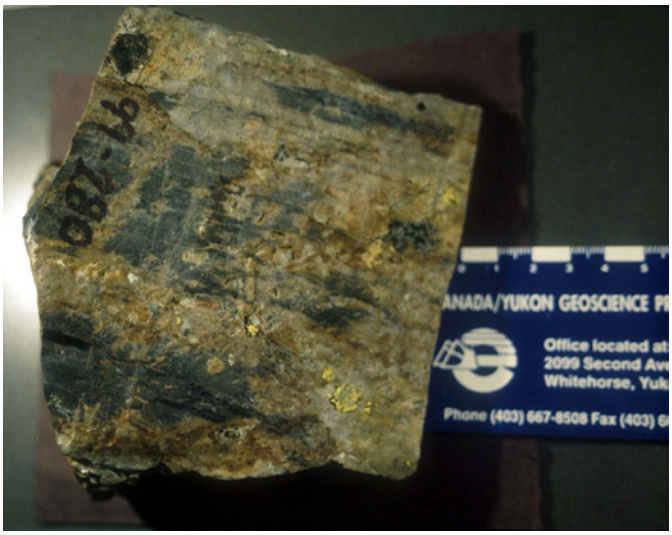

Figure 32. *Black argillite of Duo Lake Formation. Field station 98LP099.*

(Orchard, 2001). In the Ace High Creek area, the Duo Lake Formation also locally overlies the platy siltstone unit Ssp which has an inferred Silurian age. These stratigraphic relations indicate the lower contact of the Duo Lake Formation is diachronous and ranges in age from Middle Ordovician into Silurian. In the extreme northeast part of the mapped area, the Duo Lake Formation is overlain by the Steel Formation, indicating an upper age of Silurian. Elsewhere, the uppermost age for the formation cannot be determined because an upper stratigraphic contact does not occur in the Anvil District. However, Middle Devonian fossils in the formation indicate an upper age limit of at least Eifelian. The inferred age range for the Duo Lake Formation is therefore Middle Ordovician to Middle Devonian.

Table 2. *Fossil localities for Duo Lake Formation.*

Locality no.	UTM E*	UTM N*	Material	Age range	Reference
O-080030	603 249	6 925 328	brachiopod	Ordovician, Llanvirnian to Caradoc	Tempelman-Kluit (1972)
O-080031	600 628	6 924 958	graptolite	Ordovician, Llanvirnian to Silurian, Llandovery	Tempelman-Kluit (1972)
C-107902	597 505	6 924 588	graptolite	Ordovician, Arenigian to basal Llanvirnian	Norford (1982)
80033	607 476	6 918 254	conodont	Late Middle Devonian	Templeman-Kluit (1972)
66L3	601 857	6 897 304	2-hole crinoid	Early Devonian, Emsian to Middle Devonian, Eifelian	Templeman-Kluit (1972)
98LP231	602 111	6 896 349	2-hole crinoid	Early Devonian, Emsian to Middle Devonian, Eifelian	this report
C-304793	604 405	6 919 435	conodont	Indeterminate-barren	Orchard (2000)
C-305665	580 995	6 909 886	conodont	Middle Devonian	Orchard (2001)

* NAD83 UTM coordinates, zone 8

In its type area, the Duo Lake Formation has an age range from earliest Early Ordovician to late Early Silurian (Cecile, 1982), and both upper and lower contacts are diachronous. In the Nahanni area, the Duo Lake Formation ranges from Arenigian (Early Ordovician) to mid-Wenlockian (early Late Silurian) in age (Gordey and Anderson, 1993). In the Anvil District, the upper age range of the formation is extended from Silurian upward to Middle Devonian.

Duo Lake Formation shales were deposited in a quiet, euxinic marine basin starved from clastic input (Gordey and Anderson, 1993). Water depth was below wave base, but is otherwise unconstrained.

Duo Lake Formation correlates with unit 4 of Tempelman-Kluit (1972). Gordey and Irwin (1987) and Gordey (1990a) mapped a regionally extensive Cambro-Ordovician unit (COt), consisting dominantly of resistant dark and light siltstone and chert, extending east from the map area. The hornfelsed sedimentary rocks of the Duo Lake Formation correspond to this previously mapped unit. The COt unit, as mapped, probably demarcates the extent of hornfelsing of the Duo Lake Formation northwest of the Orchay pluton (Pigage, 2000a). Because of its poor exposure southwest of Anvil Batholith, the Duo Lake Formation was not differentiated in this area by Tempelman-Kluit (1972). In different areas, it corresponds to parts of his units 5, 6, or 7. Similarly, Gordey and Irwin (1987) and Gordey (1990a, b) generally considered it to be part of the Rabbitkettle Formation in the same area. It corresponds to unit 2 of Pigage (1999a) in the Rose Mountain area.

Steel Formation

In the extreme northeast part of the map area, the Duo Lake Formation is conformably overlain by massive, tan-weathering, pale grey, slightly dolomitic, bioturbated siltstones of the Steel Formation (604 500 E, 6 928 000 N – Plate 12). In the area mapped, the siltstone occurrence consists of rubble of large angular blocks on a broad plateau. The lower contact of the Steel Formation was not observed. The upper contact of the unit occurs to the east and northeast of the map area. Mapping by Gordey (1990b) indicates the Steel Formation in this immediate area is less than 30 m thick.

Absence of depositional current structures in the Steel Formation type area indicates deposition of this unit in a relatively quiet-water, off-shelf setting (Gordey and Anderson, 1993). Bioturbation reflects a change to oxygenated bottom waters from the prevailing euxinic conditions existing during the time of Duo Lake deposition.

The age of the Steel Formation in the type area is poorly constrained to be of definite Ludlovian (early Late Silurian) age, but may range from late Wenlockian (late Early Silurian) to earliest Devonian (Gordey and Anderson, 1993). In the Anvil District, the unit is younger than the immediately underlying Duo Lake Formation which contains middle Ordovician fossils. In other areas of the District, however, the Duo Lake Formation contains Middle Devonian fossils, suggesting that the Steel Formation has an aerially restricted extent and is laterally equivalent to the upper part of the Duo Lake Formation.

Platy siltstone

Northeast of Mount Mye (609 650 E, 6 916 150 N – Plate 13), Jennings and Jilson (1986) described a series of outcrops with an estimated thickness of approximately 100 m, as consisting of dark grey, tan-weathering, laminarly bedded, dolomitic siltstone. Gordey and Irwin (1987) and Gordey (1990c) also differentiated these outcrops as a separate unit, consisting of a dolomitic, platy siltstone. Upper and lower contacts of this unit were not observed. Map patterns suggest this unit overlies the Menzie Creek formation. It may occur entirely within the Duo Lake Formation.

The age range of the platy siltstone unit is poorly constrained. It is overlain by a carbonaceous argillite containing a dolostone with late Middle Devonian conodonts (Tempelman-Kluit, 1972). The presumed underlying Menzie Creek and possibly Duo Lake formations have a suggested upper age of Ordovician to Silurian (see above). Therefore this unit has an inferred age range of Silurian to late Middle Devonian. Gordey (1990c) considered the unit to be broadly Silurian and Devonian. Jennings and Jilson (1986) correlated this unit with the late Early Silurian to Middle Devonian Askin Group (Campbell, 1967) that outcrops 130 km southeast of the Anvil District (Blusson, 1966).

Quartz sandstone and dolostone

Scattered resistant outcrops north and northeast of Mount Mye consist of medium to dark grey, medium-grained, massive, noncalcareous quartz sandstone with lesser discontinuous interbeds up to 10 m thick of tan-weathering, massive dolostone. Locally, the sandstone also contains limestone concretions up to 25 cm in diameter. Interbeds of black, pale grey to bluish grey to pinkish white weathering, silty shale also occur within the

sandstone intervals. Late cross-cutting white quartz veins up to 30 cm thick are abundant.

Sandstone grains consist dominantly of monocrystal–line quartz and have a high sphericity. Minor fine opaque dust outlines individual quartz grains. Approximately 10 to 20% of the clasts are about 0.5 mm in diameter; these are enclosed in a matrix of smaller grains. Very minor tourmaline was noted in one thin section. The sandstone is clast supported, and cement is not readily visible.

This unit occurs in two major areas north and northeast of Mount Mye. In both instances, it is enclosed by dark grey to black silty shales. Fossil control for each occurrence indicates that the sandstone-dolostone unit occurs as separate horizons at different stratigraphic levels. Near 600 600 E, 6 924 700 N (Plate 9) the quartz sandstone is 5 to 15 m thick, and occurs within carbonaceous silty shales of the Duo Lake Formation. Fossil graptolites collected from the Duo Lake Formation immediately above the quartz sandstone horizon restrict the age of the sandstone to be slightly older than Middle to Late Ordovician (Llanvirnian to Caradoc; fossil localities F_1 and F_2 of Tempelman-Kluit, 1972). The other occurrence of this unit (607 500 E, 6 918 300N – Plate 12) consists of 10 to 20 m of quartz sandstone overlain by approximately 30 m of massive dolostone (Jennings and Jilson, 1986). Conodonts collected from this upper dolostone have a probable late Middle Devonian age (fossil locality F_3 of Tempelman-Kluit, 1972).

In both occurrences upper and lower contacts of the unit are conformable with the enclosing shales. This unit correlates with units 5 (quartz sandstone) and 6 (dolostone) of Tempelman-Kluit (1972) and unit Dc of Gordey and Irwin (1987).

Earn Group

The northernmost extent of this map compilation contains poorly exposed outcrop and rubble of black, carbonaceous phyllite and chert with lesser massive grey to black quartzite and chert-pebble conglomerate. Two poorly preserved fossil collections from a location just north of the area included in this report and map contain brachiopods with a tentative age determination of Early Carboniferous (Osagian or early Meramecian; Tempelman-Kluit, 1972).

These lithologies and ages are consistent with the above strata being correlative with the Earn Group (Campbell, 1967; Gordey et al., 1982). It is equivalent to unit 7 of Tempelman-Kluit (1972). Regionally in Yukon, the age of the base of the Earn Group is diachronous with ages locally as old as Early Devonian. Earn Group is unconformably overlain by Visean (mid-Mississippian) quartz sandstone of the Tay Formation. Earn Group deposition marks a dramatic change in sedimentation pattern as shale deposition transgressed far to the east of earlier limits of Selwyn Basin, and coarse clastic interbeds within shale and chert delineated accumulation in a number of submarine fan complexes within the Basin (Gordey et al., 1982).

In the Anvil District, the Earn Group is structurally overlain by Menzie Creek formation along a southerly dipping thrust fault at the northern extent of this compilation. Gordey and Irwin (1987) have mapped the regional Twopete thrust fault both to the northwest and southeast, which also places Cambrian-Ordovician sedimentary rocks on top of Mississippian to Permian sedimentary units. The fault indicated in Geoscience Map 2004-7 (Plate 7) has therefore been tentatively identified as the Twopete thrust.

YUKON-TANANA TERRANE STRATIGRAPHY

Greater than 3000 m of Paleozoic micaceous quartzite and phyllite of inferred Paleozoic age constituting Yukon-Tanana Terrane underlie the southwest part of the map area. These rocks are unconformably overlain by up to 600 m of coarse- to fine-grained clastic sedimentary rocks of Triassic age. The Yukon-Tanana and Triassic assemblages are peripheral to the main Anvil District and are therefore not extensively discussed in this report.

Micaceous quartzite

Medium to dark grey micaceous quartzite forms cliff outcrops along Vangorda Creek just north of the town of Faro (near 586 000 E, 6 901 000N – Plate 8). These outcrops represent some of the most accessible exposures of the micaceous quartzite unit of the Yukon-Tanana Terrane. Additional exposures occur as rounded elongate outcrop ridges within the town of Faro. The dominant rock type consists of a medium to very dark grey, quartzose schist to micaceous quartzite. The schist contains a pervasive foliation disrupted and contorted by a less pervasively developed cross-cutting, spaced crenulation cleavage. The quartzose schist commonly weathers silvery grey, although more carbonaceous phyllites weather to a dull sooty black. The micaceous schist contains interbeds of medium to light grey, massive quartzite and coarse-grained, medium grey, micaceous psammite. Psammite intervals typically contain clasts of bluish quartz and black

quartz. One massive quartzite bed is greater than 15 m thick.

Quartzose phyllite also contains about 30% interbands of medium to pale green, foliated, chloritic phyllite. Thinner bands are 1 to 3 m thick, and thicker bands are locally greater than 100 m thick. Thicker intervals have relict igneous equigranular texture. Chloritic phyllites commonly contain fine acicular actinolite. Locally the greenstones are extensively altered to a pale tan weathering, fine-grained quartz-carbonate-muscovite-fuchsite(?) assemblage. Equigranular textures for thicker intervals suggest that at least some of the greenstones are intrusive dykes or sills rather than extrusive flows.

Tempelman-Kluit (1970a,b) first reported the presence of eclogite lenses within the micaceous quartzites in close proximity to the Vangorda fault. Eclogites from northwest of Faro (580 300 E, 6 907 850 N – Plate 8) and northwest of Ross River (616 900 E, 6 884 350 N – Plate 14) have been studied extensively (Erdmer and Helmstaedt, 1983; Erdmer, 1987; Erdmer and Armstrong, 1988; Erdmer et al., 1998; Perchuk et al., 1999; Philippot et al., 2001). Additional eclogite localities occur along strike between these two locations. Primary eclogite metamorphic assemblages consist of garnet-omphacite-quartz-rutile. Retrograde minerals locally include clinozoisite, paragonite, phengite and amphibole. Enclosing metasedimentary rocks contain quartz-muscovite-

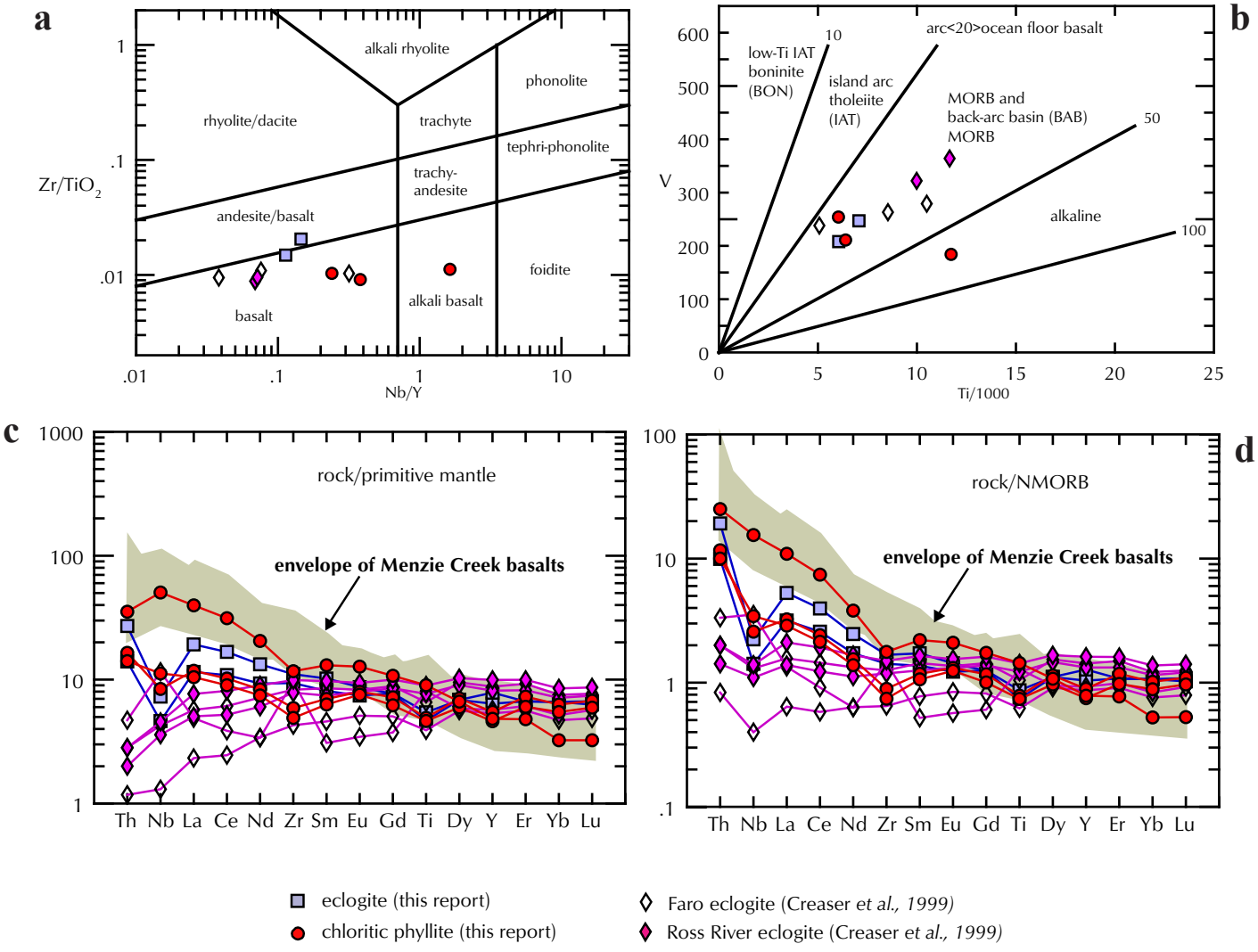

Figure 33. *Discriminant and multi-element diagrams for eclogites and greenstones in Yukon-Tanana Terrane, Anvil District.* ***(a)*** *Zr/Ti-Nb/Y diagram of Winchester and Floyd (1977) as modified by Pearce (1996);* ***(b)*** *Ti-V diagram of Shervais (1982);* ***(c)*** *Primitive mantle normalized multi-element diagram (primitive mantle values from Sun and McDonough, 1989);* ***(d)*** *NMORB normalized multi-element diagram (NMORB values from Sun and McDonough, 1989).*

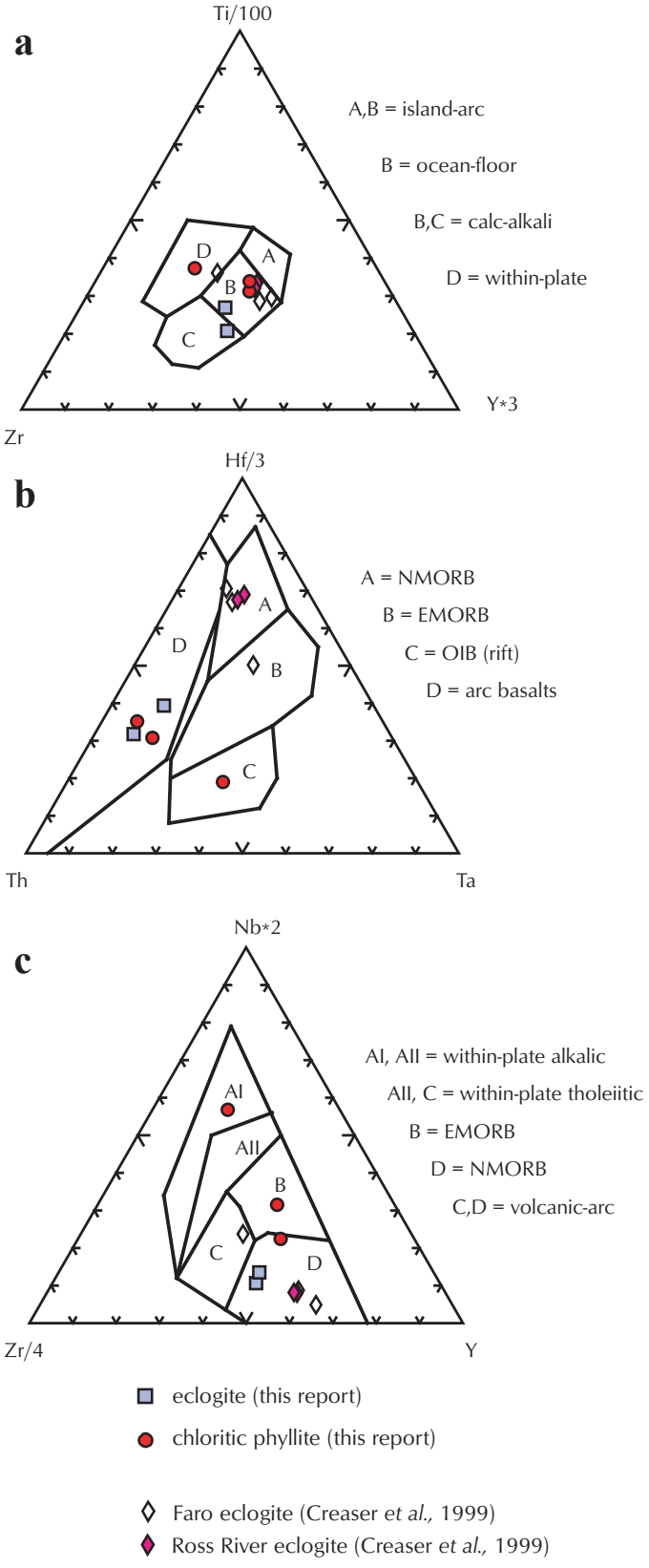

Figure 34. *Tectonic discriminant diagrams for eclogites and greenstones within the Yukon-Tanana Terrane.* ***(a)*** *Zr-Ti-Y diagram of Pearce and Cann (1973);* ***(b)*** *Th-Hf-Ta diagram of Wood (1980);* ***(c)*** *Zr-Nb-Y diagram of Meschede (1986).*

glaucophane±garnet and have undergone the same high-pressure/low-temperature metamorphism as the eclogites. Petrography, chemistry, and association with blueschists all indicate the eclogites are type C of Coleman et al. (1965).

Table I-3 (see Appendix I) contains geochemical analyses for two samples from the chloritic phyllites, one sample from the Faro eclogite locality, and one sample from another eclogite occurrence just northeast of the town of Faro. Figures 33 and 34 summarize the geochemical characteristics of these analyses using discriminant diagrams and multi-element normalized diagrams. Included on the same figures are analyses for Faro and Ross River eclogites published by Creaser et al. (1999). Based on their analyses, Creaser et al. (1999) suggested the eclogites show either within-plate or mid-ocean ridge protolith chemistry. Discriminant plots for eclogite analyses in this report are generally consistent with the Creaser et al. (1999) analyses except for thorium values. Eclogite analyses in Table I-3 also have much higher silica values than the previously published analyses. These discrepancies suggest that the analyses presented in this report are contaminated with metasedimentary crustal material and are not truly representative of the eclogite protoliths. Further fieldwork and analytical work are required to resolve these differences.

The two analysed chloritic phyllite samples were collected from localities within 570 m of each other in the town of Faro. In spite of this close spatial association, the chemistries of these two samples are significantly different. Sample LP99-055 is geochemically similar to the eclogite samples (see Figs. 33 and 34) and consistently plots within the same cluster of points on the discriminant diagrams. In contrast, sample LP99-056 is alkali basalt with a distinctive oceanic island basalt signature. This contrasting geochemical signature is similar to that of alkalic mafic rocks described by Piercey et al. (2002) in Yukon-Tanana Terrane in the Finlayson Lake area. These preliminary differences in only a few outcrop locations demonstrate overlapping geological settings and a complicated geologic history which requires further analytical work and detailed fieldwork to unravel.

The micaceous quartzite unit is nonfossiliferous. It corresponds to unit 1 of Tempelman-Kluit (1972) and was originally correlated with the Proterozoic "Grit Unit." Subsequently Tempelman-Kluit (1979a,b) grouped it with the Nisutlin allochthon of the Yukon-Tanana Terrane (YTT), considering it to be largely Triassic in age. Gordey and Irwin (1987) also considered this unit to be part of

the Nisutlin allochthon of the YTT only with an expanded age range of Carboniferous to Triassic. Mortensen and Jilson (1985) mapped this unit as part of the Devonian-Mississippian layered metamorphic sequence of the YTT. More recently, Murphy et al. (2002) have mapped their Grass Lakes succession of the YTT as being the probable correlative unit further to the southeast to the micaceous quartzite. This correlation would imply a middle Paleozoic age for the micaceous quartzite in the map area.

A poor minimum age of formation for at least some of the unit can be determined from the extensive isotopic dating of the eclogite bodies (Table 3). These dates reflect varying closure temperatures for the different minerals and isotopic systems. All dates are metamorphic cooling dates for the various minerals. Metamorphism indicated by the dates is Early to Middle Permian (using the time scale of Okulitch, 2001). Depositional age of the enclosing sediments must be older than this metamorphic cooling age. The unit is broadly constrained to being Paleozoic (pre-Permian).

Faro Peak formation (new)

Mountain ridges immediately northeast of the Tintina Trench are commonly underlain by a thick succession of massive, brown-weathering conglomerate, interbedded with mafic greywacke, sandstone, black argillite, dark grey limestone, chert and basalt. This succession is here termed the Faro Peak formation for one of the large accumulations of conglomerate on Faro Peak northwest of the town of Faro. Accessible outcrop is located on the mine access road at the "Fingers" tourist viewing area. The Faro Peak formation only occurs southwest of the Vangorda fault. It unconformably overlies the Yukon-Tanana Terrane quartzite unit. The upper contact is consistently removed by erosion, making it the youngest stratigraphic formation southwest of the Vangorda fault in the map area. It is thickest in the vicinity of Faro Peak where it has an interpreted thickness of greater than 560 m. Tempelman-Kluit (1979a) estimated an aggregate thickness of 840 m in the same general area (described as being near Rose Mountain).

Table 3. *Isotopic age dates for metamorphic minerals in Yukon-Tanana Terrane eclogites.*

Sample	Date±2σ	System	Material	Comments	Reference
Faro eclogite					
GSC76-157	258±13	K-Ar	muscovite		1
PE80-F3a	260±3	^{40}Ar-^{39}Ar	muscovite	plateau	2
PE80-F3a	256±3	^{40}Ar-^{39}Ar	muscovite	integrated	2
PE80-F3b	261±2	^{40}Ar-^{39}Ar	muscovite	laser spot integrated	2
Faro IIIa	252±7	Lu-Hf	whole rock - garnet-omphacite	isochron	3
Faro IIIa	255±7	Lu-Hf	garnet-omphacite	isochron	3
Faro IIIc	257±6	Lu-Hf	whole rock - garnet-omphacite	isochron	3
Faro IIIc	264±6	Lu-Hf	garnet-omphacite	isochron	3
PE80-F1	281±15	Sm-Nd	whole rock - garnet-pyroxene	isochron	5
Ross River eclogite					
PE85-25-1	246±14	Rb-Sr	whole rock - muscovite	isochron	4
PE85-25-2	243±12	Rb-Sr	whole rock - muscovite	isochron	4
PE85-25-2	246±8	Rb-Sr	whole rock - muscovite	isochron	4
PE85-25-21	255±8.1	Sm-Nd	whole rock - garnet-pyroxene	isochron	5
PE85-25-1	273±3	^{40}Ar/^{39}Ar	muscovite	plateau + integrated	2
PE85-21-10	267±3	^{40}Ar/^{39}Ar	muscovite	plateau	2
PE85-21-10	274±3	^{40}Ar/^{39}Ar	muscovite	integrated	2

References 1=Wanless et al., 1978; 2=Erdmer et al., 1998; 3=Philippot et al., 2001; 4=Erdmer and Armstrong, 1988; 5=Goodwin-Bell, 1998.

The Faro Peak formation can be divided into two stratigraphic units: a lower member consisting of interbedded argillite, conglomerate, sandstone, greywacke, siltstone, bedded chert, basalt and limestone, and an upper member consisting of massive, unbedded, polymictic conglomerate. Extensive outcrop exposures of the lower member occur in two adjacent streams located approximately 3 km southwest of Rose Mountain (567 500 E, 6 913 300 N and 568 800 E, 6 912 700 N – Plate 5). A series of outcrops along the ridge starting at 570 500 E, 6 911 700 N (lower contact) and extending to 571 800 E, 6 911 800 N (Plate 5) encompass the upper member from its basal contact upward.

Interbedded dark grey, rusty weathering, thick-bedded siltstones and sandstones with thick mafic greywackes, black, noncalcareous argillites interbedded with medium to dark grey, fine-grained limestones and dark green, aphanitic basalts with interbedded cherts form the lowermost lithologies in the Faro Peak formation. Individual lithologies range from a few metres to greater than 150 m in thickness. In the section described by Templeman-Kluit (1979a) near Rose Mountain, this lower succession was estimated as being greater than 340 m thick. In other areas this lower member of the formation appears to be missing.

South of Rose Mountain (572 110 E, 6 912 320 N – Plate 5), the lowermost-mapped lithology within the Faro Peak formation is a dark to medium green, aphanitic, rusty brown-weathering basalt (Jennings et al., 1978b). The basalt locally contains minor epidote streaks associated with a tan-weathering carbonate. Weathered surfaces in some instances have a primary breccia texture. Table I-4 (see Appendix I) lists the geochemical analysis for this basalt, and Figures 35 and 36 show discriminant and multi-element diagrams for the analysis. The various discriminant diagrams indicate the sample is typical for NMORB (normal mid-oceanic ridge) basalt. Geochemistry of this sample is very similar to that of the Permian Campbell Range formation basalt (see below); it is possible that this basalt actually is a previously unrecognized outlier of the Campbell Range formation.

The uppermost member of the Faro Peak formation is a massive, matrix-supported, polymictic conglomerate which forms the dominant rock type in the formation. The conglomerate contains rounded to subangular clasts up to 1 m across in a dark grey- to dark brown-weathering, argillaceous sandstone matrix. The matrix contains similar lithologies to the clasts and also contains disseminated detrital muscovite. A crude foliation is visible in the matrix. Clasts consist predominantly of metaquartzite (50%), chert (20%), basalt (20%) and limestone (10%) (Tempelman-Kluit, 1972, 1979a). Other pebble clasts include granitic gneiss (biotite quartz monzonite and hornblende granodiorite) and serpentinite. Limestone clasts are typically the largest clasts in any one outcrop. In at least one locality, the conglomerate contains an interbed of fine-grained, dark grey limestone with discontinuous black chert bands up to 10 cm thick. The lower contact of this upper member appears to be unconformable as it cuts down section through the lower member in a southwest direction until it rests directly on the YTT micaceous quartzite unit.

Tempelman-Kluit originally mapped the polymictic conglomerate of the Faro Peak formation as unit 10. Interbedded finer grained lithologies were described as unit 10a. Subsequently, he considered this coarse clastic package as being synorogenic flysch of the Nisutlin allochthonous assemblage (Tempelman-Kluit, 1979a,b). Gordey and Irwin (1987) retained the association with the Nisutlin assemblage. Clasts within the polymictic conglomerate are considered to be locally derived from older lithologies.

Table 4 contains fossil collections from the Faro Peak formation. Fossil samples C-103825 and C-157777 were collected from limestone clasts within a polymictic conglomerate tentatively assigned to the upper member.

Table 4. *Fossil localities from the Faro Peak formation.*

Locality no.	Member	UTM E*	UTM N*	Material	Age range	Reference
C-103825	Upper?	594 784	6 896 994	conodont	Late Triassic, Late Carnian	Orchard (1992a)
C-157777	Upper?	586 525	6 902 540	conodont	Late Triassic, Carnian	Orchard (2004)
C-304121	Upper?	587 731	6 902 228	conodont	Late Triassic, early Norian	Orchard (2004)
O-086347	Lower	568 032	6 913 290	conodont	Late Triassic, Late Norian-Rhaetian	Orchard (2004)
O-086348	Lower	568 032	6 913 290	conodont	Late Triassic, Late Carnian	Orchard (2004)

*NAD83 UTM coordinates, zone 8; M. Orchard (2004, pers. comm.)

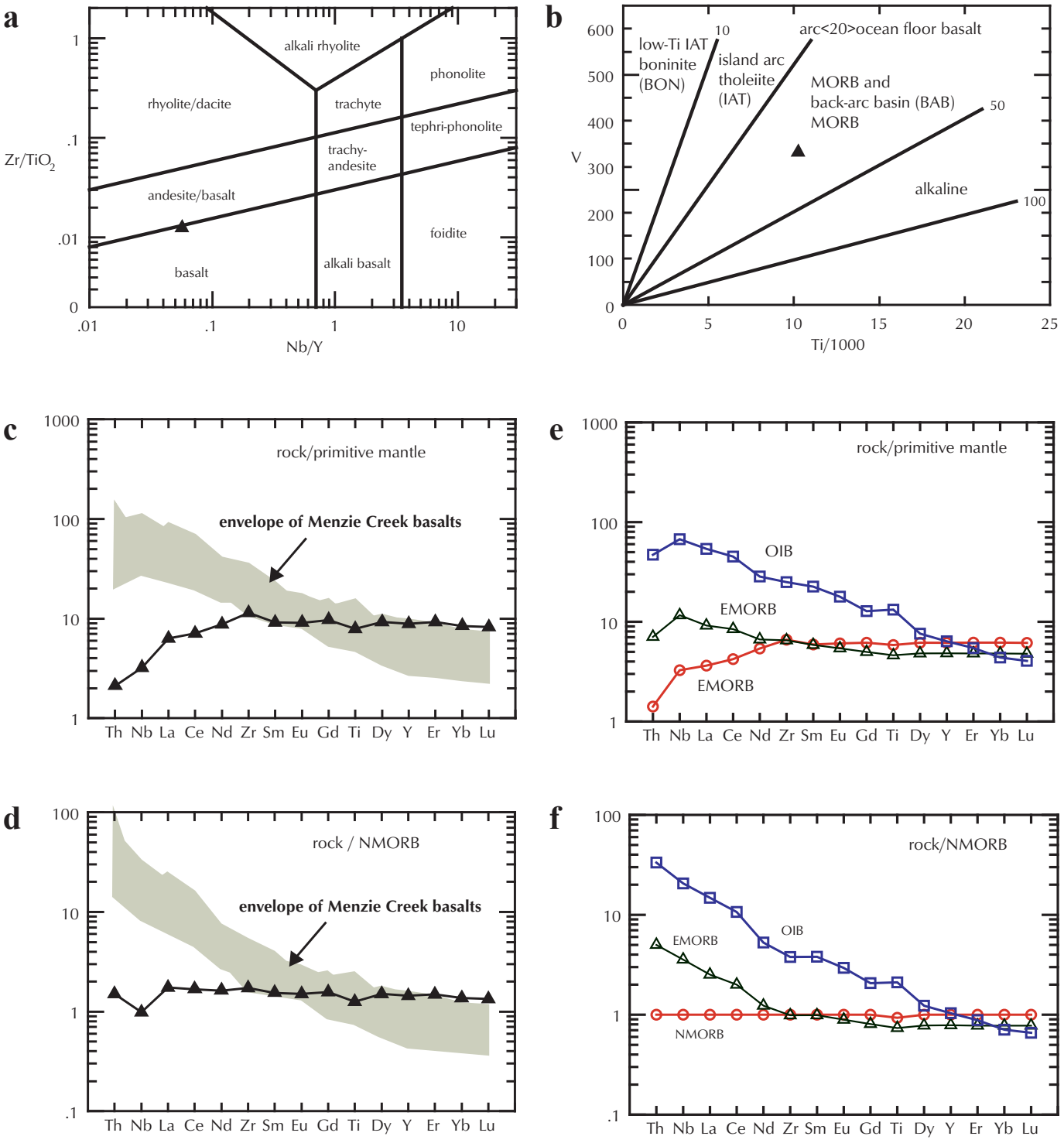

Figure 35. *Discriminant and multi-element diagrams for basalt in Faro Peak formation.* ***(a)*** *Zr/Ti-Nb/Y diagram of Winchester and Floyd (1977) as modified by Pearce (1996);* ***(b)*** *Ti-V diagram of Shervais (1982);* ***(c)*** *Primitive mantle normalized multi-element diagram;* ***(d)*** *NMORB normalized multi-element diagram;* ***(e)*** *primitive mantle normalized multi-element diagram for oceanic island basalt (OIB), enriched mid-occeanic ridge basalt (EMORB), and normal mid-oceanic ridge basalt (NMORB);* ***(f)*** *NMORB normalized multi-element diagram for OIB, EMORB and NMORB.* ***(c-f)*** *Primitive mantle and NMORB values from Sun and McDonough (1989).*

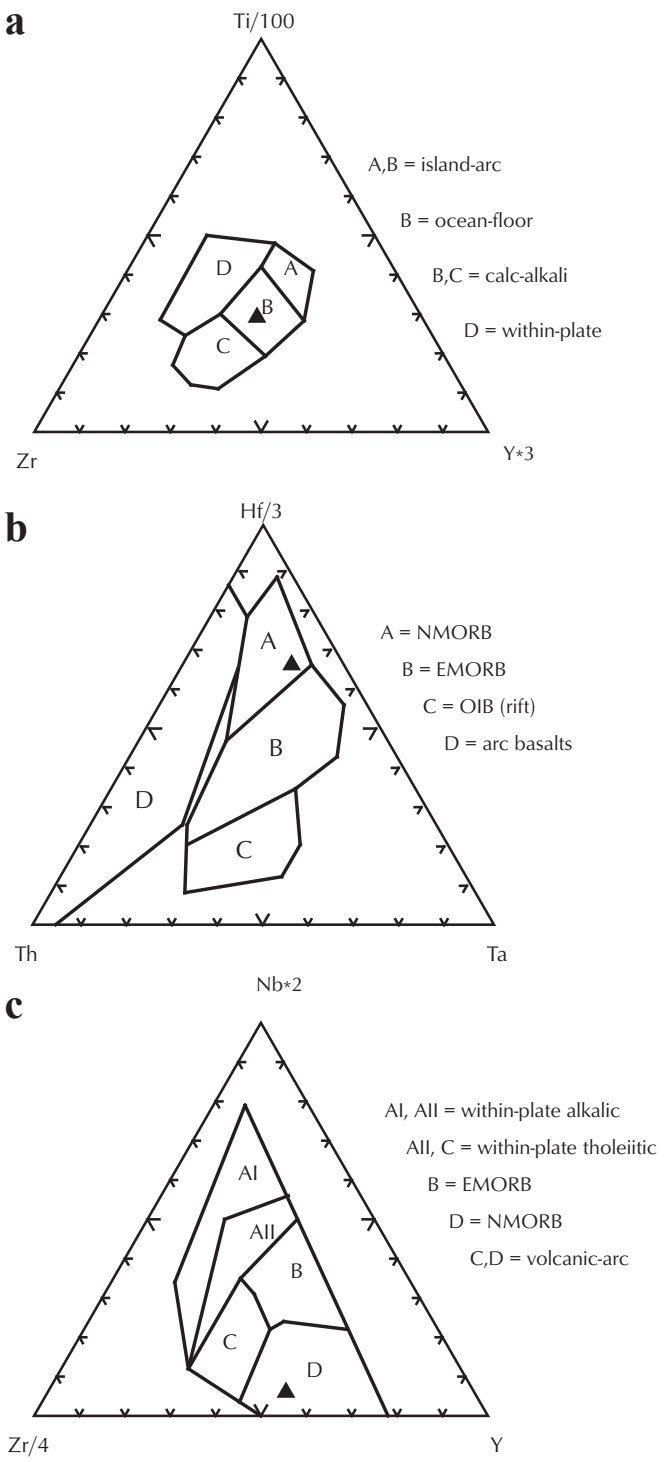

Figure 36. *Tectonic discriminant diagrams for basalt in Faro Peak formation.* ***(a)*** *Zr-Ti-Y diagram of Pearce and Cann (1973);* ***(b)*** *Th-Hf-Ta diagram of Wood (1980);* ***(c)*** *Zr-Nb-Y diagram of Meschede (1986).*

Sample C-304121 was collected from a large limestone bed interbedded with the same conglomerate at the site of the Faro NorthwesTel repeater station. Limestone clasts within the conglomerate have ages of Late Triassic-Carnian. In contrast, the fossil collection from limestone interbedded with the conglomerate has a Late Triassic (early Norian) age. A Late Triassic age for both members of the Faro Peak formation is consistent with the fossil collections.

Clasts from the Faro Peak formation conglomerate are largely locally derived from stratigraphic units presently exposed both northeast (ultramafic, Campbell Range formation basalt and chert) and southwest (YTT micaceous quartzite) of the Vangorda fault. The one source unit not presently exposed in the immediate area is the limestone forming the large clasts in the conglomerate. The massive, unsorted nature of the conglomerate suggests a proximal submarine fan fault scarp complex (Tempelman-Kluit, 1972). The base of the Faro Peak formation is a profound unconformity. Internal unconformities are also present within the Faro Peak formation. Depositional environment of the lower member is relatively quiet marine basin with local influx of coarser clastics. Some of the coarser clastic rocks (greywackes) indicate proximal volcanism.

SLIDE MOUNTAIN STRATIGRAPHY

Between the Anvil District and the Yukon-Tanana/Triassic successions is a Carboniferous to Permian stratigraphic succession of bedded chert, fine and coarse marine clastic rocks, and basalt up to 2300 m thick that has Slide Mountain Terrane affinities. This succession is best exposed in the area of Rose Mountain, northwest of the town of Faro. In this report, the succession has been divided into three formations (from oldest to youngest): the Mount Aho formation, the Rose Mountain formation, and the Campbell Range formation. The entire succession is intruded by ultramafic rocks and is bounded by faults on both the northeast and southwest margins.

This succession corresponds to the Anvil Range Group as redefined by Tempelman-Kluit (1972). As originally defined by Campbell (1967) for the Glenlyon map sheet (105L), the Anvil Range Group corresponded to the early Paleozoic North American succession of rock units described as the Mount Mye, Vangorda, and Menzie Creek formations in this report. Tempelman-Kluit (1972, 1979b) redefined Anvil Range Group to correspond to late Paleozoic volcanic and associated sedimentary rocks of Slide Mountain Terrane. Recently, Ward and Jackson

Figure 37. *Mount Aho formation, pale green argillite. Field station 98LP057.*

Figure 38. *Maroon chert and siliceous argillite, Mount Aho formation – lower member DCMAgr. Maroon chert and argillite is intimately interbedded with green chert and argillite. Field station 98LP049.*

(2000) have used the term Anvil Range Group to refer to the rocks of ancient North America as originally defined by Campbell (1967). Due to the confusion associated with use of the term Anvil Range Group and its connection to two radically different stratigraphic successions, it is suggested herein that use of the term Anvil Range Group be abandoned.

Mount Aho formation (new)

Northeast-facing slopes of Rose Mountain consist of two members constituting the Mount Aho formation. Ridge exposures which encompass both members extend from 577 700 E, 6 913 950 N (lower contact – Plate 7) to 576 300 E, 6 912 500 N (upper contact – Plate 5). The upper contact with the overlying Rose Mountain formation is conformable. The lower contact with the Duo Lake Formation is not exposed. Interpreted thicknesses range from 400 to 860 m. The different members are only differentiated in the Rose Mountain area. The lower member ranges from 0 to 600 m in thickness, and the upper member ranges in thickness from 300 to 900 m. To the southeast, the Mount Aho formation has been combined with the Rose Mountain formation for mapping purposes because of limited exposure.

In the Rose Mountain area, the lowermost member (DCMAgr) is a mixed unit consisting dominantly of a noncalcareous, pale silvery green, silty argillite (Fig. 37) with lesser sandstone, pale green bedded and massive cherts, maroon chert and argillite, and chert-pebble conglomerate. Interbedding of the lesser lithologies with the argillite is on a scale of a few centimetres to tens of metres. Sandstone and conglomerate locally constitute up to 50% of the member. Maroon chert and argillite (Fig. 38) occur largely at the top and bottom of the member and are most abundant on Cornice Ridge. The dominant argillite is soft and weathers with a patchy, medium brown surface coating. Bedding is delineated by subtle centimetre-scale colour banding caused by thin pale grey to tan siltstone interbeds. Argillite consists dominantly of fine-grained intergrown quartz with disseminated fine sericite, minor chlorite and minor equant opaques. Lesser subangular monocrystalline quartz grains are locally scattered within the argillite. Locally, biotite and epidote are randomly oriented as overgrowths within the matrix.

Sandstone and chert-pebble conglomerate (Fig. 39) contain matrix-supported, subangular to angular clasts of pale green to white chert, light greenish grey siltstone, green or dark grey argillite, and monocrystalline quartz with or without K-feldspar or plagioclase. Clasts up to

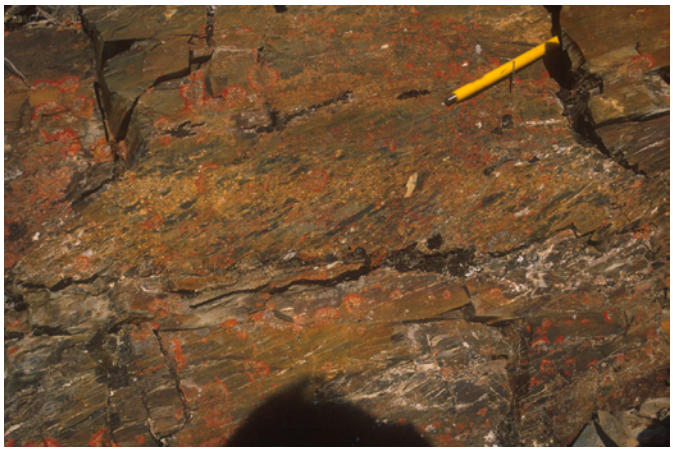

Figure 39. *Mount Aho formation – lower member DCMAgr. Chert-pebble conglomerate interval within argillite. Bedding is nearly horizontal. Conglomerate is in centre of picture. Slaty cleavage is oriented parallel to the pencil magnet, going from lower left to upper right across the picture. Pencil magnet is 12.5 cm long. Field station 98LP044.*

Figure 40. *Mount Aho formation – upper member DCMAbl. Black silty chert interbedded with dark grey, fine-grained, silty limestone. A 35-cm-thick limestone bed occurs under the rock hammer. Bedding dips steeply to the right side of the picture. Field station 98LP114.*

3 cm across are strongly flattened within the plane of the foliation with aspect ratios ranging from 2:1 to 8:1 (Pigage, 1999). Monocrystalline quartz clasts range from a low of about 5% of the conglomerates to a maximum of about 40%.

The upper member of the Mount Aho formation (DCMAbl) contains similar lithologies to the lower member, with the predominant colour of the upper member being dark grey to black. Black silty argillite with lesser black bedded chert is the dominant lithology. Bedded cherts have rhythmic bedding with 5 to 20 cm thick black chert beds alternating with thin dark grey to black argillite interbeds. In several exposures along the northeast slope of Rose Mountain, the lowermost lithology consists of an interval of black siliceous argillite alternating with medium to dark grey, finely laminated limestone (Fig. 40). Individual limestone beds range up to 35 cm in thickness. Intermixed with the argillite and chert are interbeds of sandstone and chert-pebble conglomerate.

Clast-supported, chert-pebble conglomerates (Fig. 41) within the argillite range up to 50 m in thickness. Typically, clasts within the conglomerate are subangular and consist of dark grey to black chert, light to dark grey siltstone, fine-grained sandstone, argillite, and monocrystalline quartz, K-feldspar, or plagioclase. Monocrystalline clasts constitute up to 50% of the clasts locally. Sandstone beds within the upper member consist of subangular monocrystalline quartz clasts with minor chert and argillite clasts.

The lower contact of the upper member with the lower member is transitional with interbedding of pale green and dark grey lithologies, and mixing of pale green and dark grey clasts within the sandstones and conglomerates of both members. This internal contact between the two members is placed at the first occurrence of dark grey to black argillite, sandstone, or conglomerate.

Figure 41. *Mount Aho formation – upper member DCMAbl. Black chert-pebble conglomerate. Field station 98LP055.*

Figure 42. *Mount Aho formation. Interbedded grey barite and pale tan chert. Field station 99LP131.*

Figure 43. *Mount Aho formation, bedded barite. Slaty cleavage oriented horizontally in this picture. Field station 99LP131.*

The upper contact with Rose Mountain formation is conformable, with a sharp change to pale bedded cherts of the Rose Mountain formation from dark coloured, intermixed cherts, argillites, sandstones and chert-pebble conglomerates.

Both upper and lower members contain stratiform barite horizons (DCMAba) which have been differentiated as separate map units in the Rose Mountain area. Barite horizons (Figs. 42 and 43) occur within pale cream to silvery green phyllitic bedded chert intervals ranging up to 40 m in thickness. Barite is nodular to massive within the bedded cherts. Sulphide minerals are not visibly associated with the barite. These barite horizons have previously been sampled at several locations for possible extraction as industrial minerals (Franzen, 1978; Read, 1982). The major gangue mineral associated with the barite is quartz.

The age range of the Mount Aho formation is not well constrained. Table 5 contains the one fossil locality from within the Mount Aho formation. Fossil locality C-304787 was collected from near the middle of the upper member, immediately beneath a barite horizon which has been mapped laterally for a distance of at least 2.5 km. The overlying Rose Mountain formation has a lower limit age of Early Carboniferous-?Visean from a sample collected just above the contact between the two units. No fossils were collected from the lower pale green member. The Mount Aho formation is interpreted to be Early Carboniferous in age, possibly extending downward into Devonian.

Mount Aho formation was deposited in a quiet, deeper water, marine basin. Deposition of the upper member occurred within an euxinic environment. Irregular influxes of coarse sedimentary and igneous clasts are possibly related to turbidity currents. The presence of monocrystalline quartz and feldspars among the clasts indicates that felsic volcanic or plutonic rocks were present in the source region. Stratiform barite suggests local synsedimentary rifting with siliceous hydrothermal fluids venting to the basin floor.

The Mount Aho formation corresponds to the lowermost chert unit of the Anvil Range Group (unit 8a) as mapped by Tempelman-Kluit (1972). Gordey and Irwin (1987) similarly considered the formation to

Table 5. *Fossil localities from the Mount Aho formation.*

Locality no.	Member	UTM E*	UTM N*	Material	Age range	Reference
C-304122	Upper	567 600	6 916 185	conodont	indeterminate-barren	Orchard (1999)
C-304123	Upper	567 600	6 916 185	conodont	indeterminate-barren	Orchard (1999)
C-304124	Upper	567 600	6 916 185	conodont	indeterminate-barren	Orchard (1999)
C-304782	Lower	578 200	6 912 292	conodont	indeterminate-barren	Orchard (2000)
C-304787	Upper	571 664	6 915 306	conodont	Early Carboniferous	Orchard (2000)
C-304788	Upper	571 756	6 915 420	conodont	indeterminate-barren	Orchard (2000)

*NAD83 UTM coordinates, zone 8

represent cherts that were part of the Anvil allochthonous assemblage (CPat). In contrast, Jennings and Jilson (1986) tentatively correlated Mount Aho formation with Earn Group on the basis of extensive chert-pebble conglomerate interbeds and barite horizons within the formation. This formation corresponds with units 3 and 4 of Pigage (1999a). Pigage (1999a) concurred with Jennings and Jilson on a possible correlation with Earn Group because of lithologic similarity and difficulties defining a clear structural break between Mount Aho formation and underlying and overlying units. With this correlation, the lower contact of the Mount Aho formation would be stratigraphic and the lower age range of the formation would be Late Devonian to Early Carboniferous. The upper age limit of the Mount Aho formation appears to extend beyond the regionally determined ages of Earn Group (Gordey et al., 1982).

Recent mapping by Murphy et al. (2002) in the Finlayson Lake area to the east delineated a succession of dark grey siliceous phyllite, grey, white, pink and green chert, mottled grey-white chert-pebble conglomerate, quartzofeldspathic grit, meta-felsic volcanic rocks and barite, which they called the Finlayson succession of Yukon-Tanana Terrane. This succession had previously been mapped as Earn Group (Plint and Gordon, 1997); with the position of the Finlayson succession relative to the unconformably overlying basalts of the Campbell Range succession and its lithologic similarity to the Mount Aho and Rose Mountain formations, Murphy et al. (2002) tentatively correlated the Finlayson succession with these two units mapped in the Anvil District. With this correlation, the lower contact of the Mount Aho formation and the underlying Duo Lake Formation would be a thrust fault (correlative with the Inconnu Thrust; Murphy et al., 2002). More recently, Murphy (2004) has renamed this succession the Fortin Creek group and re-interpreted it as belonging to Slide Mountain Terrane on the basis of its basinal character and lithologic similarity to Sylvester Allochthon (Nelson, 1993). This interpretation is tentatively preferred over the interpretation placing the Mount Aho formation in North American stratigraphy.

Rose Mountain formation (new)

Rose Mountain formation consists dominantly of pale green to cream, noncalcareous, phyllitic, bedded cherts (Fig. 44). Chert beds are 2 to 15 cm thick and alternate with thin, pale green argillite interbeds. The bedded cherts typically weather orange-brown to tan-brown; locally they have an intense dark brown manganese oxide surface coating. In thin section the cherts consist of fine-grained intergrown quartz with variable amounts of disseminated fine sericite and chlorite.

Figure 44. *Rose Mountain formation, pale cream, phyllitic, bedded chert. Field station 98LP107.*

The unit is well exposed on the northeast slopes of Rose Mountain. A good type section extends from 576 200 E, 6 912 800 N (lower contact) upslope to 574 700 E, 6 912 800 N (upper contact) (Plate 5). Interpreted thicknesses range from 200 to 600 m. Away from the Rose Mountain area, poor exposures resulted in this unit being grouped with the Mount Aho formation to make a combined mapping unit.

The pale cherts locally contain intervals up to 15 m thick of dark grey to black chert and silty argillite. Other interbedded lithologies occurring in minor amounts include thin-bedded limestone, medium to dark grey sandstone, and dark grey to grey chert-pebble conglomerate. Sandstone intervals consist of subequal proportions of subangular to subround phyllitic chert clasts and monocrystalline quartz clasts. Monocrystalline quartz clasts typically have undulatory extinction. Minor clasts of dark grey to black argillite are also present. Cross-cutting fractures are infilled with coarser-grained quartz, chlorite, and locally carbonate minerals.

The upper portion of the formation contains variable amounts of dark maroon to red argillite with lesser bedded chert (Fig. 45). The proportion and thickness of these interbedded maroon to red units varies dramatically along strike, with intervals over 60 m thick changing rapidly laterally to zero thickness. Locally, the red units have a mottled appearance with lenses and irregular shapes of pale green chert and argillite within the overall red chert and argillite.

Figure 45. *Rose Mountain formation red chert. Bedding is near vertical. Spaced fracture cleavage dips steeply left. Field station 99LP068.*

Both upper and lower contacts of this unit are conformable. The lower contact boundary is placed at the first occurrence of pale bedded chert. The upper contact is gradational with interbedding of basalt and chert and is placed at the first occurrence of basalt. Mapping southeast of Rose Mountain shows that this upper contact with the basalt is interfingering and diachronous.

The Rose Mountain formation denotes predominantly slow deposition of siliceous fine clastic rocks within a starved, deeper water, marine basin. Irregular and minor influxes of limestone debris, sands and gravels are probably related to turbidity currents. Lithologies represented by the formation do not pinpoint the depth of the basin beyond below wavebase and above the calcite compensation depth. The marine basin was euxinic for only very short intervals.

Table 6 lists fossil localities within the Rose Mountain formation. Fossil localities O-080025 and O-093500 located about 60 m below the top of the formation contain latest Carboniferous to earliest Permian fusulinids and Late Carboniferous conodonts (Tempelman-Kluit, 1972, 1979a,b; Orchard, 1992b). The conodont collection from this site is considered to be a mixed fauna with some species indicating an early Carboniferous age (Orchard, 1992b). A conodont fossil locality (C-304786) from near the base of the unit has an age of Early Carboniferous-?Visean (Orchard, 2000). Radiolarians collected from near the top contact of the formation have an age range within Early Permian (Asselian to Sakmarian; Cordey, 2000). Fossils from within this formation are consistent with an age range of Early Carboniferous (?Visean) to early Permian (Asselian-Sakmarian).

Rose Mountain formation correlates with the bedded cherts of the Anvil Range Group (unit 8a) as defined by Tempelman-Kluit (1972). Jennings and Jilson (1986) also included it with their Anvil Range Group. Gordey and

Table 6. *Fossil localities in Rose Mountain formation.*

Locality no.	UTM E*	UTM N*	Material	Age range	Reference
C-304784	566 674	6 916 482	conodont	indeterminate-barren	Orchard (2000)
C-304786	572 610	6 914 109	conodont	Early Carboniferous, ?Visean	Orchard (2000)
C-304785	572 029	6 914 337	conodont	Early Carboniferous, ?Serpukhovian	Orchard (2000)
C-304789	570 676	6 915 452	conodont	indeterminate-barren	Orchard (2000)
O-080025	575 127	6 913 000	fusulinids	Latest Pennsylvanian to Earliest Permian	Tempelman-Kluit (1972)
O-093500	575 127	6 913 000	conodont	Late Carboniferous (mixed fauna)	Orchard (1992b)
LP99-180	570 736	6 914 888	radiolarian	Early Permian, Asselian-Sakmarian	Corday (2000)

*NAD83 UTM coordinates, zone 8

Irwin (1987) mapped it as part of the Anvil allochthonous assemblage (CPat). It corresponds with unit 5 as previously reported by Pigage (1999a). Pigage (1999a) suggested the Rose Mountain formation corresponded to Mount Christie Formation (Gordey and Anderson, 1993) which would place it within North American stratigraphy. Regionally, however, recent mapping by Murphy et al. (2002) in the Finlayson Lake area delineated a correlative succession which was called the Fortin Creek group and considered to be part of the Slide Mountain Terrane (Murphy, 2004).

Campbell Range formation

Rose Mountain immediately northeast of the Tintina Trench is capped by resistant basaltic volcanic rocks and associated bedded cherts. These volcanic rocks and associated bedded cherts collectively form the Campbell Range formation (Murphy, 2004; formerly called the Campbell Range succession, Murphy et al., 2002). A well exposed section for the volcanic rocks extends from a lower contact at (573 450 E, 6 913 800 N) to an upper extent of outcrop at (572 700 E, 6 913 000 N – Plate 5). A minimum thickness for the volcanic rocks is approximately 800 m with the upper contact being eroded.

Dark reddish brown-weathering, dark green, massive, aphanitic basalts characterize Campbell Range formation. Autobreccia textures with subangular to rounded clasts of basalt in a dark green to reddish green aphanitic volcanic matrix are commonly visible (Fig. 46). Patchy epidote alteration in the matrix locally gives the basalt a medium-green colour. In places the basalts are slightly to moderately magnetic. Foliation is rarely visible within the basalt. Pillows were not observed. Locally, basalt outcrops contain irregular, discontinuous lenses and pods of green or red, poorly bedded chert. Petrographically, the basalts typically contain clinopyroxene microphenocrysts and glomerocrysts in a fine-grained, felted matrix of plagioclase microlites, chlorite, epidote and opaque minerals. Plagioclase is typically partly to completely altered. Locally, hornblende occurs as acicular brown to green grains in the matrix.

The lower contact of the Campbell Range formation with the underlying Rose Mountain formation is gradational with interbedding of basalt and chert on a scale of 5 m or less. This gradational contact was also recognized by Tempelman-Kluit (1972). The lower contact is placed at the lowermost major basalt flow. Mapping in the Rose Mountain area has documented that this contact is interfingering and diachronous. The upper contact of the

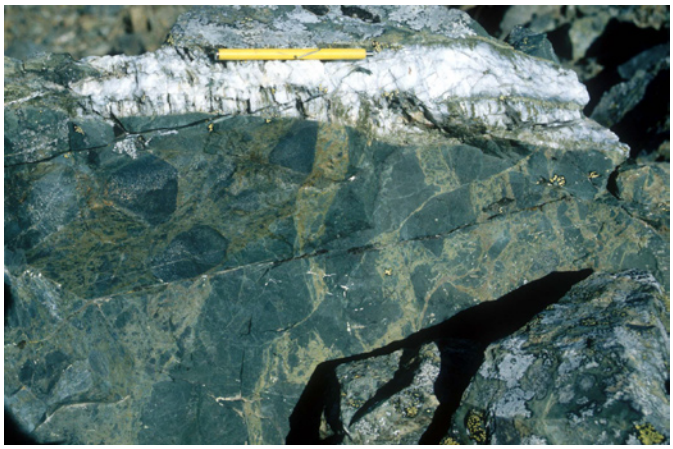

Figure 46. *Campbell Range formation. Autobrecciated texture with epidote well developed in matrix. Pencil magnet is 12.5 cm long. Late cross-cutting quartz vein. Field station 99LP207.*

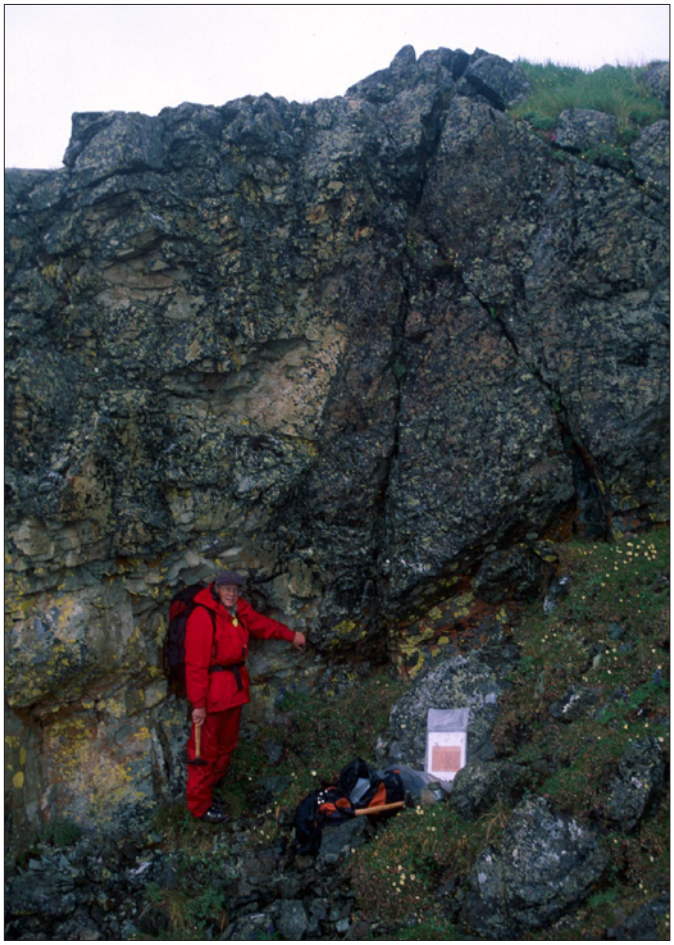

Figure 47. *Campbell Range formation green chert interbedded with basalt. Field station 99LP048. Bedding contact is near-vertical in centre of photo with chert being on the left.*

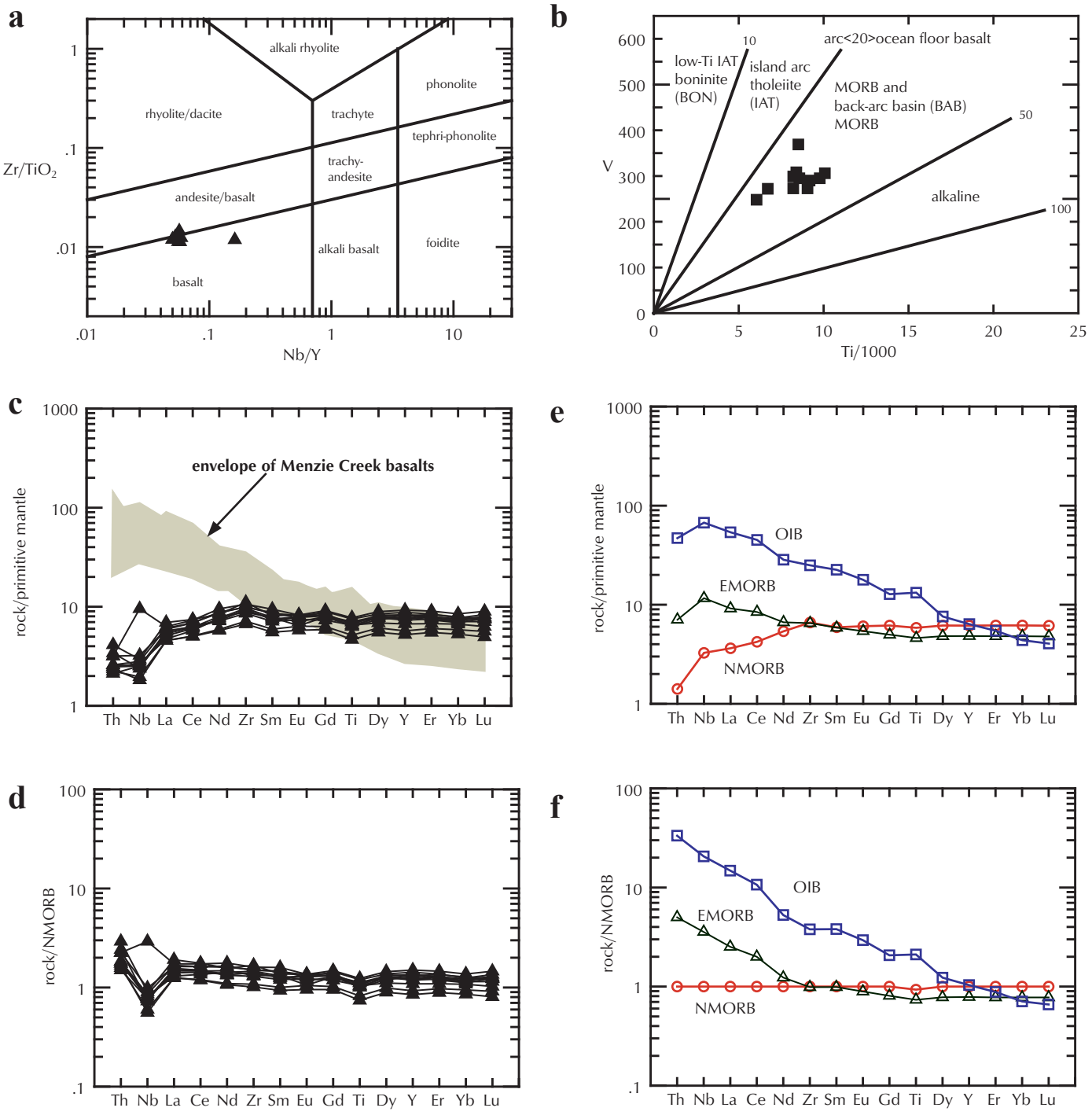

Figure 48. *Discriminant and multi-element diagrams for basalt in Campbell Range formation.* ***(a)*** *Zr/Ti-Nb/Y diagram of Winchester and Floyd (1977) as modified by Pearce (1996);* ***(b)*** *Ti-V diagram of Shervais (1982);* ***(c)*** *primitive mantle normalized multi-element diagram;* ***(d)*** *N-MORB normalized multi-element diagram;* ***(e)*** *primitive mantle normalized multi-element diagram for oceanic island basalt (OIB), enriched mid-occeanic ridge basalt (EMORB), and normal mid-oceanic ridge basalt (NMORB);* ***(f)*** *NMORB normalized multi-element diagram for OIB, EMORB and NMORB.* ***(c-f)*** *Primitive mantle and NMORB values from Sun and McDonough (1989).*

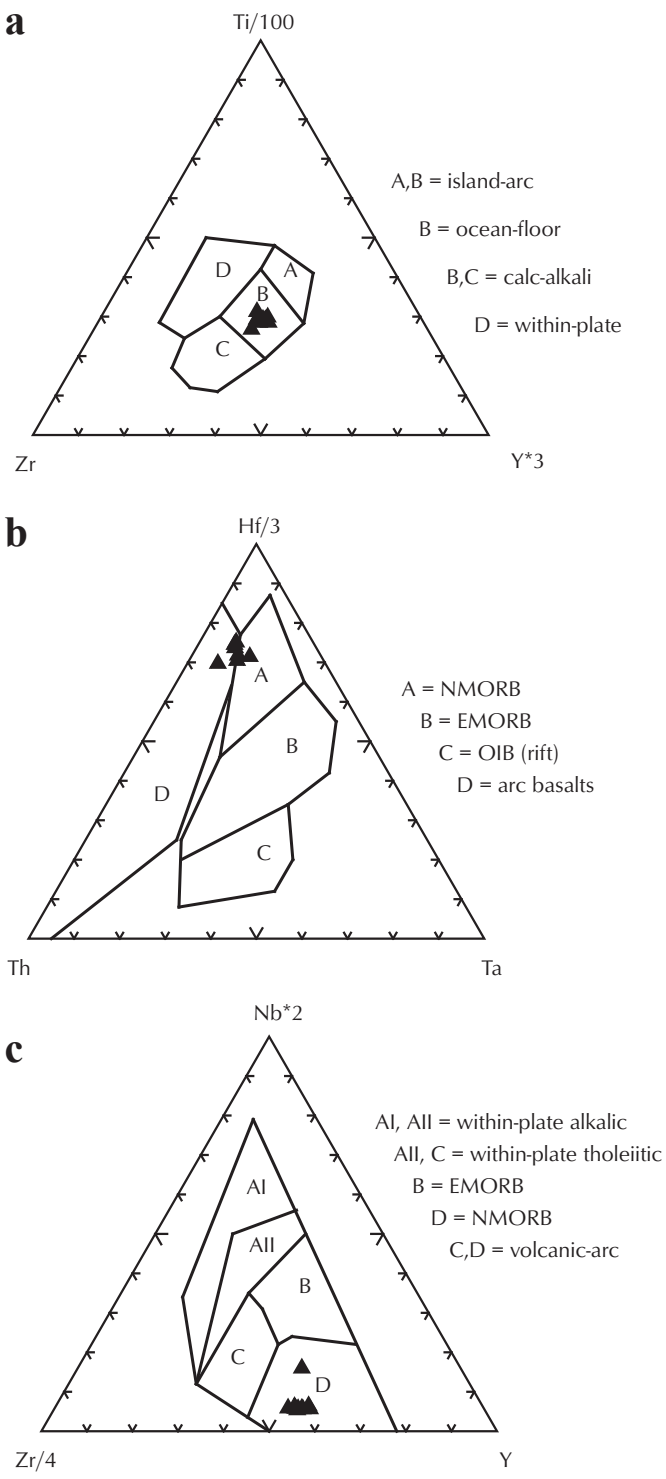

Figure 49. *Tectonic discriminant diagrams for basalt in Campbell Range formation.* ***(a)*** *Zr-Ti-Y diagram of Pearce and Cann (1973);* ***(b)*** *Th-Hf-Ta diagram of Wood (1980);* ***(c)*** *Zr-Nb-Y diagram of Meschede (1986).*

Campbell Range formation has been removed by erosion or is faulted.

Basalt flows are interbedded with red, green, dark grey and black, bedded to massive chert and argillite (Fig. 47). Sedimentary chert intervals constitute about 20% of the unit and are up to 60 m thick. Bedded cherts consist of chert beds 5 to 30 cm thick, separated by thin argillaceous intervals. Typically the argillite intervals are less than 20% of the bedded cherts; locally however they constitute up to 80% of a chert interval. In one outcrop, sedimentary rocks within the Campbell Range formation consist of pale green, matrix-supported, volcaniclastic sandstone to conglomerate with subangular to angular chert and volcanic clasts up to 30 cm across suspended in a sandstone matrix. On the southeast ridge of Rose Mountain, one phyllitic chert interval contains a 1.5-m-thick bed of medium to dark grey, immature sandstone with clasts of light chert, dark chert, and "black" quartz grains.

Geochemical analyses of the Campbell Range formation basalts are presented in Table I-5 (see Appendix I). Trace element discriminant and multi-element normalized diagrams indicate the basalts are subalkalic and are consistent with NMORB chemistry (Figs. 48 and 49). Tectonic discriminant diagrams are consistent with a either a mid-ocean ridge or a back-arc basin paleotectonic setting. The negative Nb anomaly and positive Th anomalies in Figures 48c and d are consistent with a slight crustal or subduction component. Figure 48 shows evidence that Campbell Range formation basalts have a strikingly different normalized geochemical signature from the Menzie Creek formation basalts. Chemistry for the basalts in the Faro area is very similar to those for the CRB2 suite of the Campbell Range belt metabasalts from the Finlayson Lake region (Piercey et al., 1999).

Tempelman-Kluit (1972, 1979a,b) considered the Campbell Range formation basalts to be Pennsylvanian to Permian on the basis of conodonts and fusulinids collected from a limestone approximately 60 m beneath the lowermost basalt. Radiolarians collected from red chert immediately beneath the lower formation contact on Rose Mountain yielded an Asselian-Sakmarian (Early Permian age; Cordey, 2000, see Appendix II). The basalts in the Rose Mountain area are therefore considered Early to possibly Late Permian in age.

Correlative basalts include Campbell Range formation basalts located within the Slide Mountain Terrane in the Finlayson area (Plint and Gordon, 1997; Murphy and Piercey, 1999; Murphy, et al., 2002; Murphy, 2004).

Regionally, Campbell Range formation basalts have a mid-Pennsylvanian to Early Permian age based on radiolaria (Plint and Gordon, 1997). Plint and Gordon (1997) also correlated Campbell Range formation with Slide Mountain Terrane and Sylvester Allochthon-Division II (Nelson, 1993). The correlations, lithologies and lithogeochemistry all support these basalts and underlying sediments being deposited in a marginal or back-arc oceanic basin (i.e., the Anvil Ocean) during Late Paleozoic time. Campbell Range formation basalts have a chemical signature consistent with formation from a depleted mantle source.

INTRUSIVE ROCKS

INTRODUCTION

Early and Late Paleozoic intrusions in the Faro area consist of mafic and ultramafic tabular bodies. Early Paleozoic metabasites occur as locally extensive dykes and sills within the Mount Mye, Vangorda, and Menzie Creek formations. Permian (?) gabbros and ultramafic intrusions are associated with Campbell Range formation basalts.

Late- to post-metamorphic intermediate to felsic intrusive rocks occur as major bodies, dykes, sills and plugs in the Anvil District. The largest bodies in the current map area are the Anvil and Orchay batholiths. Three intrusive suites have been recognized, largely on the basis of geochemistry and intrusion ages. These intrusive bodies range in age from mid-Cretaceous to Eocene.

INTRUSIVE SUITES

Ordovician-Silurian gabbro and pyroxenite

Mount Mye, Vangorda, and Menzie Creek formations all contain metabasite lenses which range from a few centimetres up to 100 m in thickness and locally extend along strike for several kilometres. These bodies mainly appear to be conformable with observed or inferred bedding but in detail are locally cross-cutting. The margins of the lenses are pervasively recrystallized and foliated, and the interiors of thicker bodies are massive and commonly preserve relict diabasic to hypidiomorphic-granular igneous textures (Fig. 50). Typically the metabasite lenses have a gabbroic to diabasic appearance. Present mineralogy consists of chlorite-plagioclase-quartz ±carbonate±actinolite±biotite±epidote. Locally, however, the intrusive bodies consist of variably serpentinized pyroxenite. The pyroxenites are commonly magnetic and are readily visible on airborne magnetic surveys.

Locally, the intrusive bodies exhibit extensive quartz-carbonate alteration. With increasing alteration, the dark green rock becomes a rusty weathering, light tan, quartz-carbonate-muscovite rock (Fig. 51) which locally contains minor amounts of a bright green layer silicate resembling fuchsite. Modene (1982) identified this mineral as most probably being a Ni-bearing serpentine mineral. These heavily carbonate-altered rocks resemble quartz-carbonate altered mafic and ultramafic igneous rocks described worldwide.

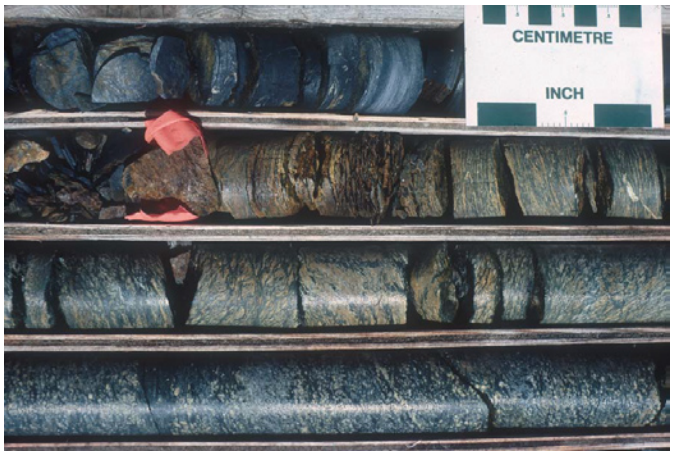

Figure 50. *Ordovician-Silurian gabbro sill in Vangorda formation. Margin of sill is located immediately to right of flagging in the second row from the top. The sill margin is strongly foliated. Lower rows are less foliated and display relict igneous texture. Drill Hole CNR76-04. Depth 67 feet to 90 feet (20 to 27 m). BQ-size core.*

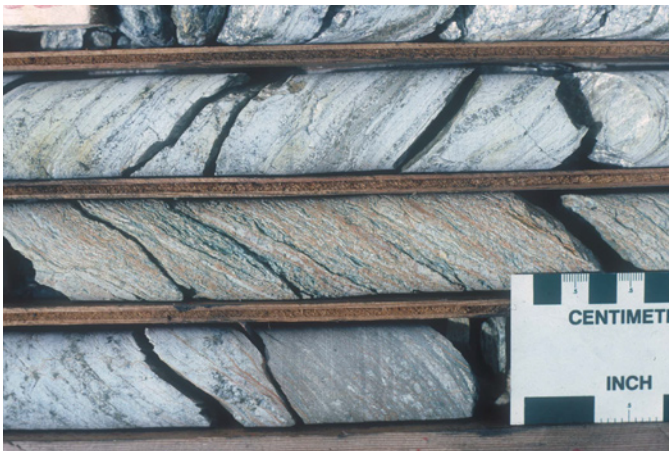

Figure 51. *Strongly quartz-carbonate altered Ordovician-Silurian gabbro sill in Grum deposit. Sill is strongly foliated and is located in middle row of core. Drill hole FAGU189, 17.9-25 m. BQ-size core.*

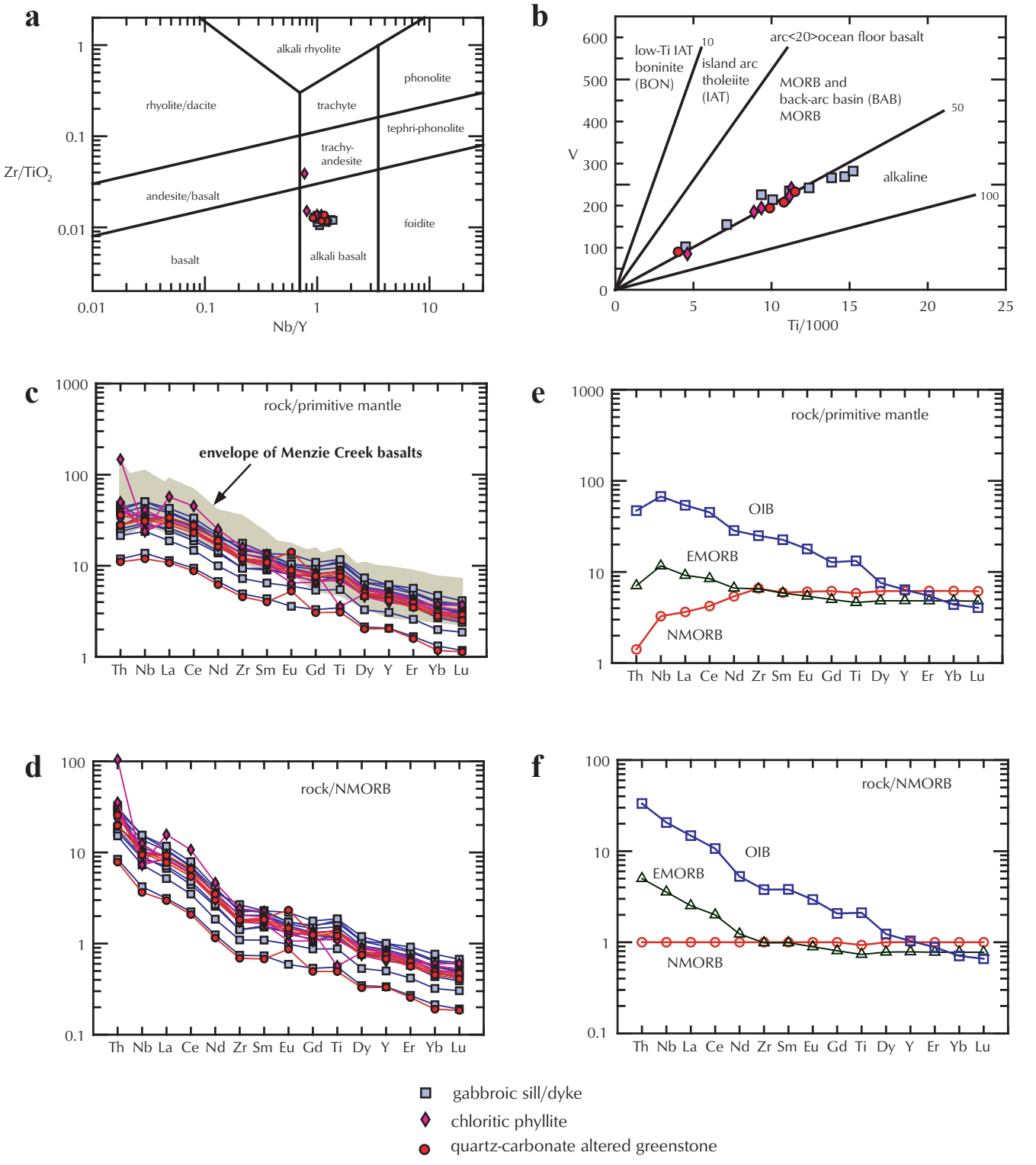

Figure 52. *Discriminant and multi-element diagrams for Ordovician-Silurian mafic intrusive dykes and sills within the Vangorda and Mount Mye formations.* ***(a)*** *Zr/Ti-Nb/Y diagram of Winchester and Floyd (1977) as modified by Pearce (1996);* ***(b)*** *Ti-V diagram of Shervais (1982);* ***(c)*** *primitive mantle normalized multi-element diagram;* ***(d)*** *NMORB normalized multi-element diagram;* ***(e)*** *primitive mantle normalized multi-element diagram for oceanic island basalt (OIB), enriched mid-occeanic ridge basalt (EMORB), and normal mid-oceanic ridge basalt (NMORB);* ***(f)*** *NMORB normalized multi-element diagram for OIB, EMORB and NMORB.* ***(c-f)*** *Primitive mantle and NMORB values from Sun and McDonough (1989).*

Figures 52 and 53 are discriminant and multi-element diagrams for intrusive dykes and sills within the Mount Mye and Vangorda formations. Comparison of Figures 52 and 53 with Figures 28 and 29, respectively shows that the metabasite dykes and sills are chemically very similar to the basalts of the Menzie Creek formation. This overall compositional similarity supports the interpretation that the metabasites in the Vangorda and Mount Mye formations are subvolcanic dykes and sills that fed the Menzie Creek formation flows.

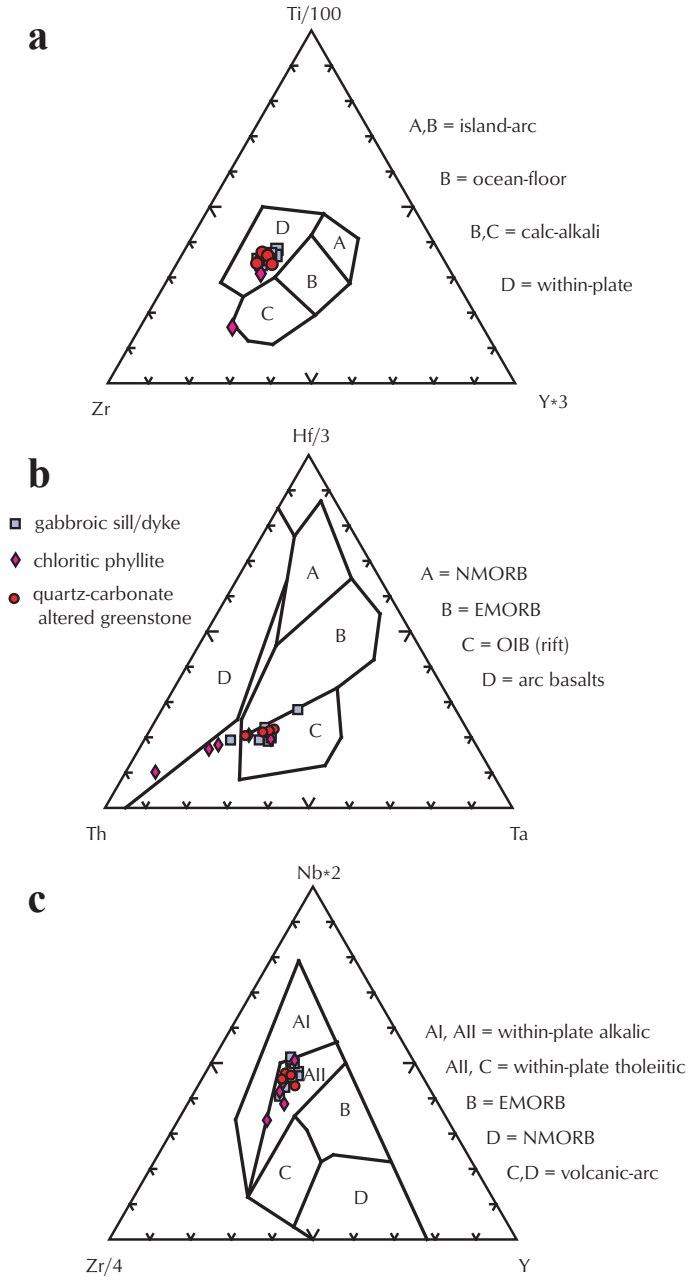

Figure 53. *Tectonic discriminant diagrams for Ordovician-Silurian mafic intrusive dykes and sills within the Mount Mye and Vangorda formations.* ***(a)*** *Zr-Ti-Y diagram of Pearce and Cann (1973);* ***(b)*** *Th-Hf-Ta diagram of Wood (1980);* ***(c)*** *Zr-Nb-Y diagram of Meschede (1986).*

Permian(?) mafic and ultramafic intrusions

Limited exposures of the ultramafic and mafic intrusive rocks (harzburgite, gabbro, diabase, serpentinite) spacially associated with the Campbell Range formation basalts occur on the southwest-facing slope of Rose Mountain. A reasonably well exposed section occurs from 567 800 E, 6 915 200 N to 567 000 E, 6 914 100 N (Plate 5). Marginal and internal contacts of the intrusive rocks are poorly exposed. Areas of harzburgite, gabbro and diabase are contained within serpentinite zones. Commonly the serpentinite is unfoliated, and relict igneous textures are visible. Locally, however, serpentinite is strongly foliated, especially on margins of the ultramafic intrusive. The geophysical map pattern from the 1996 airborne survey (Woolham, 1996) indicates that the ultramafic rocks dip toward the southwest. The ultramafic rocks are considered to be intrusive into the Campbell Range formation basalts because near the mine access road the location of the ultramafic rocks shifts from southwest of Campbell Range basalt to northeast of the basalt. This map pattern is more easily explained by intrusion, rather than structural interleaving. In the Rose Mountain area, the southwest contact of the intrusive complex is a southwest-dipping normal fault (Vangorda fault). Table I-6 (see Appendix I) contains geochemical analyses of the ultramafic intrusive rock. One of the samples identified as a diabase in the field has the same chemical signature as a gabbro sample.

Ultramafic intrusive rocks are undated in the Anvil District. Juxtaposition of the ultramafic rocks against the Triassic Faro Peak formation and the presence of ultramafic clasts in the Faro Peak formation indicates the intrusives are older than Norian (approximately 215 Ma). Similar ultramafic intrusions in the Campbell Range formation basalts in the Finlayson Lake area have been isotopically dated as 274.3±0.5 Ma (upper Early Permian; Mortensen, 1992). A similar assumed age for the ultramafic rocks in the Faro area is consistent with the ultramafic rocks being intrusive into associated Early Permian Campbell Range formation basalt.

Anvil plutonic suite (revised)

The oldest recognized granitic intrusive rocks in the Anvil District consist of biotite±muscovite granite (Fig. 54) which forms the core of the Anvil Batholith. Proportions of muscovite and biotite vary widely. Other

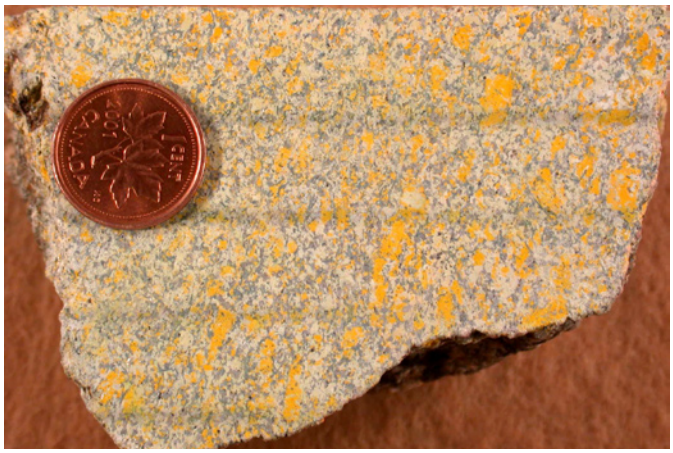

Figure 54. *Anvil plutonic suite. Slightly foliated biotite-muscovite granite. Stained for K-feldspar. Penny is 1.9 cm across. Field station 84-50.*

Figure 55. *Anvil plutonic suite. Granite contact with overlying Vangorda formation calc-silicate rock. Contact proceeds from upper left to lower right across photograph. Left end of pencil is approximately on the contact. Pencil is 14.5 cm long. Field station 99LP014.*

accessory minerals include apatite, zircon, allanite, monazite and tourmaline. Biotite is characterized by reddish brown pleochroism which is identical to that of biotite in the country-rock schist. K-feldspar commonly forms megacrysts which are locally oriented.

Intrusive contacts of the granite with surrounding metasedimentary rocks are sharp. Locally, they are parallel to the S_2 fabric, although regionally they cross-cut stratigraphy (Fig. 55). Granitic and aplitic sills occur in the metasedimentary rocks adjacent to the main intrusive bodies. Locally the batholith contains a poorly developed, shallow-dipping fabric defined largely by oriented micas and/or feldspar phenocryst orientation. On the south side of Mount Mye, the Anvil Batholith contains a well developed S-C banding caused by extensional faults.

Metamorphic isograds in the surrounding metasedimentary rocks are concentric around the Anvil Batholith. Foliations and compositional banding in the surrounding metasedimentary rocks are arched over the batholith. A band of metasedimentary rock within the batholith can be traced from east to west completely across the batholith. This pattern suggests the intrusion should be considered as two overlapping sill-like bodies, rather than a single intrusive body. The upper sill has limited lateral extent with exposures occurring only between the mine access road and Blind Creek.

This unit was originally mapped as unit 11 by Tempelman-Kluit (1972). It was identified as the Mount Mye phase of the Anvil plutonic suite by Pigage and Anderson (1985). Gordey and Irwin (1987) mapped this unit as a non-hornblende bearing phase of the Selwyn Plutonic Suite (defined by Anderson, 1983; Gordey and Anderson, 1993). More recently, Mortensen et al. (2000) have divided Early and mid-Cretaceous intrusions of the Selwyn Plutonic Suite in Yukon into different intrusive suites based on age, lithology and geochemistry. This report follows their lead and retains the term Anvil plutonic suite only for these biotite±muscovite granites. Geochemically it is peraluminous, and some geochemical criteria suggest an S-type character for the suite (Pigage and Anderson, 1985).

Table 7 contains the various isotopic ages completed on samples from the Anvil plutonic suite. Two samples from widely separated localities (GAR-1 and GAR-2) give U-Pb monazite ages of 109.3±1.2 Ma (2-sigma error) and 103.9±1.5 Ma (2-sigma error). These are interpreted to be crystallization ages for the two samples and indicate that intrusion of the Anvil suite occurred over a period of at least 4 to 8 Ma. The single Rb-Sr whole rock-mineral isochron reported by Pigage and Anderson is significantly younger and appears to reflect substantial post-emplacement mobility of Rb and/or Sr. The initial $^{87}Sr/^{86}Sr$ ratio from this isochron is 0.7405. K-Ar biotite and muscovite ages range from 97 Ma to 81 Ma. Biotite ages are older than muscovite ages for biotite-muscovite sample pairs from the same rock, suggesting possible post-intrusion disturbance of the K-Ar system. The younger range in K-Ar, Rb-Sr, and ^{39}Ar-^{40}Ar ages for the granites may partially reflect heat effects from the younger Tay River plutonic suite (see following).

Table 7. *Isotopic ages for Anvil plutonic suite (Mount Mye phase).*

Sample	UTM E*	UTM N*	Date± 2σ	System	Material	Interpretation	Reference
GAR-1	586 262	6 917 974	109.3±1.2 Ma	U-Pb	monazite	intrusion age	1
GAR-2	590 051	6 906 867	103.9±1.5 Ma	U-Pb	monazite	intrusion age	1
GSC92-39	598 492	6 916 106	100.6±1.3 Ma	^{40}Ar-^{39}Ar	muscovite	intrusion alteration age	2
GSC92-40	598 492	6 916 106	101.1±1.1 Ma	^{40}Ar-^{39}Ar	muscovite	intrusion alteration age	2
9088	593 636	6 909 787	100.9±2 Ma	Rb-Sr	whole rock - mineral	intrusion cooling age	3
GSC65-41	579 549	6 925 261	92±5 Ma	K-Ar	biotite	intrusion cooling age	4
GSC65-42	601 172	6 907 266	81±6 Ma	K-Ar	muscovite	intrusion cooling age	4
GSC65-43	601 172	6 907 266	89±5 Ma	K-Ar	biotite	intrusion cooling age	4
GSC70-45	589 944	6 907 127	96±5 Ma	K-Ar	muscovite	intrusion cooling age	5
GSC70-46	589 944	6 907 127	97±5 Ma	K-Ar	biotite	intrusion cooling age	5

References: 1 = This report (see Appendix III); 2 = Mortensen and Ballantyne (1992); 3 = Pigage and Anderson (1985); 4 = Wanless et al. (1967); 5 = Wanless et al. (1972)
*NAD83 UTM coordinates, zone 8

Tay River plutonic suite

The Anvil plutonic suite is cross-cut by unfoliated plutons, dykes and sills of biotite-hornblende granodiorite to granite composition (Fig. 56) that are part of the Tay River plutonic suite (Mortensen et al., 2000). Accessory minerals in these intrusions include apatite, zircon, allanite, tourmaline, and rare monazite. Biotite is pleochroic with dark chocolate brown colours. Hornblende also has strong absorption colours ranging from pale green-brown to deep olive or brownish green. Locally clinopyroxene is associated with hornblende.

This unit occurs as a large intrusive body at the northwest end of Anvil Batholith, and constitutes the entire Orchay Batholith. It also occurs as smaller dykes and sills which are commonly elongate in an east to northeast direction. It forms a moderately large dyke at the northwest end of the Faro open pit. Intrusive dykes that are correlated with the Tay River suite have also been noted in the metasedimentary units that underlie Rose Mountain (Rose Mountain formation and Campbell Range formation).

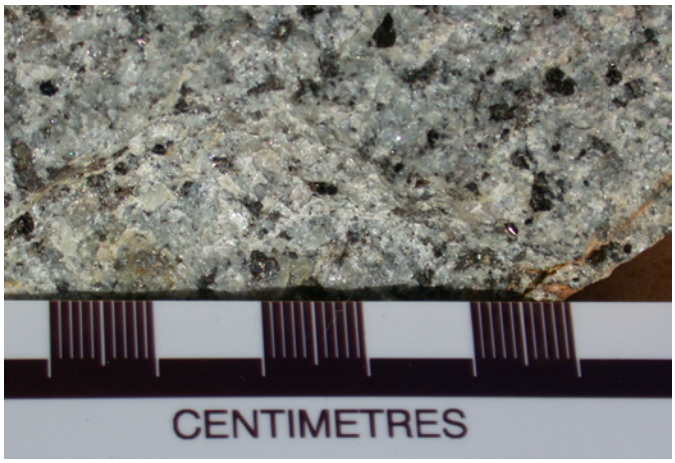

Figure 56. *Tay River plutonic suite. Equigranular biotite-plagioclase-K-feldspar-quartz granite. Sample from northwest wall of Faro open pit.*

Marginal contacts are sharp and cross-cut compositional layering of the enclosing metasedimentary rocks. Locally, the intrusions contain a marginal phase consisting of unoriented, large, dark green hornblende and smaller white feldspar phenocrysts in a dark grey aphanitic matrix. Alteration of this fine-grained marginal phase of the intrusions is common.

Large bodies of the Tay River plutonic suite are surrounded by a thin contact metamorphic aureole. Northwest of the Orchay Batholith, a large area of fine-grained hornfels is probably related to a shallowly buried extension of the batholith.

Tempelman-Kluit (1972) did not distinguish the medium- to coarse-grained, equigranular phase of this rock type from the Anvil plutonic suite and therefore considered the Tay River plutonic suite as part of his unit 11. He noted several examples of the porphyritic marginal phase of the Tay River suite occurring as dykes within the batholith on the south slopes of Mount Mye and mapped them as unit 13. Pigage and Anderson (1985) described and classified this unit as the Orchay phase of the Anvil plutonic suite. Some of the geochemical and petrographic features of the Orchay phase suggest I-type affinities (Pigage and Anderson, 1985). This suite is less radiogenic than the above Anvil plutonic suite, with an

Table 8. *Isotopic ages for Tay River plutonic suite in the Anvil District.*

Sample	UTM E*	UTM N*	Date±2σ	System	Material	Interpretation	Reference
A098	591 185	6 906 521	98.6±0.2 Ma	U-Pb	zircon	intrusion age	1
AR4	563 471	6 937 050	95.3±1.3 Ma	U-Pb	monazite	intrusion age	1
GGA-85-30F1	628 325	6 913 200	97.4±0.2 Ma	U-Pb	zircon	intrusion age	6, 7
AR2	559 020	6 926 786	61±1.5 Ma	Rb-Sr	whole rock - mineral	intrusion cooling age ?	2
AR14,15,17	619 732	6 889 800	99±2.5 Ma	Rb-Sr	whole rock isochron	intrusion cooling age	2
AR14,15,17	622 164	6 909 167					
GSC72-32	584 102	6 915 503	101±4 Ma	K-Ar	biotite	intrusion cooling age	3
GSC90-62	622 145	6 890 726	89.3±9.9 Ma	K-Ar	biotite	intrusion cooling age	4
GSC90-66	622 145	6 890 726	97.8±3.4 Ma	K-Ar	hornblende	intrusion cooling age	4
GSC92-36	578 083	6 918 002	96.7±1.0 Ma	^{40}Ar-^{39}Ar	biotite	intrusion cooling age	5
GSC92-37	583 873	6 915 604	95.6±1.0 Ma	^{40}Ar-^{39}Ar	biotite	intrusion cooling age	5

References: 1 = This report (see Appendix III); 2 = Pigage and Anderson (1985); 3 = Wanless et al. (1973); 4 = Hunt and Roddick (1991); 5 = Hunt and Roddick (1992); 6=Breitsprecher et al., 2002; 7 = Gordey and Mortensen, unpublished data
*NAD83 UTM coordinates, zone 8

initial ^{87}Sr/^{86}Sr ratio of 0.7161 (Pigage and Anderson, 1985). Gordey and Irwin (1987) classified the Tay River suite as a hornblende-bearing phase of the Selwyn Plutonic Suite. Recent regional studies by Mortensen et al. (2000) have indicated that intrusive rocks of similar age, geochemistry and mineralogy are more extensive in eastern Yukon Territory than previously thought; consequently they reclassified this intrusive rock type as the Tay River plutonic suite.

Table 8 lists isotopic age data for Tay River plutonic suite samples in the Anvil District. Three samples have been dated by U-Pb methods. Sample A098 gives a U-Pb zircon age of 98.6±0.2 Ma, sample AR4 gives a U-Pb monazite age of 95.3±1.3 Ma, and sample GGA-85-30F1 gives a U-Pb zircon age of 97.4±0.2 Ma. All of these ages are interpreted to be crystallization ages for separate bodies of the suite. Most of the K-Ar and ^{40}Ar-^{39}Ar dates in Table 8 indicate intrusion and cooling in the 96-98 Ma range. This age range and initial ^{87}Sr/^{86}Sr is consistent with that for other Tay River suite intrusions farther to the east. It is also similar to the mid-Cretaceous South Fork volcanics, indicating that the Tay River suite is the intrusive equivalent of the South Fork volcanics (Mortensen, personal communication, 2001). Overlap of ages for the U-Pb, K-Ar, and ^{40}Ar-^{39}Ar dates denotes rapid intrusion and cooling for this plutonic suite. Sample AR2 gives an unusually young Rb-Sr whole rock-mineral isochron (61 Ma), suggesting substantial post-emplacement mobility of Rb and/or Sr.

Table 9. *Isotopic ages for Eocene quartz-feldspar porphyry in the Anvil District.*

Sample	UTM E*	UTM N*	Date±2σ	System	Material	Interpretation	Reference
LP99-228	601 176	6 924 097	55.8±0.1 Ma	U-Pb	zircon	intrusion age	1
LP98-22	597 124	6 905 694	53.8±0.2 Ma	U-Pb	zircon	intrusion age	1
GSC90-58	601 548	6 924 228	54.3±1.2 Ma	K-Ar	whole rock	intrusion age	2

References: 1 = This report (see Appendix III); 2 = Hunt and Roddick (1991)
*NAD83 UTM coordinates, zone 8

Figure 57. *Eocene quartz-feldspar porphyry. Flow-banded with scattered clear and grey quartz phenocrysts. Field station 99LP228. Penny is 1.9 cm across.*

Figure 58. *Eocene quartz-feldspar porphyry. Smokey quartz and small white feldspar phenocrysts. Sample from northeast wall of Faro open pit. Penny is 1.9 cm across.*

Eocene quartz-feldspar porphyry

Small dykes and intrusive plugs of opaque white-weathering, aphanitic, quartz-feldspar porphyry are scattered throughout the District. The largest of these occurs as a small rhyolitic plug north of Mount Mye (601 340 E, 6 924 220 N – Plate 10). This plug is crudely circular in plan with a diameter of 700 m. It contains concentric flow banding, delineated by millimetre-scale white laminae (Fig. 57). The porphyry contains sparse white K-feldspar phenocrysts and abundant smokey grey and clear quartz phenocrysts. Quartz phenocrysts are typically slightly to moderately embayed. Biotite is disseminated in the matrix. Radiating K-feldspar crystallites in the matrix suggest devitrification from glass.

Small dykes are associated with zones of faulting on the south side of Anvil Batholith. Typically, these dykes contain dark smoky grey quartz phenocrysts in a clay-weathered, pale tan, aphanitic matrix (Fig. 58). Examples occur on the northeast side of the Faro pit, and between the Grum and Vangorda deposits.

Tempelman-Kluit (1972) mapped these igneous bodies as unit 14. Gordey and Irwin (1987) classified them as unit Tv. Pigage and Anderson (1985) tentatively correlated smoky quartz-feldspar porphyry dykes in the Faro mine area with the Marjorie phase of the Anvil plutonic suite. Geochronological studies clearly indicate that this correlation is wrong, and the dykes must be considered as part of the Eocene intrusive activity.

Table 9 lists isotopic ages that have been completed for this porphyritic unit. All dates indicate an early Eocene age of intrusion. Complete overlap of the U-Pb and K-Ar dates indicates quenching of the porphyry during intrusion. This quenching is consistent with extrusive flow-banding textures and partially embayed quartz phenocrysts. Although volumes of Eocene intrusive and extrusive rocks are small, distribution of the porphyries is widespread throughout the Anvil District.

STRUCTURE

INTRODUCTION

The Anvil District is complexly polydeformed and polymetamorphosed. Jennings and Jilson (1986) documented five deformation phases within the District. The first two phases (D_1 and D_2) are most important in that they are regionally developed and accompanied by regional structural fabrics. D_1 and D_2 folding was coaxial and trends northwest-southeast with a type 3 interference pattern (Ramsay, 1967). Major differences in axial planar cleavage orientations and vergence sense between D_1 and D_2 minor structures indicate a change in orientation of maximum compressive stress from horizontal (D_1) to vertical (D_2) for these two deformation phases. The remaining deformation events (D_3-D_5) are only locally developed and have not been correlated throughout the District, although one of these later deformation events had important influences on mining of the Faro deposit. Regionally, northeast-verging thrust faults have been documented as a significant feature of the D_1 deformation phase (Gordey and Irwin, 1987; Jennings and Jilson, 1986). Different studies have identified significant differences in the number of thrust faults and the extent of displacement for each fault.

Stratigraphic units in the District are domed to form a northwest-trending structural culmination called the Anvil Arch (Tempelman-Kluit, 1972) which is cored by the mid-Cretaceous plutons of the Anvil and Tay River plutonic suites. Metamorphic grade decreases radially away from the granites in the core of the Arch. Metamorphic intensity near the plutonic core reaches middle amphibolite facies, although much of the District has only undergone lower greenschist facies metamorphism.

D_1 DEFORMATION (FOLDING)

A pervasive planar fabric (S_1) defined by alignment of micas and chlorite in phyllites and schists was recognized and described by Tempelman-Kluit (1972). He was unable to substantiate any folds related to this S_1 fabric and speculated that it may have formed parallel to S_0 (primary depositional bedding) rather than being deformation related. Jennings and Jilson (1986) confirmed the presence of small scale D_1 minor folds, with S_1 being a pervasively developed axial planar cleavage, and large-scale D_1 macroscopic folds being locally responsible for distribution of mineralization at the Grum deposit. They also noted that D_1 folds are not commonly observed. Figure 59 illustrates a small D_1 minor fold overprinted by later coaxial D_2 minor folds. This D_1 minor fold is located over the Dy deposit and was also shown by Jennings and Jilson (1986; Fig. 21a). It occurs adjacent to a large mafic intrusive sill within the Vangorda formation; possibly part of the reason it is so well preserved is because it is located in a pressure strain shadow related to the more competent rock of the sill. Rare D_1 minor folds are visible in drill core (Fig. 60). Figure 61 shows a D_1 minor fold observed

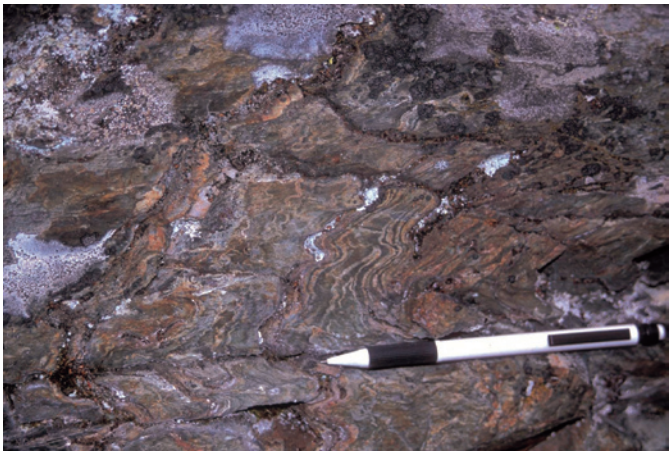

Figure 59. *Small D_1 fold in Vangorda formation adjacent to Ordovician-Silurian gabbro sill. Outcrop located in Dy/Grizzly deposit area. D_1 axial plane is near vertical. Re-folded by near-horizontal D_2 minor fold. Pencil (14 cm long) is oriented parallel to the S_2 axial planar crenulation cleavage.*

Figure 60. *D_1 minor fold defined by siltstone bed in Vangorda formation. Drill hole 76X-11, 72 ft (22 m). Drill hole located in Dy/Grizzly deposit area. NQ-size core.*

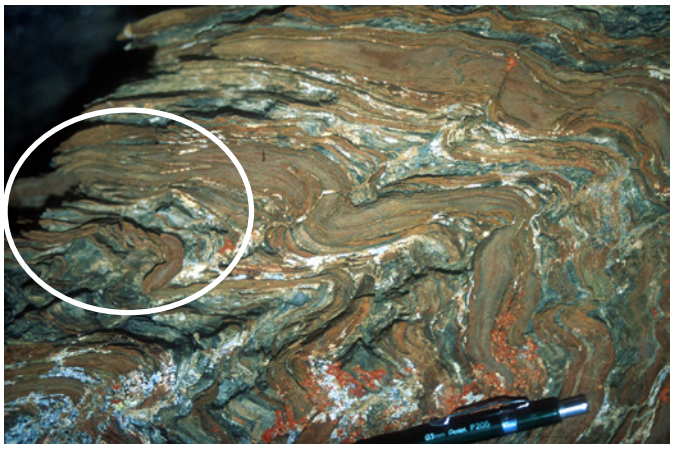

Figure 61. *D_1 minor fold in silty limestone beds, Vangorda formation. Fold closure visible on left side of photo. Field station 98LP164.*

Figure 62. *Macroscopic northeast-verging, D_1 minor fold on northeast slope of Rose Mountain. Looking north, person is standing in steep limb. Beds in upper left and lower right parts of picture are structurally upright. Field station 99LP164.*

in outcrop northeast of the Anvil Batholith. Figure 62 is a small D_1 minor fold on the northeast slope of Rose Mountain. All observed D_1 minor folds on both northeast and southwest sides of the Anvil Batholith are steep to upright and have northeast vergence.

More commonly, outcrops contain L_1 intersection lineations caused by the overprinting of S_0 bedding by S_1 slaty cleavage. L_1 lineations dominantly plunge gently northwest and southeast. In the Rose Mountain area, some of the L_1 lineations plunge gently to moderately to the southwest. Most measurements have been in the area of extensive exploration activity on Vangorda Plateau.

Only a few macroscropic D_1 folds have been recognized in the District. These all occur southwest of the Anvil Batholith. Rees (1989) interpreted a small northeast-verging D_1 fold northwest of the Faro deposit largely on the basis of repetition of stratigraphy at the base of the Vangorda formation. Detailed definition drilling for the Grum deposit confirmed the presence of a large macroscopic D_1 anticline-syncline pair outlined by ore horizons (see Jennings and Jilson, 1986, Fig. 33). This compilation has outlined an anticline-syncline pair occurring southeast of Shrimp Lake and southwest of the Grum and Vangorda deposits.

D_1 DEFORMATION (THRUST FAULTS)

The Ordovician-Silurian Menzie Creek formation has been structurally thrust northeast over Devonian-Carboniferous Earn Group along the northeast margin of the map area. Gordey and Irwin (1987) and Gordey (1990a,b,c) interpreted this fault as the gently dipping Faro thrust and recognized it on both the northeast and southwest sides of the batholith (it is eroded over the Anvil Arch). In this report this thrust is tentatively correlated with the Twopete thrust of Gordey and Irwin (1987).

Near the batholith, the Faro thrust as mapped by Gordey and Irwin (1987) separates greenschist facies phyllites of Vangorda formation from amphibolite facies Cambrian-Ordovician calc-silicate rock on both northeast and southwest sides of the batholith. Detailed geological mapping and drill core logging southwest of Anvil Batholith has indicated the Faro thrust in that area can be interpreted as a metamorphic transition from calcareous phyllites to calc-silicate rock within the Vangorda formation (Jennings et al., 1978a,b; Rees, 1989). On the northeast side of the batholith Pigage (2000a) suggested that for one area the interpreted Faro thrust actually represents interbedding of dark Duo Lake Formation shales and Menzie Creek formation basalts rather than

thrusting of volcanic rocks over the carbonaceous shales. For these reasons the structural interpretation presented in this report excludes the Faro thrust.

The most significant northeast-verging thrust faults occur on the southwest margin of the Anvil District. Figure 63 illustrates the differing structural-stratigraphic interpretations for the Rose Mountain area on the southwest margin of the District. Based on regional considerations, Tempelman-Kluit (1979a,b), Gordey and Irwin (1987), and Gordey (1990b) interpreted several major thrust faults stacking Nisutlin and Anvil allochthon rocks of the Yukon-Tanana Terrane over ancient North American sedimentary rocks. In contrast, Jennings and Jilson (1986) considered the ultramafic rocks an allochthonous ophiolite wedged between Yukon-Tanana Terrane and ancient North America along steep faults forming the Vangorda fault zone. They described a structurally and stratigraphically continuous sequence of lithologies on the northeast flank of Rose Mountain and the difficulties of inserting a thrust fault within that sequence. In spite of the difficulties, they proposed a major thrust within the sequence, separating coarse clastic rocks considered to be deformed Earn Group of North American affinity, from overlying Anvil Range Group basalts, ultramafic rocks, and cherts of allochthonous origin. Pigage (1999) re-iterated the difficulty of locating a thrust fault within this sequence and suggested the entire sequence may have North American affinities.

Recent regional mapping in the Finlayson Lake area to the southeast (Murphy et al., 2002) delineated a Paleozoic coarse clastic sequence within Yukon-Tanana Terrane that has been thrust northeastward over North American lithologies. Ultramafic rocks are shown to be intrusive into Paleozoic basalt flows, and both mafic and ultramafic lithologies are interpreted to be part of the Slide Mountain Terrane. Extrapolation of their units and structural relations into the Rose Mountain area indicates the basal northeast-directed thrust emplacing Yukon-Tanana Terrane and Slide Mountain Terrane over North American lithologies is located at the base of the Mount Aho formation. The Mount Aho and the Rose Mountain formations correlate with their Fortin Creek group, and the Campbell Range formation correlates with their Campbell Range succession. This basal thrust fault is not exposed anywhere in the Anvil District. The Vangorda fault zone is interpreted in this report to be a later extensional fault.

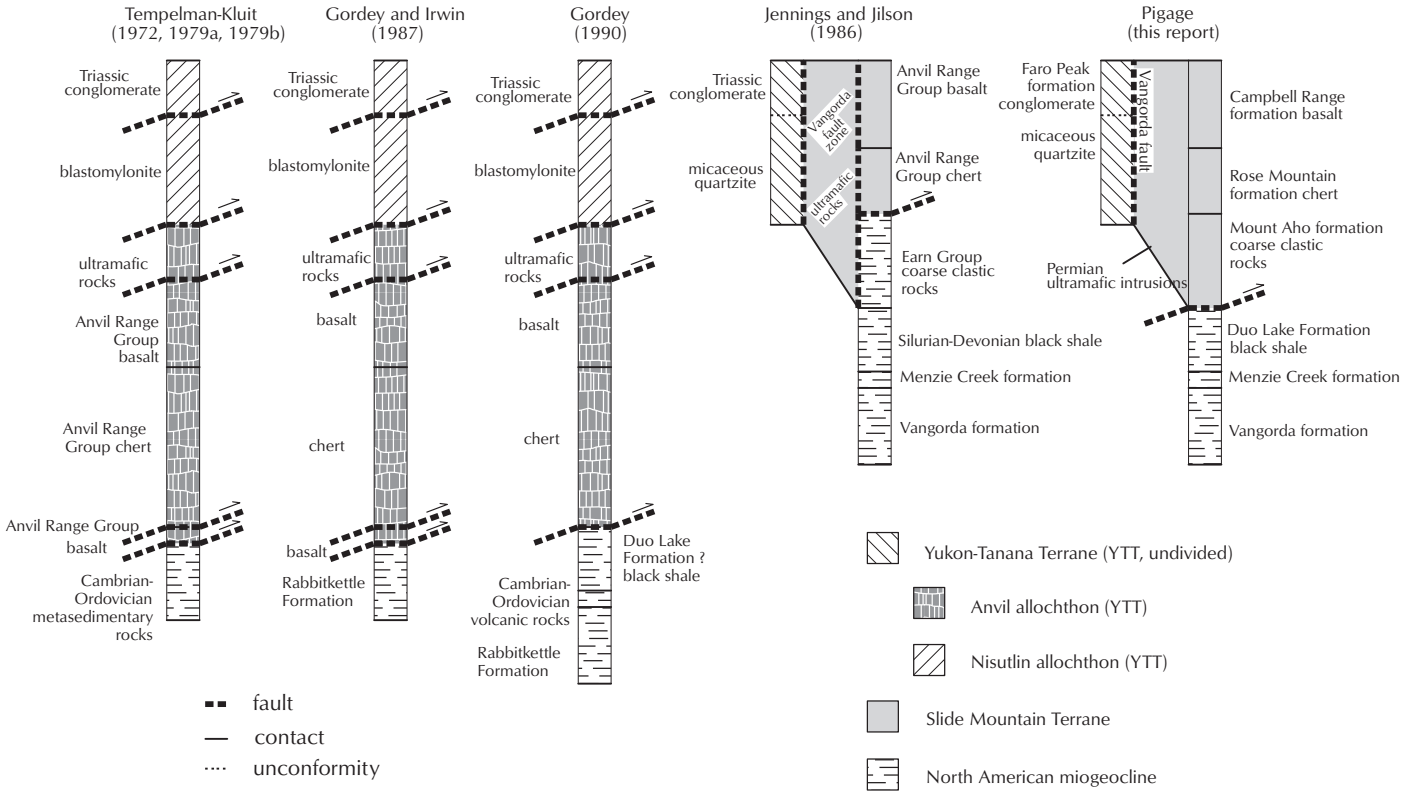

Figure 63. *Comparison of recent interpretations of stratigraphy and structure in the Rose Mountain area.*

D_2 DEFORMATION (FOLDING)

The predominant fabric in most of the Anvil District is a gently dipping axial planar crenulation cleavage (S_2) formed during the D_2 deformation. The S_2 cleavage is domed over the northwest-trending Anvil Arch (Tempelman-Kluit, 1972). To the southwest of the arch axis, it generally dips moderately to gently to the southwest; northeast of the arch axis, it generally dips moderately to gently to the northeast. Local dip reversals, however, are present in each of these domains.

The arch axis is also a locus for reversal in vergence of the D_2 minor folds. On the southwest side of the arch axis, D_2 minor folds consistently have a southwest vergence. On the northeast side of the arch axis, D_2 minor folds have a northeast vergence. The arch axis represents a D_2 structural culmination with folds cascading off of the Anvil Arch to the southwest and northeast.

The D_2 structures are most intensely developed in the core of the Anvil Arch. D_2 folds immediately adjacent to the mid-Cretaceous intrusions are tight to isoclinal (Fig. 13) with long straight limbs. L_2 minor fold axes and intersection lineations plunge northwest and southeast. The S_2 axial planar crenulation cleavage is very closely spaced, and earlier fabrics are not readily visible, even with a hand lens. The S_1 pervasive fabric and the S_0 primary depositional bedding have been strongly transposed into a subparallel orientation. These earlier fabrics are also subparallel with the S_2 axial planar crenulation cleavage. D_1 minor folds are not visible. These areas also correspond to the highest metamorphic grades, generally with mica schists in the amphibolite facies of metamorphism. Smith and Erdmer (1990) have detailed the relict S_1 fabric preserved in microlithons and inclusion trails of metamorphic porphyroblasts, forming and growing during the D_2 deformation and metamorphism immediately adjacent to the Anvil Batholith.

Both deformation intensity and metamorphic grade decrease farther away from the core of the Anvil Arch. D_2 minor folds are more open with rounded hinges and a well developed, spaced, axial-planar crenulation cleavage (Fig. 14). M_2 metamorphism ranges from lower to upper greenschist facies. The earlier D_1 pervasive axial planar cleavage occurs as well developed microlithons between the thin S_2 cleavage zones. D_2 deformation fabric and minor folds are also readily visible in drill core (Figs. 15, 64). S_0 primary bedding and S_1 axial planar cleavage are transposed into subparallelism. These earlier fabrics, however, can be clearly discerned and have a different overall orientation than the S_2 crenulation cleavage. On both sides of the Anvil Arch, the earlier S_0 and S_1 fabrics dip more steeply away from the arch axis than the S_2 fabric. D_2 minor folds are common on an outcrop scale. One larger D_2 fold has been delineated at the Grum deposit through exploration and development drilling (see cover of bulletin and section A-B on Plate 11). This fold has a frequency of 180 m and a half-amplitude of approximately 160 m.

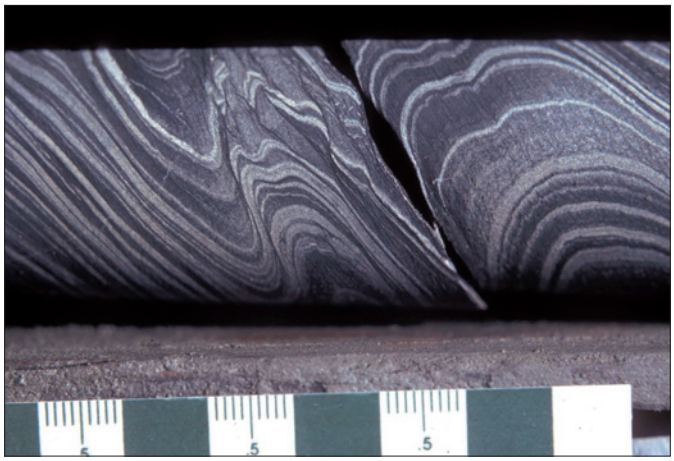

Figure 64. *D_2 minor fold in Vangorda formation. S_2 axial plane crenulation cleavage dips steeply to right in picture. NQ-size core. Drill hole 72X-23, 84 ft (26 m).*

Intensity of the D_2 fabric decreases with increasing lateral distance from the Anvil arch axis. In the area around Rose Mountain, for example, the S_2 fabric is not readily visible. However D_2 minor folds and axial planar crenulation cleavage are well developed in unit PYq immediately north of the town of Faro in outcrops on Vangorda Creek (Fig. 65).

The gentle to moderately dipping orientation of the D_2 crenulation cleavage and the gentle plunge of D_2 minor folds constrain the maximum compressive stress during deformation and metamorphism to be oriented vertically. The close association of decreasing D_2 deformation intensity away from the axis of the Anvil Arch, the presence of D_2 deformation textures in the Anvil Batholith, and the reversal in vergence of D_2 minor structures over the Anvil Arch, all indicate that D_2 deformation is caused by intrusion of the Anvil plutonic suite (with the locus of intrusion being along the Anvil Arch). Vertical-directed compressive stress could be modeled as resulting from buoyant intrusion of the Anvil plutonic suite.

Figure 65. *D_2 minor fold with incipiently developed S_2 axial-planar crenulation cleavage, micaceous quartzite in Yukon-Tanana Terrane. Field station 99LP149. S_2 fabric parallel to handle of rock hammer.*

Figure 66. *Extensional fault rock, Vangorda Plateau. Clasts of quartz vein and highly altered mafic gabbro dyke in sheared and gouged carbonaceous phyllite fault rock matrix. NQ size core. Drill hole 81VX-01, 395-400 m.*

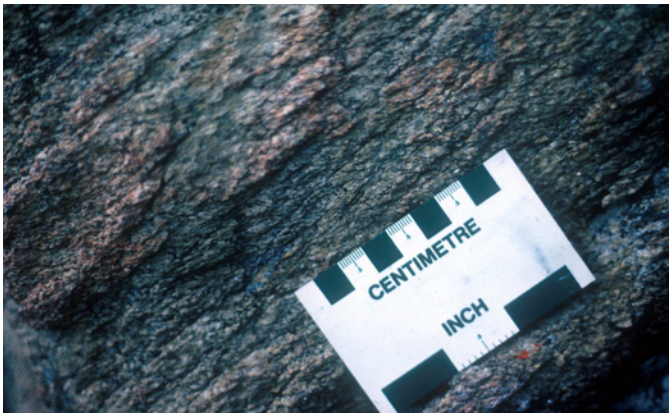

Figure 67. *S-C banding in Anvil Batholith in immediate footwall of Tie fault. S-foliation dips gently to west. C-bands are parallel to edge of scale card. Field station 84-4.*

D_2 DEFORMATION (NORMAL FAULTS)

Regional-scale extensional faults on the southwest side of Anvil Batholith have been delineated through detailed property geology mapping (Pigage and Jilson, 1985; Bradford, 1989). The best documented of these faults is the Tie fault which truncates the northwest end of the Grum deposit. The Tie fault has been mapped for a strike length of 6 km, is up to 150 m thick, and has a minimum displacement of 1 km on the fault surface. It juxtaposes rocks of amphibolite facies metamorphic grade in the footwall, against phyllites of lower greenschist facies metamorphic grade in the hanging wall. In drill core, the fault zone consists of highly sheared, carbonaceous phyllite containing an irregular, slickensided and polished, anastamosing planar fabric. Irregular, angular clasts of quartz-carbonate-altered gabbro and vein quartz are abundantly scattered through the carbonaceous phyllite. In outcrop, metamorphic rocks and granite extending away from the fault zone for a distance of almost 1 km, contain a shear banding or S-C banding texture which gradually fades with increasing distance from the fault. The S-C banding is developed exclusively in granites of the Anvil plutonic suite; granitic rocks of the Tay River plutonic suite are unfoliated. Orientation of shear banding textures is consistent with the 'upthrown' side of the fault being on the northern high metamorphic grade and granite side of the fault with the hanging wall displacement being in a south direction (approximately 180° azimuth). Figure 66 illustrates a typical extensional fault in drill core, and Figure 67 shows S-C banding developed in Anvil Batholith in the immediate footwall of the Tie fault.

Drilling under the Dy/Grizzly deposit has confirmed the existence of another extensional fault with similar textures that truncates the northwest extension of the Dy deposit. Jennings and Jilson (1986) also suggested the possibility of a similar extensional fault underneath the Swim deposit, based on extensive fault gouge intersected in several drill holes. A southwest-northeast oriented cross section through the Swim deposit suggests however, that the gouge in the Swim holes is not related to an extensional fault with major displacement.

Jennings and Jilson (1986) described the occurrence of similar faults on the northeast side of Anvil Batholith, including their "Graphite fault." The "Graphite fault" was interpreted on the basis of a change in S_2 orientation and apparent truncation of stratigraphy and metamorphic isograds across the fault. The author was unable to discern shear band or gouge textures within the graphitic phyllite demarcating the "Graphite fault" in either outcrop or thin section. The Graphite fault is therefore re-interpreted in this report as a stratigraphic carbonaceous phyllite unit within the Mount Mye formation.

These extensional faults are clearly post-metamorphic because they truncate and displace metamorphic isograds. However, movement along the fault was occurring while rocks were still at pressure-temperature conditions suitable for coherent recrystallization during displacement. Shear band textures within the fault zones have the same orientation as the S_2 crenulation cleavage in rocks adjacent to the fault zones. These different metamorphic and structural relations denote that the extensional faults are late D_2 features and represent the last deformation event related to D_2 vertical compressive deformation. Extensional faults may be related to gravitational collapse of the metasedimentary and intrusive rock pile with buoyant intrusion and uplift centred along the northwest-southeast axis of the Anvil Arch. Uplift was apparently asymmetric with the southwest side of the Arch being uplifted to a greater extent (and thereby developing extensional faults). Faulting displacement for the best documented extensional faults is in a southerly direction which is not symmetric with the northwest trend of the Arch.

METAMORPHISM

D_1 and D_2 deformation minor structures have associated axial planar structural fabrics defined by aligned metamorphic minerals. Metamorphic grade indicated by mineral associations ranges from muscovite-chlorite zone of greenschist facies to garnet-biotite-sillimanite-muscovite zone of amphibolite facies (Tempelman-Kluit, 1972; Jennings and Jilson, 1986; Smith and Erdmer, 1990). Metamorphic grade decreases radially outward from a central metamorphic welt, cored by the Anvil Batholith. Metamorphic grade also decreases outward away from Orchay pluton and the small pluton northwest of Rose Mountain. Large areas of hornfels northwest of Orchay pluton and schist near Swim Lakes indicate the probable presence of shallowly buried intrusions in those areas.

In pelites of the Mount Mye formation, Smith and Erdmer (1990) documented a sequence of isograds marked by the first appearance of biotite, andalusite, staurolite, garnet and fibrolite, progressing inward toward the Anvil Batholith intrusive contact. In the maps presented with this report, a single 'pseudo-isograd' in the pelites has been indicated by an approximate line marking the transition from fine-grained phyllite to coarse-grained schist. This transition is gradational, but occurs rapidly over a very short distance. It crudely corresponds to the garnet-in isograd as mapped by Smith and Erdmer (1990).

A similar transition occurs in calcareous rocks of the Vangorda formation. Calcareous muscovite-chlorite phyllites undergo a rapid transition to calc-silicate rock with appearance of biotite, diopside and epidote. The resulting calc-silicate rock is very distinctive with a prominent green and brown striping on a scale of millimetres to centimetres. The brown color is related to the presence of abundant biotite in the pelitic bands, and the pale green color is caused by diopside and epidote growing in the calcite-quartz siltstone bands in phyllites of lower metamorphic grade. Colour striping, hardness and density differences between calc-silicate rock and calcareous phyllites are so extensive that the correlation of Vangorda formation lithologies across this metamorphic transition was not recognized for some twenty years after geological mapping was initiated in the District (Jennings and Jilson, 1986). This metamorphic transition occurs at slightly lower metamorphic grade than the phyllite to schist transition.

Metamorphic micas defining S_1 lithons within the S_2 crenulation cleavage have the same mineralogy as the S_2 cleavage. Jennings and Jilson (1986) suggested that M_1 and M_2 metamorphisms therefore have comparable pressure-temperature ranges and distributions. Smith and Erdmer (1990) provided convincing textural and paragenetic evidence that textures and mineral assemblages recorded in the pelites are related solely to the D_2 deformation and M_2 metamorphism. Brown (1994) analysed chlorites from S_2 cleavage planes and S_1 microlithons near the Vangorda deposit by electron microprobe and found no difference in composition. He interpreted the similar compositions as indicating the S_1 chlorites had been overprinted and re-equilibrated during the M_2 metamorphism, and did not contain any information concerning P-T conditions during the M_1 metamorphism. The following discussion on metamorphic conditions follows this inference and considers all pressure-temperature conditions as relating solely to the M_2 metamorphism.

The absence of kyanite in the pelite mineral assemblages constrains metamorphic conditions to being at lower pressures than the aluminosilicate triple point (approximately 4 kilobars). Figure 68 illustrates the range of conditions for M_2 metamorphism in Anvil District on a pressure-temperature bathozone diagram (Carmichael, 1978). An upper temperature limit is provided by the second sillimanite isograd reaction, marking the breakdown of muscovite to form fibrolite which does not occur in the Anvil District. M_2 metamorphism corresponds to the low pressure bathozones 2 or 3. Classic areas containing similar metamorphic grades are Buchans (bathozone 2) and the Pyrenees (bathozone 3).

Smith and Erdmer (1990) estimated metamorphic pressure conditions using the plagioclase-garnet-aluminosilicate-quartz geobarometer (Ghent et al., 1979) and metamorphic temperatures using the Ferry-Spear biotite-garnet geothermometer (Ferry and Spear, 1978) for samples ranging in metamorphic grade from biotite zone through sillimanite zone. The resulting estimates ranged from 2.8 to 6.5 kilobars and 509° to 872° Centigrade. When combined with petrogenetic restrictions based on experimental studies, they concluded metamorphic pressures were 3 kilobars with temperatures ranging up to 600°-620°C adjacent to the Anvil Batholith.

Brown (1994) estimated metamorphic conditions for M_2 metamorphism in the Vangorda deposit from mineral assemblages in pelites and in sulphide mineral ore. The pelite mineral assemblage of the Vangorda deposit is muscovite-chlorite zone of greenschist facies. Using tetrahedral $Al_{(IV)}$ occupancy of chlorite grains (Cathelineau, 1988), a mean temperature of 363°C was calculated. This corresponded reasonably well with a mean temperature of 336°C calculated from the arsenopyrite-pyrite-pyrrhotite geothermometer using the calibration of Barton (1969). A mean pressure estimate of 4.0 kilobars was attained using sphalerite-pyrrhotite-pyrite geobarometer. These different pressure-temperature estimates for M_2 metamorphism are in reasonable agreement with temperatures and pressures inferred by Smith and Erdmer (1990) from petrogenetic grids and pelite geobarometers and geothermometers.

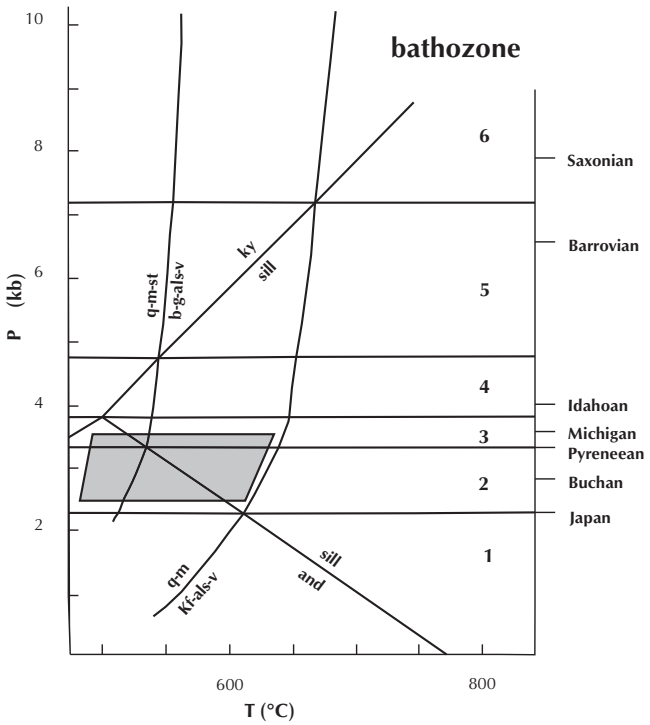

Figure 68. *Metamorphic pressure-temperature diagram for M_2 metamorphism, Anvil District. Bathozones from Carmichael (1978) are indicated. q = quartz, Kf = K-feldspar, als = aluminosilicate, m = muscovite, St = staurolite, b = biotite, g = garnet, v = vapour, ky = kyanite, sill = sillimanite, and = andalusite.*

AGE OF DEFORMATION AND METAMORPHISM

D_1 DEFORMATION AND M_1 METAMORPHISM

Timing of the D_1 deformation and accompanying M_1 metamorphism is poorly constrained. Compositional studies of D_1 aligned metamorphic chlorite from phyllites near the Vangorda deposit show that the M_1 chlorite has re-equilibrated during M_2 metamorphism and D_2 deformation (Brown, 1994). Any isotopic dating of metasedimentary rocks containing a well developed D_2 fabric, therefore, will generally result in M_2/D_2 ages. Initial attempts to date metasedimentary rocks with only a D_1 structural fabric (sample LP98-44, Mount Aho formation) or a weakly developed D_2 fabric (sample LP98-38, Vangorda formation) by ^{40}Ar-^{39}Ar were unsuccessful because the isotopic ages did not plateau with stepwise heating of the samples (see Figs. 69a and 69b: M. Villeneuve, personal communication, 2000).

Tempelman-Kluit (1972) originally postulated the D_1 deformation and M_1 metamorphism was pre-Devonian and possibly pre-late Ordovician because metamorphic effects were noted only in Ordovician and older rocks. Subsequently, Jennings and Jilson (1986) documented the presence of a D_1 structural fabric in Permian Campbell Range formation, constraining deformation and metamorphism to be uppermost Paleozoic or later. Triassic Faro Peak formation also contains a pervasive structural fabric with an orientation consistent with the D_1 fabric in Paleozoic metasedimentary rocks immediately to the northeast, suggesting D_1 deformation postdates late Triassic.

The regional development of minor folds, thrust faults, and pervasive structural fabrics in both Yukon-Tanana and ancient North American stratigraphic units supports the correlation of D_1 structures with convergence of Yukon-Tanana Terrane against ancestral North America. Structural relations in Anvil District indicate a maximum post-Triassic age for this convergence. Similar maximum ages are required in the Finlayson Lake area to the southeast by thrusting of Yukon-Tanana stratigraphy over Triassic North American stratigraphy (Murphy et al., 2002).

D_2 structures and M_2 metamorphism clearly cross-cut and are later than the D_1/M_1 deformation and metamorphism. Timing for D_2/M_2 therefore provides a minimum age for the D_1/M_1 event. As will be shown in the following section, the age of D_2/M_2 is between 110 Ma and 96 Ma. The D_1/M_1 deformation and metamorphism must therefore be older than mid-Cretaceous.

Extensive radiometric dating of eclogite lenses (Pygre) in micaceous quartzites of Yukon-Tanana Terrane near Faro and Ross River has resulted in consistent Permian dates for the time of metamorphism leading to formation and isotopic closure of the eclogites (see Table 4). In central Yukon, radiometric dates for several eclogite

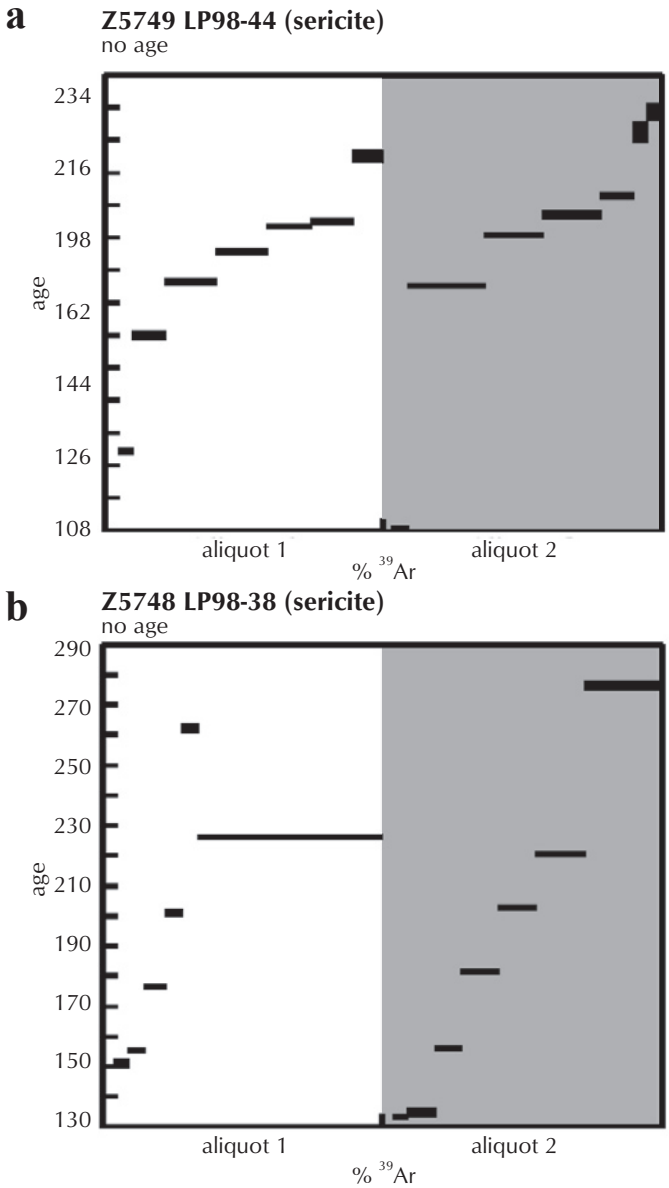

Figure 69. (a) *Ar release diagram for pale green phyllite, Mount Aho formation. Field station 98LP044.* ***(b)*** *Ar release diagram for pale grey phyllite, Vangorda formation. Field station 98LP038.*

localities within Yukon-Tanana Terrane rocks indicates multiple high pressure metamorphic events that range in age from Mississippian to Early Triassic (Erdmer et al., 1998). The Faro-Ross River eclogite radiometric dates cannot therefore be correlated with D_1 deformation and M_1 metamorphism since they apparently pre-date Triassic time.

D_2 DEFORMATION AND M_2 METAMORPHISM

Detailed mapping studies have all documented the strong correlation of D_2/M_2 deformation and metamorphism with intrusion of the Anvil plutonic suite (Pigage and Anderson, 1985; Jennings and Jilson, 1986; Smith and Erdmer, 1990). Metamorphic isograds are concentric around the Anvil plutonic suite. Anvil plutonic suite sills and the margins of the main Anvil Batholith are moderately to weakly foliated with a S_2 planar fabric. The D_2 structural fabric is most intensely developed in the core of the Anvil Arch which also marks the locus of the most extensive intrusion by the Anvil plutonic suite. Intrusion of the Anvil plutonic suite is synkinematic to late synkinematic. U-Pb dates of monazites from the Anvil plutonic suite have a crystallization date of 109 to 104 Ma. This provides a maximum age for the D_2/M_2 deformation and metamorphism.

In contrast, intrusions of the Tay River plutonic suite are unfoliated. Similarly, on the southwest side of Anvil Batholith, Tay River plutonic suite dykes and sills cross-cut and postdate late D_2 extensional faults. D_2/M_2 deformation and metamorphism must therefore predate intrusion of the Tay River plutonic suite. Radiometric dates of plutons from the Tay River suite range from 96 to 98 Ma. D_2/M_2 deformation and metamorphism must therefore occur before 96 Ma (early Late Cretaceous time). The minimum and maximum dates for D_2/M_2 constrain metamorphism and deformation to the time interval between 110 Ma and 96 Ma.

D_3-D_5 DEFORMATION AND METAMORPHISM

As documented by Jennings and Jilson (1986), D_3 through D_5 folding deformations are delineated by open folds accompanied by an axial planar crenulation cleavage. These textures are only locally developed. They must have formed while the rock was still hot enough to recrystallize metamorphic muscovite, chlorite, or biotite in an axial planar orientation. This implies that these deformations may be related to local stresses during waning stages of the D_2/M_2 deformation and metamorphism. The steep orientation of the crenulation cleavage and gentle plunge of the minor folds indicates main compressive stress during these local strain events reverted to a largely horizontal orientation.

NORMAL AND STRIKE SLIP FAULTS

Numerous strike-slip and normal slip faults have been documented in the District. Two orientations are dominant: north (azimuth 340°-025°) and northeast (azimuth 050°-090°). In most cases the faults are steep with small displacements. Drill holes through some of these faults have intersected mud gouge zones. In at least some instances, the faults offset the Tie fault and the Vangorda fault. Faulting is interpreted as being post-intrusion of the mid-Cretaceous Anvil and Tay River plutonic suites and may be related to extension and relaxation following intrusion of the plutonic suites. One small normal fault north of the Vangorda deposit offsets the Tie fault and contains a 55 Ma Tertiary quartz-feldspar porphyry dyke intruding along the trend of the fault zone. This places a loose age restriction on this particular fault as displacement occurring sometime between 110 and 55 Ma.

Jennings and Jilson (1986) suggested some of the faults may be subsidsidiary structures related to strike-slip displacement along the Tintina Fault. Orientation of the faults and sense of displacement however, is not always consistent with second or third order structures that would be expected to be associated with the Tintina Fault.

VANGORDA FAULT

The Vangorda fault (Tempelman-Kluit, 1972) juxtaposes Permian (?) ultramafic intrusive rocks and Permian Campbell Range formation basalts to the northeast, against Triassic Faro Peak formation and underlying Yukon-Tanana Terrane (YTT) quartzite to the southwest. Tempelman-Kluit (1972) postulated a complex fault history with northeast-directed reverse movement being followed by southwest-side down normal displacement. Jennings and Jilson (1986) considered the Vangorda fault to be a transpressive suture juxtaposing North American stratigraphy against Yukon-Tanana Terrane. In both interpretations, the fault would represent a structural boundary between major geologic terranes.

The restriction of the Triassic Faro Peak formation to the southwest side of the Vangorda fault is consistent with the fault being a southwest-dipping, normal fault with

the southwest side being downthrown. Extent of normal displacement is unknown but must be at least as much as the thickness of the Faro Peak formation (600 m). The Faro Peak formation contains clasts of Permian ultramafic intrusive rocks and YTT quartzites; possibly it represents proximal deposition of material eroding from the fault scarp. Normal fault movement is syn- to post-Triassic (Norian). This interpretation of the Vangorda fault as a normal fault refers to the latest displacement along the fault; it does not preclude the possibility that the fault may have had a long history with an earlier reverse sense of displacement.

TINTINA FAULT

Tintina Trench is a prominent topographic linear valley extending some 960 km from northwest to southeast through the Yukon (Roddick, 1967). The Trench is also the locus of a major northwest-trending, strike-slip fault, the Tintina Fault, juxtaposing dramatically different geology on southwest and northeast sides (Roddick, 1967). Roddick (1967) and Tempelman-Kluit (1970b) independently estimated right lateral strike-slip displacement of approximately 420 km across the fault. Roddick (1967) suggested most of the movement occurred in Late Cretaceous. Tempelman-Kluit (1970b) postulated most of the movement was in Late Cretaceous to early Tertiary. More recent studies confirmed the 420 km offset and proved the 65 Ma McQuesten plutonic suite was offset the same amount as earlier structures and geologic contacts, restricting displacement to post-Cretaceous time (Murphy and Mortensen, 2003).

COOLING, UPLIFT AND EROSION

Metamorphic assemblages of the coarse-grained schists around the Anvil plutonic suite denote a rock column of about 10 km overlying the present erosion surface during intrusion of the Anvil Batholith (see above). In contrast, the hornfels associated with the Tay River plutonic suite at the northeast margin of the map area suggests that these intrusions occurred at much shallower levels in the crust. The presence of large caldera-filling units of South Fork volcanics (coeval with the Tay River plutonic suite) immediately adjacent to the Orchay Batholith also indicates very shallow to near-surface depths of emplacement for Tay River intrusions. This extremely shallow level of intrusion is further supported by deposition of subaerial coarse clastic rocks in the Ross River area during the same time interval as Tay River suite intrusion (Long et al., 2001).

Smith and Erdmer (1990) suggested uplift and erosion of 10 km of cover rock in a 5-million-year interval between intrusion of the Anvil plutonic suite and eruption of the South Fork volcanics. The new isotopic ages for the Anvil and Tay River plutonic suites and correlation of Tay River plutonic suite with the South Fork volcanics allow revision of this estimate. With these considerations, uplift and erosion of the 10 km of cover rock over the Anvil Batholith probably occurred largely over the approximately 10-million-year-interval between 109 Ma and 97 Ma. The occurrence of near-extrusive flow-banding textures in the Eocene quartz-feldspar porphyry plug in the northeast part of the map area, further indicates that present erosion levels have not changed significantly since 97 Ma.

ECONOMIC GEOLOGY

INTRODUCTION

In 1953, prospector Alan Kulan staked mineral claims encompassing exposures of massive sulphide mineralized rock on the northwest bank of Vangorda Creek (Fig. 70) that had been brought to his attention by Ross River residents George Sterriah and Robert Etzel. He immediately optioned the claims to Prospectors Airways Company Limited. Diamond drilling done as a followup to extensive ground geochemical and geophysical surveys delineated the small zinc-lead-silver-barite massive sulphide Vangorda deposit. It was not developed at the time because of its small size, low metal prices, and the remoteness of the discovery. The orientation ground surveys (Chisholm, 1957) became benchmark studies for further exploration in the District.

Between 1965 and 1976, four additional zinc-lead-silver-barite massive sulphide mineral deposits were discovered in the area. Discovery of the Faro deposit in 1965 resulted in the largest staking rush in the Yukon to that time. Exploration in the District indicated an estimated 225 million tonnes of sulphide-bearing rock (Jennings and Jilson, 1986). Mining in the District began in 1969 and continued with interruptions until 1997.

These early exploration successes resulted in extremely focused exploration activity, directed towards the discovery of additional massive sulphide deposits. Yukon MINFILE occurrences within the Anvil District identify additional mineral deposit models relevant to the District (Deklerk, 2003). These include volcanic-hosted massive sulphide mineralization, sediment-hosted barite mineralization, and high-grade polymetallic quartz vein showings. The District presents fresh opportunities for discoveries unrelated to the massive sulphide bodies already outlined. In the following sections, the different types of mineral occurrences previously identified within the District are briefly presented.

Figure 70. *Discovery showing on Vangorda Creek. Exposed outcrop consists of highly weathered quartzose mineralization. Staked in 1953 by Al Kulan. Camera lens on left side of photograph is 49 mm across.*

SEDIMENTARY-EXHALATIVE (SEDEX) ZINC-LEAD-SILVER-BARITE MASSIVE SULPHIDE DEPOSITS

Table 10 lists the discovery dates and exploration methods leading to the discoveries of the known zinc-lead-silver-barite deposits in the District. The initial discovery of the Vangorda deposit utilized conventional prospecting. Early exploration successes (Swim, Faro, Grum) were based on anomalies defined by regional magnetic, electromagnetic, and gravity surveys. Follow-up on these regional surveys typically consisted of geology, ground magnetic and electromagnetic surveys, and geochemical surveys (Chisholm, 1957; Brock, 1973). Geophysical surveys in the District have been difficult to interpret because of the presence of carbonaceous metasedimentary rocks, greenstones, and widely variable overburden depth. However, the geophysical data is extremely informative when combined with independent geological control. With increased understanding of the geologic setting of the deposits, the discovery drill hole for Dy/Grizzly in 1976 was collared based on geological reasoning and constraints.

Table 10. *Discovery dates for SEDEX deposits, Anvil District.*

Deposit	Discovery date	Principal discovery method
Vangorda	1953	Conventional prospecting, confirmed by drilling in 1953
Swim	1964	Airborne magnetic/ground gravity, confirmed by drilling in 1965
Faro	1965	Airborne magnetic/ground electromagnetic, confirmed by drilling in 1965
Grum	1973	Gravity/airborne magnetic/geology, confirmed by drilling in 1973
Dy/ Grizzly	1976	Geology, confirmed by drilling in 1976

The zinc-lead-silver-barite pyritic massive sulphide deposits of the Anvil District have been classified as the SEDEX (sedimentary-exhalative) type (Carne and Cathro, 1982; Jennings and Jilson, 1986; Pigage, 1990). The deposits occur as single or multiple, stratiform horizons within a 150-m stratigraphic interval which straddles the geological contact between the Vangorda and Mount Mye formations. Their internal metal zonation, asymmetric facies, tabular and stratiform nature, and mineralogy are all consistent with this deposit type (see Jennings and Jilson, 1986; Pigage, 1990; Goodfellow et al., 1993). Detailed structural studies verify that mineralized horizons have experienced all the same deformation and metamorphism as the enclosing host metamorphosed sedimentary rocks (Brown, 1993; Brown, 1994; Brown and McClay, 1994) and are therefore probably syngenetic to diagenetic in origin.

A feeder or vent zone has not been identified in any of the five known deposits. These massive sulphide deposits however, occur along a northwest curvilinear trend suggesting a primary structural control on the depositional sites for mineralization (see Plates 1 and 2). This curvilinear trend also marks a change in thickness of the graphitic phyllites associated with the mineralized horizons, with the carbonaceous phyllites becoming significantly thinner northeast of the curvilinear trend.

The east portion of the Anvil District also contains two iron-rich disseminated sulphide mineral showings (SB and Sea, Yukon MINFILE 105K 043 and 105K 042, respectively; Deklerk, 2003) located along the curvilinear trend defined by the zinc-lead-silver-barite massive sulphide deposits and one additional showing northeast of Mount Mye (Ace, Yukon MINFILE 105K 034; Deklerk, 2003). These occurrences are dominated by pyrite-pyrrhotite-magnetite-chalcopyrite bands and stringers in strongly silicified Mount Mye formation phyllites. Locally, the phyllites contain abundant irregular chlorite-quartz-pyrrhotite stringers and veinlets.

Existing rotary and diamond drill hole collars within the Anvil District are clustered predominantly in the immediate vicinity of the known deposits (see 1:25,000-scale maps with collar locations, Plates 3-17). Much of the strike length of the geological contact between the Mount Mye and Vangorda formations has not been drill tested for down-dip occurrence of stratiform sulphide deposits. Even along the general trend between the different deposits, areas of incomplete drill hole coverage leave room for further deposits. Exploration potential remains high for additional SEDEX deposits within the District.

SEDIMENT-HOSTED BARITE DEPOSITS

Mount Aho formation contains several barite showings (Figs. 46 and 47) within a strike length of 9 km from multiple horizons (Yukon MINFILE 105K 106, Deklerk, 2003). Surface samples from several of the showings indicate the main impurity is quartz (Read, 1982). Thickness and grade variations, and down-dip extent of the best showings have not been delineated. No drilling has been completed anywhere along the strike extent of the baritic horizons.

POLYMETALLIC INTRUSION-RELATED QUARTZ VEINS

The northeast margin of the mid-Cretaceous Anvil Batholith (Anvil plutonic suite) contains polymetallic-precious metal-bearing veins and fracture-filled breccia bodies (Mortensen and Ballantyne, 1992; Yukon MINFILE occurrences 105K 051, 105K 052, 105K 053, Deklerk, 2003). Early exploration efforts were directed toward trying to link the vein occurrences with possible deeper pyritic massive sulphide mineralization. Starting in the mid-1980s exploration efforts on these occurrences were guided by intrusion-related vein and stockwork geologic deposit models. Zones of quartz veinlets and stockwork zones occur within the granite associated with strong, pervasive, sericitic alteration. Dating of the sericitic alteration at 100 Ma indicates veins and stockwork developed shortly after intrusion of the muscovite-biotite granite. Bedrock occurrences corresponding to spectacular mineralized glacial float boulders (Fig. 71) occurring along Ace High Creek have not been discovered to date.

Figure 71. *Float boulder of sulphide mineral breccia in Anvil plutonic suite granite. JRV property, Ace High Creek, north of Mount Mye.*

VOLCANIC-HOSTED MASSIVE SULPHIDE MINERALIZATION (VHMS)

Exploration in the interval 1966 to 1978 indicated the presence of low-grade zinc-mineralized rock in the Menzie Creek formation northeast of Anvil Batholith (Yukon MINFILE 105K 083, Deklerk, 2003). In drill core, disseminated sphalerite blebs and sphalerite-carbonate veinlets occur in both massive volcanic rocks and volcanic breccias. Sphalerite is coarsely crystalline and black in colour. Minor chalcopyrite is closely associated with the sphalerite. Pyrite and pyrrhotite locally occur in the veins. Rare galena occurs in coarse aggregates in cross-cutting quartz-carbonate veins. The mineralized area is strongly quartz-carbonate altered and has pale tan colour.

The mineralized interval has been compared with a feeder stockwork occurring beneath a massive sulphide black smoker formed on the seafloor. Present drilling has not delineated the extent of the mineralization. The presence of syngenetic mineralization within Menzie Creek formation opens other areas underlain by Menzie Creek basalts for exploration targets.

Campbell Range formation basalt represents an additional exploration target for stratiform massive sulphide mineralization. The recent discovery of a massive pyrite-chalcopyrite-bornite horizon on the Ice claims east of Ross River in correlative basalts also indicates Campbell Range formation is a favourable host for VHMS mineralization (Hunt, 1998).

SUMMARY

The Anvil District contains the most westerly off-shelf basinal facies of the Cordilleran miogeocline, a prism of sedimentary rocks of Precambrian to Jurassic age deposited along the relatively stable continental margin of western North America. The District is part of Selwyn Basin, a large area of central Yukon where deep water clastic rocks, chert, and minor carbonate accumulated along the ancient North American continental margin during late Proterozoic and early Paleozoic (Gabrielse, 1967). Northeast of the basin, a shallow carbonate platform formed the near-shore facies of ancient North America (Abbott et al., 1986). Anvil District is immediately northeast of the Yukon-Tanana Terrane and Slide Mountain Terrane, the most easterly of the allochthonous terranes (Coney et al., 1980).

Ancestral North American rocks, from Mount Mye formation through Earn Group, are documented for the District. Total interpreted present thickness of the metasedimentary rocks of North American affinity is greater than 7400 m. The depositional environment is interpreted to be an off-shelf marine basin, with locally euxinic carbonaceous shales indicating deposition in local highly reduced sub-basins. Ordovician Menzie Creek volcanic rocks have a distinctive within-plate geochemical signature. Extensive submarine volcanism was likely related to localized rifting along the continental margin.

Rocks of Yukon-Tanana and Slide Mountain terranes are thrust over North American rocks in the Anvil District along the northwest extension of the Inconnu thrust. Yukon-Tanana rocks are separated from Slide Mountain rocks by the extensional Vangorda fault. The most southwesterly Yukon-Tanana succession consists of Paleozoic micaceous quartzite and phyllite which is unconformably overlain by fine to coarse Triassic clastic rocks. Micaceous quartzite is tentatively correlated with the Grass Lakes assemblage of Yukon-Tanana Terrane mapped further to the southeast. Locally, this assemblage contains Permian eclogite occurrences within a metavolcanic/metasedimentary belt. The Triassic section consists of Faro Peak formation and has an interpreted thickness of up to 600 m. Coarse clastic rocks of the Faro Peak formation suggest deposition within proximal submarine fans, possibly related to developing fault scarps.

Northeast of Vangorda fault, Slide Mountain Terrane is dominated by argillites and bedded cherts with intervals of sandstone and conglomerate. Conglomerates and sandstones contain clasts of shale, monocrystalline quartz, monocrystalline K-feldspar and chert. Provenance for coarser clastic rocks is a shale basin with input from either eroding intrusive or felsic volcanic rocks. The succession is capped by Permian Campbell Range formation basalts which have a NMORB or BAB MORB (normal or back-arc-basin mid-oceanic ridge basalt) geochemical signature. Basalts and associated bedded cherts are intruded by Permian (?) ultramafic magmas. The succession has tentatively been correlated with the Fortin Creek group and Campbell Range formation as mapped further to the southeast in the Finlayson Lake District.

All successions have been intruded by felsic magmas during Cretaceous and Eocene. The oldest felsic intrusive rocks form the Anvil plutonic suite (104 to 109 Ma) which consists of biotite-muscovite granite with S-type geochemical and petrologic affinities. This phase forms most of the Anvil Batholith which cores the northwest-trending Anvil Arch in the central part of the District. The Tay River plutonic suite (97 Ma) consists of biotite±hornblende granodiorite to granite. It forms the large Orchay Batholith at the southeast margin of the District as well as numerous dykes and sills throughout the District. The suite has petrologic and geochemical I-type affinities; the geochemical signature and age of the plutonic suite indicates it is the subvolcanic equivalent of the South Fork volcanics which outcrop immediately to the northeast. The youngest intrusions in the District consist of quartz-feldspar porphyries (55 Ma). These Eocene intrusions occur as elongate dykes or circular plugs scattered throughout the District. Locally, they have flow-banding textures indicating near-surface intrusion.

Rocks of the Anvil District are complexly polydeformed and polymetamorphosed. The first two deformation phases (D_1 and D_2) are most important in that they are regionally developed and accompanied by regional structural fabrics. The two deformations are coaxial, trending southeast. D_1 deformation is delineated by steep, tight, northeast-verging minor folds. D_1 structural fabric is present in the Triassic Faro Peak formation; therefore D_1 deformation post-dates Triassic time and pre-dates the subsequent D_2 deformation and associated structural fabric. The TwoPete and Inconnu thrust faults are considered to have been active during D_1 deformation. D_1 deformation marks the general

convergence of Yukon-Tanana and Slide Mountain terranes with ancestral North America.

D_2 deformation is delineated by a gently dipping axial-planar crenulation cleavage and associated minor folds. S_2 fabrics and folds are most strongly developed and tightest over the Anvil Batholith and decrease in intensity both to northeast and southwest. Vergence of folds also reverses over the Anvil Batholith with southwest-verging structures occurring southwest of the batholith, and northeast-verging structures occurring northeast of the batholith. The Anvil plutonic suite contains D_2 structural fabric, and the Tay River plutonic suite is unfoliated. D_2 deformation is restricted to the time interval between 109 to 96 Ma. Major compressive stress is near vertically oriented and most intense over Anvil Batholith, indicating D_2 deformation is kinematically linked to buoyant intrusion of the Anvil plutonic suite. The latest stage of D_2 deformation consists of extensional faults locally developed along the southwest margin of Anvil Batholith and overlying metasedimentary rocks. Extensional faults have proven displacements in excess of 1 km locally, and may result from the collapse of a gravitationally unstable topographic high created by intrusion of the Anvil plutonic suite.

D_2 deformation was accompanied by pervasive M_2 metamorphism. Metamorphic isograds are concentric around the Anvil Batholith. Metamorphic assemblages range from lower greenschist facies to sillimanite-muscovite zone in the amphibolite facies. Maximum temperatures and pressures during metamorphism were approximately 620°C and 4 kilobars. This corresponds to a depth of burial of up to 12 km during metamorphism. M_2 metamorphism has totally overprinted earlier M_1 metamorphism associated with D_1 deformation.

The Anvil District contains significant sedimentary-exhalative (SEDEX) zinc-lead-silver-barite mineralization. Exploration in the District has discovered an estimated 225 million tonnes of sulphide-bearing rock (Jennings and Jilson, 1986) distributed in five base metal deposits that occur within a 150-m stratigraphic interval straddling the Mount Mye-Vangorda contact in the ancestral North America succession. Mining in the District began in 1969 and continued with interruptions until 1997. Known deposits occur along a curvilinear trend which has been postulated to be a syndepositional fault structure that was active during deposit formation. Despite exploration efforts for more than 45 years in the District, substantial areas of the Mount Mye-Vangorda geological contact remain untested for undiscovered, deeply buried massive sulphide mineralization.

Yukon MINFILE occurrences within the District document mineralized showings and prospects for sediment-hosted barite, intrusion-related polymetallic veins, and volcanic-hosted sulphide deposit models (Deklerk, 2003). Only recently have exploration efforts within the District been directed towards these other exploration targets. As with SEDEX mineralization, exploration potential for these additional deposit models has not been fully tested to date.

RECOMMENDATIONS FOR FURTHER WORK

The compilation presented in this report summarizes geology known thus far in the Anvil District. It provides a common geologic and geographic framework for private and public sector geological studies completed during the extensive exploration activity since the 1953 discovery of the Vangorda deposit. Where possible, drill hole collar locations have been indicated on the compilation maps.

The interpretation presented in this report simplifies some of the structural complexity in the North American succession suggested by previous workers and argues for stratigraphic interbedding rather than structural interleaving northeast of the Anvil Batholith. Further, the suggested trace of the break juxtaposing North America and Yukon-Tanana successions has been placed based on proposed correlations of units from farther to the southeast.

The present report outlines a stratigraphic succession immediately northeast of the town of Faro that has been correlated with Slide Mountain Terrane. More detailed work is required to augment and more fully understand this package of rocks and its stratigraphic and/or structural relations to both Yukon-Tanana and North America successions.

The Yukon-Tanana micaceous quartzites contain eclogites which form a band along the northeast margin of the quartzites. Additional eclogite occurrences have been documented in this report. Further detailed work, including field relations and geochemistry research, is required to delineate depositional setting of the eclogites and their structural and stratigraphic relations to the enclosing metasedimentary rocks.

The time and extent of D_1 deformation and M_1 metamorphism has only been loosely constrained by geological studies. More detailed constraints on the D_1 deformation are required. This includes possible radiometric dating of the deformation through isotopic studies.

Existing isotopic dating of large felsic granitic bodies was largely completed in the 1960s and early 1970s. These early age determinations have large errors and therefore cannot be readily used to construct pressure-temperature-time loops for delineation of regional intrusion, metamorphism, uplift and erosion. Better constrained dating of the intrusive suites by several isotopic methods would greatly improve our understanding of the post-deposition history in the Anvil District.

The present study is a first attempt to place the economic and exploration geology of the Anvil District within a common stratigraphic and structural framework. Early in the study, a drill-hole database was initiated to attempt to capture the original lithology logging of the core and re-interpret that geology using the stratigraphic units described in this report. Unfortunately that effort to update the drill hole information eventually had to be abandoned because of time constraints. Ideally it should be completed to supplement the common framework presented in this compilation.

SELECTED REFERENCES

Abbott, J.G., Gordey, S.P. and Tempelman-Kluit, D.J., 1986. Setting of stratiform, sediment-hosted lead-zinc deposits in Yukon and northeastern British Columbia. *In:* Mineral Deposits of Northern Cordillera, J.A. Morin (ed.), Canadian Institute of Mining and Metallurgy, Special Volume 37, p. 1–18.

Anderson, R.G., 1983. Selwyn plutonic suite and its relationship to tungsten skarn mineralization, southeastern Yukon and District of Mackenzie. *In:* Current Research, Part B, Geological Survey of Canada, Paper 83-1B, p. 151–163.

Blusson, S.L., 1966. Geology, Frances Lake, Yukon Territory and District of Mackenzie, 105H. Geological Survey of Canada, Map 6-1966 (1: 253 440 scale).

Bond, J.D., 2001. Quaternary geology and till geochemistry of the Anvil district (parts of 105K/2,3,5,6,7), central Yukon Territory. Exploration and Geological Services Division, Yukon Region, Indian and Northern Affairs Canada, Bulletin 11, 39 p., (includes 11 1:25 000-scale maps).

Bostock, H.S., 1948. Physiography of the Canadian Cordillera, with special reference to the area north of the fifty-fifth parallel. Geological Survey of Canada, Memoir 247, 106 p.

Breitsprecher, K., Mortensen, J.K. and Villeneuve, M.E. (compilers), 2002. Yukonage 2002 – a database of isotopic age determinations from rock units from Yukon Territory. Exploration and Geological Services Division, Yukon Region, Indian and Northern Affairs Canada, CD-ROM.

Brock, J.S., 1973. Geophysical exploration leading to the discovery of the Faro deposit. Canadian Institute of Mining and Metallurgy Bulletin, vol. 66, p. 97–116.

Brown, D., 1994. Low temperature, lower pressure deformation and metamorphism of the Vangorda massive sulphide orebody, Yukon, Canada. Mineralium Deposita, vol. 29, p. 330–340.

Brown, D. and McClay, K.R., 1994. Structural geology of the Vangorda Pb-Zn deposit. Ore Geology Reviews, vol. 9, p. 61–78.

Campbell, R.B., 1967. Reconnaissance geology of Glenlyon map area, Yukon Territory. Geological Survey of Canada, Memoir 352, 92 p.

Carmichael, D.M., 1978. Metamorphic bathozones and bathograds: a measure of the depth of post-metamorphic uplift and erosion on the regional scale. American Journal of Science, vol. 278, p. 769–797.

Carne, R.C. and Cathro, R.J., 1982. Sedimentary exhalative (sedex) zinc-lead deposits, northern Canadian Cordillera. Canadian Institute of Mining and Metallurgy, Bulletin, vol. 75, No. 840, p. 66–78.

Chisholm, E.O., 1957. Geophysical exploration of a lead-zinc deposit in Yukon Territory. *In:* Methods and Case Histories in Mining Geophysics, Sixth Commonwealth Mining and Metallurgy Congress, p. 269–277.

Coney, P.J., Jones, D.L. and Monger, J.W.H., 1980. Cordilleran suspect terranes. Nature, vol. 288, p. 329–333.

Cordey, F., 2000. Report on radiolarians, fieldwork 1999, 2 samples (chert) by Lee Pigage. Geological Survey of Canada, Report No. FC2000-GSC-4, 2 p.

Creaser, R.A., Goodwin-Bell, J.S. and Erdmer, P., 1999. Geochemical and Nd isotopic constraints for the origin of eclogite protoliths, northern Cordillera: implications for the Paleozoic tectonic evolution of the Yukon-Tanana Terrane. Canadian Journal of Earth Sciences, vol. 36, p. 1697–1709.

Deklerk, R., 2003. Yukon MINFILE – a database of mineral occurrences. Yukon Geological Survey, CD-ROM.

Duk-Rodkin, A., Barendregt, R.W., Tornacai, C. and Philips, F.M., 1996. Late Tertiary to late Quaternary record in the Mackenzie Mountains, Northwest Territories, Canada: Stratigraphy, paleosols, paleomagnetism, and chlorine-36. Canadian Journal of Earth Sciences, vol. 33, p. 875–895.

Erdmer, P., 1987. Blueschist and eclogite in mylonitic allochthons, Ross River and Watson Lake areas, southeastern Yukon. Canadian Journal of Earth Sciences, vol. 24, p. 1439–1449.

Erdmer, P. and Armstrong, R.L., 1988. Permo-Triassic isotopic dates for blueschist, Ross River area, Yukon. *In:* Yukon Geology, Volume 2, Exploration and Geological Services Division, Yukon Region, Indian and Northern Affairs Canada, p. 33–36.

Erdmer, P., Ghent, E.D., Archibald, D.A. and Stout, M.Z., 1998. Paleozoic and Mesozoic high-pressure metamorphism at the margin of ancestral North America in central Yukon. Geological Society of America Bulletin, vol. 110, p. 615–629.

Erdmer, P. and Helmstaedt, H., 1983. Eclogite from central Yukon: a record of subduction at the western margin of ancient North America. Canadian Journal of Earth Sciences, vol. 20, p. 1389–1408.

Ferry, J.M. and Spear, F.S., 1978. Experimental calibration of the partitioning of Fe and Mg between biotite and garnet. Contributions to Mineralogy and Petrology, vol. 66, p. 113–117.

Franzen, J., 1978. Geological report Urn claim group. Unpublished Assessment Report #090345. Energy, Mines and Resources, Yukon Government.

Froese, D.G., Barendregt, R.W., Enkin, R.J. and Baker, J., 2000. Paleomagnetic evidence for multiple Late Pliocene-Early Pleistocene glaciations in the Klondike area, Yukon Territory. Canadian Journal of Earth Sciences, vol. 37, p. 863–877.

Gabrielse, H., 1967. Tectonic evolution of the northern Canadian Cordillera. Canadian Journal of Earth Sciences, vol. 4, p. 271–298.

Gabrielse, H., Blusson, S.L. and Roddick, J.A., 1973. Geology of Flat River, Glacier Lake, and Wrigley Lake map-areas, District of Mackenzie and Yukon Territory. Geological Survey of Canada, Memoir 366, 153 p.

Ghent, E.D., Robbins, D.B. and Stout, M.Z., 1979. Geothermometry, geobarometry, and fluid compositions of metamorphosed calc-silicates and pelites, Mica Creek, British Columbia. The American Mineralogist, vol. 64, p. 874–885.

Goodfellow, W.D., Lydon, J.W. and Turner, R.J.W., 1993. Geology and genesis of stratiform sediment-hosted (SEDEX) zinc-lead-silver sulphide deposit. *In:* Mineral Deposit Modelling, R.V. Kirkham, W.D. Sinclair, R.I. Thorpe and J.M. Duke (eds.), Geological Association of Canada, Special Paper 40, p. 201–251.

Goodfellow, W.D., Cecile, M.P. and Leybourne, M.I., 1995. Geochemistry, petrogenesis and tectonic setting of lower Paleozoic alkalic and potassic volcanic rocks, Northern Canadian Cordilleran miogeocline. Canadian Journal of Earth Sciences, vol. 32, p. 1236–1254.

Goodwin-Bell, J.S., 1998. A geochemical and Sm-Nd isotopic study of Cordilleran eclogites from the Yukon-Tanana Terrane. Unpublished MSc thesis, University of Alberta, Edmonton, Alberta.

Gordey, S.P., 1983. Thrust faults in the Anvil Range, and a new look at the Anvil Range Group, south-central Yukon Territory. Geological Survey of Canada, Paper 83-1A, p. 225–227.

Gordey, S.P., 1990a. Geology of Tenas Creek (105K/1), Swim Lakes (105K/2), and Faro (105K/3) map areas, Yukon Territory. Geological Survey of Canada, Open File 2249 (1:50 000 scale).

Gordey, S.P., 1990b. Geology of Mount Atherton (105K/4), Rose Mountain (105K/5), and Mount Mye (105K/6) map areas, Yukon Territory. Geological Survey of Canada, Open File 2250 (1:50 000 scale).

Gordey, S.P., 1990c. Geology of Blind Creek (105K/7), Teddy Creek (105K/10), and Barwell Lake (105K/11) map areas, Yukon Territory. Geological Survey of Canada, Open File 2251 (1:50 000 scale).

Gordey, S.P., Abbott, J.G. and Orchard, M.J., 1982. Devono-Mississippian (Earn Group) and younger strata in east-central Yukon. Geological Survey of Canada, Paper 82-1B, p. 93–100.

Gordey, S.P. and Anderson, R.G., 1993. Evolution of the northern Cordilleran miogeocline, Nahanni map area (105I), Yukon and Northwest Territories. Geological Survey of Canada, Memoir 428, 214 p.

Gordey, S.P. and Irwin, S.E.B., 1987. Geology, Sheldon Lake and Tay River map areas, Yukon Territory. Geological Survey of Canada, Map 19-1987 (3 sheets) (1:250 000 scale).

Hunt, J.A., 1998. The setting of volcanogenic massive sulphide deposits in the Finlayson Lake district. *In:* Yukon Exploration and Geology 1997, Exploration and Geological Services Division, Yukon Region, Indian and Northern Affairs Canada, p. 99–104.

Hunt, P.A. and Roddick, J.C., 1991. A compilation of K-Ar ages, Report 20. *In:* Radiogenic and Isotopic Studies, Report 4. Geological Survey of Canada, Paper 90-2, p. 113–143.

Hunt, P.A. and Roddick, J.C., 1992. A compilation of K-Ar and ^{40}Ar-^{39}Ar ages, report 22. *In:* Radiogenic and Isotopic Studies: Report 6. Geological Survey of Canada, Paper 92-2, p. 179–226.

Jackson, D.E. and Lenz, A.C., 1962. Zonation of Ordovician and Silurian graptolites in northern Yukon, Canada. American Association of Petroleum Geologists, Bulletin, vol. 46, p. 30–45.

Jackson, L.E., Jr., 1994. Terrain inventory and Quaternary history of the Pelly River area, Yukon Territory. Geological Survey of Canada, Memoir 437, 41 p. (1:100 000 scale).

Jenner, G.A., 1996. Trace element geochemistry of igneous rocks: geochemical nomenclature and analytical geochemistry. *In:* Trace Element Geochemistry of Volcanic Rocks: Applications for Massive Sulphide Exploration, D.A. Wyman (ed.), Geological Association of Canada, Short Course Notes, vol. 12, p. 51–77.

Jennings, D.S. and Jilson, G.A., 1986. Geology and sulphide deposits of Anvil Range, Yukon. *In:* Mineral Deposits of Northern Cordillera, J.A. Morin (ed.), Canadian Institute of Mining and Metallurgy, Special Volume 37, p. 319–361.

Long, D.G.F., Lowey, G.W. and Sweet, A.R., 2001. Age and setting of dinosaur trackways, Ross River area, Yukon Territory (105F/15). *In:* Yukon Exploration and Geology 2000, D.S. Emond and L.H. Weston (eds.), Exploration and Geological Services Division, Yukon Region, Indian and Northern Affairs Canada, p. 181–198.

McPhie, J., Doyle, M. and Allen, R., 1993. Volcanic textures: a guide to the interpretation of textures in volcanic rocks. University of Tasmania, Centre for Ore Deposit and Exploration Studies, 196 p.

Meschede, M., 1986. A method of discriminating between different types of mid-ocean ridge basalts and continental tholeiites with the Nb-Zr-Y diagram. Chemical Geology, vol. 56, p. 207–218.

Modene, Janet, 1982. Origin and sulfur isotope geochemistry of the Grum deposit, Anvil Range, Yukon Territory, Canada. Unpublished M.Sc. thesis, University of Wisconsin, 158 p.

Morrow, D.W., 1999. Lower Paleozoic stratigraphy of northern Yukon Territory and northwestern District of Mackenzie. Geological Survey of Canada, Bulletin 538, 202 p.

Mortensen, J.K., 1992. New U-Pb ages for the Slide Mountain Terrane in southeastern Yukon Territory. Radiogenic Age and Isotopic Studies, Report 5. Geological Survey of Canada, Paper 91-2, p. 167–173.

Mortensen, J.K. and Ballantyne, S.B., 1992. Age and Pb isotopic studies of Ag-Sn-base metal epigenetic mineralization in the Mount Mye area, east-central Yukon Territory. *In:* Radiogenic Age and Isotopic Studies; Report 6. Geological Survey of Canada, Paper 92-2, p. 129–134.

Mortensen, J.K., Ghosh, D.K. and Ferri, F., 1995. U-Pb geochronology of intrusive rocks associated with copper-gold porphyry deposits in the Canadian Cordillera. *In:* Porphyry Deposits of the Northwestern Cordillera of North America, T.G. Shroeter (ed.), Canadian Institute of Mining, Metallurgy and Petroleum, Special Volume 46, p. 142–158.

Mortensen, J.K., Hart, C.J.R., Murphy, D.C. and Heffernan, S., 2000. Temporal evolution of early and mid-Cretaceous magmatism in the Tintina Gold Belt. *In:* The Tintina Gold Belt: Concepts, Exploration, and Discoveries, T.L. Tucker and M.T. Smith (eds.), British Columbia and Yukon Chamber of Mines, Special Volume 2, p. 49–58.

Mortensen, J.K. and Jilson, G.A., 1985. Evolution of the Yukon-Tanana Terrane: evidence from southeastern Yukon Territory. Geology, vol. 13, p. 806–810.

Murphy, D.C., 2004. Devonian-Mississippian metavolcanic stratigraphy, massive sulphide potential and structural re-interpretation of Yukon-Tanana Terrane south of the Finlayson Lake massive sulphide district, southeastern Yukon (105G/1, 105H/3,4,5). *In:* Yukon Exploration and Geology 2003, D.S. Emond and L.L. Lewis (eds.), Yukon Geological Survey, p. 157–175.

Murphy, D.C., Colpron, M., Roots, C.F., Gordey, S.P. and Abbott, J.G., 2002. Finlayson Lake Targeted Geoscience Initiative (southeastern Yukon), Part 1: Bedrock geology. *In:* Yukon Exploration and Geology 2001, D.S. Emond, L.H. Weston and L.L. Lewis (eds.), Exploration and Geological Services Division, Yukon Region, Indian and Northern Affairs Canada, p. 189–207.

Murphy, D.C. and Mortensen, J.K., 2003. Late Paleozoic and Mesozoic features constrain displacement on Tintina Fault and limit large-scale orogen-parallel displacement in the Northern Cordillera. GAC-MAC-SEG Joint Annual Meeting, May 25-28, 2003. Abstracts, vol. 28, abstract 151.

Murphy, D.C. and Piercey, S.J., 1999. Finlayson Project: Geological evolution of Yukon-Tanana Terrane and its relationship to the Campbell Range belt, northern Wolverine Lake map area, southeastern Yukon. *In:* Yukon Exploration and Geology 1998, D.S. Emond and C.F. Roots (eds.), Exploration and Geological Services Division, Yukon Region, Indian and Northern Affairs Canada, p. 47–62.

Nelson, J.L., 1993. The Sylvester allochthon: Upper Paleozoic marginal-basin and island-arc terranes in northern British Columbia. Canadian Journal of Earth Sciences, vol. 30, p. 631–643.

Norford, B.S., 1977. Report on one collection of fossils collected from the Tay River map-area, Yukon Territory by Dr. D. Tempelman-Kluit, 1968 (NTS 105-K). Geological Survey of Canada, Report O-1-1977-BSN.

Norford, B.S., 1982. Report on 13 lots of fossils collected from the Nahanni, Sheldon Lake, Tay River and Glenlyon map-areas, Yukon Territory collected by Dr. S. Gordey, 1982 (NTS 105I, J, K, L). Geological Survey of Canada, Report O-S 17-BSN-1982.

Orchard, M.J., 1992a. Report on conodonts and other microfossils, Quiet Lake (105F), Finlayson (105G), Sheldon Lake (105J), Tay River (105K), Glenlyon (105L), 512 samples (145 productive) collected by S.P. Gordey 1980, 1982, 1983, 1985-87, 1991. Geological Survey of Canada, Report OF-1992-11, 93 p.

Orchard, M.J., 1992b. Report on conodonts and other microfossils, Tay River (105K) and Glenlyon (105L), 13 samples collected by D.J. Tempelman-Kluit 1975-1976, 1979. Geological Survey of Canada, Report OF-1992-14, 10 p.

Orchard, M.J., 1999. Report on conodonts and other microfossils, Tay River (105K), 4 samples (1 productive) collected by L. Pigage, Yukon Geoscience Office. Geological Survey of Canada, Report MJO-1999-3, 3 p.

Orchard, M.J., 2000. Report on conodonts and other microfossils, Tay River (105K), 12 samples (5 productive) collected by L. Pigage, Yukon Geoscience Office. Geological Survey of Canada, Report MJO-2000-3, 5 p.

Orchard, M.J., 2001. Report on conodonts and other microfossils, Tay River (105K), 1 sample (1 productive) collected by L. Pigage (2000). Geological Survey of Canada, Report MJO-2001-8, 2 p.

Pearce, J.A., 1996. A user's guide to basalt discrimination diagrams. *In:* Trace Element Geochemistry of Volcanic Rocks: Applications for Massive Sulphide Exploration, D.A. Wyman (ed.), Geological Association of Canada, Short Course Notes, vol. 12, p. 79–113.

Pearce, J.A. and Cann, J.R., 1973. Tectonic setting of basic volcanic rocks determined using trace element analyses. Earth and Planetary Science Letters, vol. 19, p. 290–300.

Perchuk, A., Philippot, P., Erdmer, P. and Fialin, M., 1999. Rates of thermal equilibration at the onset of subduction deduced from diffusion modeling of eclogitic garnets, Yukon-Tanana Terrane, Canada. Geology, vol. 27, p. 531–534.

Philippot, P., Blichert-Toft, J., Perchuk, A., Costa, S. and Gerasimov, V., 2001. Lu-Hf and Ar-Ar chronometry supports extreme rate of subduction zone metamorphism deduced from geospeedometry. Tectonophysics, vol. 342, p. 23–38.

Piercey, S.J., Hunt, J.A. and Murphy, D.C., 1999. Lithogeochemistry of meta-volcanic rocks from Yukon-Tanana Terrane, Finlayson Lake region, Yukon: Preliminary results. *In:* Yukon Exploration and Geology 1998, C.F. Roots and D.S. Emond (eds.), Exploration and Geological Services Division, Yukon Region, Indian and Northern Affairs Canada, p. 125–138.

Piercey, S.J., Mortensen, J.K., Murphy, D.C., Paradis, S. and Creaser, R.A., 2002. Geochemistry and tectonic significance of alkalic mafic magmatism in the Yukon-Tanana Terrane, Finlayson Lake region, Yukon. Canadian Journal of Earth Sciences, vol. 39, p. 1729–1744.

Pigage, L.C., 1990. Anvil Pb-Zn-Ag district, Yukon Territory, Canada. *In:* Mineral Deposits of the Northern Canadian Cordillera, Yukon-Northeastern British Columbia, J.G. Abbott and R.J.W. Turner (eds.), Geological Survey of Canada, Open File 2169, p. 283–308.

Pigage, L.C., 1999a. Preliminary geology of Rose Mountain, Anvil District, central Yukon (105K/05). *In:* Yukon Exploration and Geology 1998, C.F. Roots and D.S. Emond (eds.), Exploration and Geological Services Division, Yukon Region, Indian and Northern Affairs Canada, p. 91–103.

Pigage, L.C., 1999b. Geological map of Rose Mountain (105K/5NW), central Yukon (1:25 000 scale). Exploration and Geological Services Division, Yukon Region, Indian and Northern Affairs Canada, Open File 1999-11.

Pigage, L.C., 1999c. Geological map of Blind Creek (105K/7NW), central Yukon (1:25 000 scale). Exploration and Geological Services Division, Yukon Region, Indian and Northern Affairs Canada, Open File 1999-12.

Pigage, L.C., 1999d. Geological map of Blind Creek (105K/7SE), central Yukon (1:25 000 scale). Exploration and Geological Services Division, Yukon Region, Indian and Northern Affairs Canada, Open File 1999-15.

Pigage, L.C., 2000a. Preliminary geology north of Mount Mye, Anvil District (105K/6, 105K/7), central Yukon. *In:* Yukon Exploration and Geology, 1999. D.S. Emond and L.H. Weston (eds.), Exploration and Geological Services Division, Yukon Region, Indian and Northern Affairs Canada, p. 101–114.

Pigage, L.C., 2000b. Geological map of Mount Mye (105K/6NW), central Yukon (1:25 000 scale). Exploration and Geological Services Division, Yukon Region, Indian and Northern Affairs Canada, Open File 2000-2.

Pigage, L.C., 2000c. Geological map of Mount Mye (105K/6NE), central Yukon (1:25 000 scale). Exploration and Geological Services Division, Yukon Region, Indian and Northern Affairs Canada, Open File 2000-3.

Pigage, L.C., 2000d. Geological map of Swim Lakes (105K/2SE), central Yukon (1:25 000 scale). Exploration and Geological Services Division, Yukon Region, Indian and Northern Affairs Canada, Open File 2000-4.

Pigage, L.C., 2000e. Geological map of Swim Lakes (105K/2NE), central Yukon (1:25 000 scale). Exploration and Geological Services Division, Yukon Region, Indian and Northern Affairs Canada, Open File 2000-5.

Pigage, L.C., 2000f. Geological map of Swim Lakes (105K/2W), central Yukon (1:25 000 scale). Exploration and Geological Services Division, Yukon Region, Indian and Northern Affairs Canada, Open File 2000-6.

Pigage, L.C., 2000g. Geological map of Mount Mye (105K/6E), central Yukon (1:25 000 scale). Exploration and Geological Services Division, Yukon Region, Indian and Northern Affairs Canada, Open File 2000-7.

Pigage, L.C., 2000h. Geological map of Blind Creek (105K/7SW), central Yukon (1:25 000 scale). Exploration and Geological Services Division, Yukon Region, Indian and Northern Affairs Canada, Open File 2000-8.

Pigage, L.C., 2000i. Geological map of Rose Mountain (105K/5NE), central Yukon (1:25 000 scale). Exploration and Geological Services Division, Yukon Region, Indian and Northern Affairs Canada, Open File 2000-13.

Pigage, L.C., 2001a. Geological map of Rose Mountain (105K/5SE), central Yukon (1:25 000 scale). Exploration and Geological Services Division, Yukon Region, Indian and Northern Affairs Canada, Open File 2001-4.

Pigage, L.C., 2001b. Geological map of Faro (NTS 105K/3NW) & Mount Mye (NTS 105K/6SW), central Yukon (1:25 000 scale). Exploration and Geological Services Division, Yukon Region, Indian and Northern Affairs Canada, Open File 2001-26.

Pigage, L.C., 2001c. Geological map of Faro (105K/3NE) & Mount Mye (NTS 105K/6SE), central Yukon (1:25 000 scale). Exploration and Geological Services Division, Yukon Region, Indian and Northern Affairs Canada, Open File 2001-27.

Pigage, L.C., 2001d. Geological map of Mount Mye (105K/6W), central Yukon (1:25 000 scale). Exploration and Geological Services Division, Yukon Region, Indian and Northern Affairs Canada, Open File 2001-28.

Pigage, L.C., 2001e. Geological map of Anvil District (105K/2,3,5,6,7,11), central Yukon (1:100 000 scale). Exploration and Geological Services Division, Yukon Region, Indian and Northern Affairs Canada, Open File 2001-31.

Pigage, L.C. and Anderson, R.G., 1985. The Anvil plutonic suite, Faro, Yukon Territory. Canadian Journal of Earth Sciences, vol. 22, p. 1204–1216.

Pigage, L.C. and Jilson, G.A., 1985. Major extensional faults, Anvil Pb-Zn District, Yukon. Geological Society of America, Abstracts with Programs-Cordilleran Section, vol. 17, p. 400.

Plint, H.E. and Gordon, T.M., 1997. The Slide Mountain Terrane and the structural evolution of the Finlayson Lake Fault Zone, southeastern Yukon. Canadian Journal of Earth Sciences, vol. 34, p. 105–126.

Ramsay, J.G., 1967. Folding and fracturing of rocks. McGraw-Hill Book Company, Toronto, 568 p.

Read, W.S., 1982. Report on URN barite property. Unpublished assessment report #091369. Energy, Mines and Resources, Yukon Government, 28 p.

Rennae, P.R., Swisher, C.C., Deino, A.L., Karner, D.B., Owens, T.L. and DePaolo, D.J., 1998. Intercalibration of standards, absolute ages and uncertainties in $^{40}Ar/^{39}Ar$ dating. Chemical Geology, vol. 145, p. 117–152.

Roddick, J.A., 1967. Tintina Trench. Journal of Geology, vol. 75, p. 23–33.

Roddick, J.A. and Green, L.H., 1961. Tay River, Yukon Territory. Geological Survey of Canada, Map 13-1961 (1:253 440 scale).

Roddick, J.C., 1987. Generalized numerical error analysis with application to geochronology and thermodynamics. Geochimica et Cosmochimica Acta, vol. 51, p. 2129–2135.

Roddick, J.C., 1988. The assessment of errors in $^{40}Ar/^{39}Ar$ dating. *In:* Radiogenic Age and Isotopic Studies, Report 2, Geological Survey of Canada, Paper 88-2, p. 7–16.

Shervais, J.W., 1982. Ti-V plots and the petrogenesis of modern and ophiolitic lavas. Earth and Planetary Science Letters, vol. 59, p. 101–118.

Smith, J.M. and Erdmer, P., 1990. The Anvil aureole, an atypical mid-Cretaceous culmination in the northern Canadian Cordillera. Canadian Journal of Earth Sciences, vol. 27, p. 344–356.

Snyder, D.B., Clowes, R.M., Cook, F.A., Erdmer, P., Evenchick, C.A., van der Velden, A.J. and Hall, K.W., 2002. Proterozoic prism arrests suspect terranes: insights into the ancient Cordilleran margin from seismic reflection data. GSA Today, vol. 12, number 10, p. 4–10.

Stacey, J.S. and Kramer, J.D., 1975. Approximation of terrestrial lead isotope evolution by a two-stage model. Earth and Planetary Science Letters, vol. 26, p. 207–221.

Steiger, R.H. and Jäger, E., 1977. Subcommission on geochronology: convention on the use of decay constants in geo- and cosmochronology. Earth and Planetary Science Letters, vol. 36, p. 359–362.

Sun, S.-S. and McDonough, W.F., 1989. Chemical and isotopic systematics of oceanic basalts: implications for mantle composition and processes. *In:* Magmatism in the Ocean Basins, A.D. Saunders and M.J. Norry (eds.), Geological Society Special Publication 42, p. 313–345.

Tempelman-Kluit, D.J., 1970a. An occurrence of eclogite near Tintina Trench, Yukon. Geological Survey of Canada, Paper 70-1B, p. 19–22.

Tempelman-Kluit, D.J., 1970b. Stratigraphy and structure of the "Keno Hill Quartzite" in Tombstone River – upper Klondike River map-areas, Yukon Territory (116 B/7, B/8). Geological Survey of Canada, Bulletin 180, 102 p.

Tempelman-Kluit, D.J., 1972. Geology and origin of the Faro, Vangorda, and Swim concordant zinc-lead deposits, central Yukon Territory. Geological Survey of Canada, Bulletin 208 (1:125 000 scale), 73 p.

Tempelman-Kluit, D.J., 1979a. Five occurrences of transported synorogenic clastic rocks in Yukon Territory. Geological Survey of Canada, Paper 79-1A, p. 1–12.

Tempelman-Kluit, D.J., 1979b. Transported cataclasite, ophiolite and granodiorite in Yukon: evidence of arc-continent collision. Geological Survey of Canada, Paper 79-14, 27 p.

Wanless, R.K., Stevens, R.D., Lachance, G.R. and Edmonds, C.M., 1967. Age determinations and geological studies, K-Ar isotopic ages, Report 7. Geological Survey of Canada, Paper 66-17, p. 40–43.

Wanless, R.K., Stevens, R.D., Lachance, G.R. and Delabio, R.N., 1970. Age determinations and geological studies, K-Ar isotopic ages, Report 9. Geological Survey of Canada, Paper 69-2A, p. 27–28.

Wanless, R.K., Stevens, R.D., Lachance, G.R. and Delabio, R.N., 1972. Age determinations and geological studies, K-Ar isotopic ages, Report 10. Geological Survey of Canada, Paper 71-2, p. 28–29.

Wanless, R.K., Stevens, R.D., Lachance, G.R. and Delabio, R.N., 1973. Age determinations and geological studies, K-Ar isotopic ages, Report 11. Geological Survey of Canada, Paper 73-2, p. 27.

Wanless, R.K., Stevens, R.D., Lachance, G.R. and Delabio, R.N., 1978. Age determinations and geological studies, K-Ar isotopic ages, Report 13. Geological Survey of Canada, Paper 77-2, p. 32.

Ward, B.C. and Jackson, L.E., Jr., 2000. Surficial geology of the Glenlyon map area, Yukon Territory. Geological Survey of Canada, Bulletin 559, 60 p.

Winchester, J.A. and Floyd, P.A., 1977. Geochemical discrimination of different magma series and their differentiation products using immobile elements. Chemical Geology, vol. 20, p. 325–343.

Wood, D.A., 1980. The application of a Th-Hf-Ta diagram to problems of tectonomagmatic classification and to establishing the nature of crustal contamination of basaltic lavas of the British Tertiary volcanic province. Earth and Planetary Science Letters, vol. 50, p. 11–30.

ADDITIONAL REPORTS USED IN MAP COMPILATION

Adamson, R.S., 1966. Diamond drilling Ace claim group. Unpublished Assessment Report #091255, Energy, Mines and Resources, Yukon Government.

Adamson, R.S., 1966. Diamond drilling Dea claim group. Unpublished Assessment Report #091205, Energy, Mines and Resources, Yukon Government.

Allan, A., 1973. Unpublished Assessment Report #091209, Energy, Mines and Resources, Yukon Government.

Blanchflower, J.D., 1999. 1999 exploration report on the JRV property. Unpublished company report prepared by Minorex Consulting Ltd. for Pacific Ridge Exploration Ltd.

Bradford, J., 1989. Geology of the Vangorda Plateau and part of the Swim Basin. Unpublished Curragh Resources Inc. internal company report (1:5000 scale).

Bradford, J., 1989. Report on geological mapping of the Tread claims. Unpublished Curragh Resources Inc. internal company report (1:5000 scale).

Chisholm, E.O., 1976. Unpublished Assessment Report #061385. Energy, Mines and Resources, Yukon Government.

Fairley, J.F., 1965. Development work (Nasty claim group) (rotary drilling). Unpublished Assessment Report #017939, Energy, Mines and Resources, Yukon Government.

Fairley, J.F., 1965. Rotary drilling Beta claim group. Unpublished Assessment Report #091691, Energy, Mines and Resources, Yukon Government.

Fairley, J.F., 1965. Rotary drilling Cub claim group. Unpublished Assessment Report #091204, Energy, Mines and Resources, Yukon Government.

Foster, F., 1976. Diamond drilling report on the Irene 1-56 claim group. Unpublished Assessment Report #091253, Energy, Mines and Resources, Yukon Government.

Foster, F., 1977. Diamond drilling report on the Eva 1-39 claim group. Unpublished Assessment Report #091230, Energy, Mines and Resources, Yukon Government.

Foster, F., 1977. Diamond drilling report on the Mabel 1-48 and Eva 40-47 claim group. Unpublished Assessment Report #091230, Energy, Mines and Resources, Yukon Government.

Foster, F., 1977. Diamond drilling report on the Wynne 1-42 claim group. Unpublished Assessment Report #091252, Energy, Mines and Resources, Yukon Government.

Foster, F. and Brock, J.S., 1975. Geological, geochemical and geophysical report on the Eva 1-39 claim group. Unpublished Assessment Report #061507, Energy, Mines and Resources, Yukon Government.

Foster, F. and Holland, R., 1977. Geological and geochemical report on the Raz 1-182 claim group. Unpublished Assessment Report #090267, Energy, Mines and Resources, Yukon Government.

Foster, H.F., 1979. Diamond drilling report on the Rachel and Mn claim groups. Unpublished Assessment Report #091214, Energy, Mines and Resources, Yukon Government.

Gondi, J. and Stammers, M., 1976. Unpublished Assessment Report #091242, Energy, Mines and Resources, Yukon Government.

Guild, J.D., 1977. Diamond drilling program on the Dot 1-42 mineral claims. Unpublished Assessment Report #091259, Energy, Mines and Resources, Yukon Government.

Guild, J.D., 1977. Report on diamond drilling on the Raz 1-20 mineral claims. Unpublished Assessment Report #091251, Energy, Mines and Resources, Yukon Government.

Guild, J.D., 1977. Diamond drilling program on the Wynne 1-88 mineral claims. Unpublished Assessment Report #091252, Energy, Mines and Resources, Yukon Government.

Guild, J.D., 1978. Report on diamond drilling program on the Rachel-Mn mineral claims. Unpublished Assessment Report #091214, Energy, Mines and Resources, Yukon Government.

Hill, R.P. and Jennings, D.S., 1978. Unpublished Assessment Report #091211, Energy, Mines and Resources, Yukon Government.

Hitchens, A.C. and Kidlark, R.G., 1978. Tay Mountain property Tay #1-166 claims. Unpublished Assessment Report #090404, Energy, Mines and Resources, Yukon Government.

Holland, R.T., 1977. Report on diamond drilling program on the Raz 1-182 mineral claims. Unpublished Assessment Report #091251. Energy, Mines and Resources, Yukon Government.

House, G.D., 1970. Unpublished Assessment Report #091232. Energy, Mines and Resources, Yukon Government.

House, G.D., 1978. Unpublished Assessment Report #091258. Energy, Mines and Resources, Yukon Government.

House, G.D., 1978. Unpublished Assessment Report #091350. Energy, Mines and Resources, Yukon Government.

Jansons, U., 1974. Unpublished Assessment Report #091220. Energy, Mines and Resources, Yukon Government.

Jennings, D.S. and Heslop, J., 1971. Geologic map Faro area. Unpublished Anvil Mining Corporation internal company report (1:4800 scale).

Jennings, D.S., Jilson, G.A., Hanson, D.J. and Franzen, J.P., 1978a. Geology Anvil District map area. Unpublished Cyprus Anvil Mining Corporation internal company report (1:50 000 scale).

Jennings, D.S., Jilson, G.A., Hanson, D.J. and Franzen, J.P., 1978b. Geology Anvil District map area. Unpublished Cyprus Anvil Mining Corporation internal company report (1:12 000 scale).

Jilson, G.A., 1974. Summary of exploration of the Mt. Mye prospect during 1970, 1971, 1972, & 1973. Unpublished Kangaroo Exploration Corporation internal company report.

Jilson, G.A., 1977. Geology map of the Mt. Mye area. Unpublished Cyprus Anvil Mining Corporation internal company report (1:24 000 scale).

Jilson, G.A. and Pigage, L.C., 1984. Geology of the Tie-Firth area. Unpublished Cyprus Anvil Mining Corporation internal company report (1:5000 scale).

Lewis, P.F. and Simpson, J.G., 1973. A geological report on the Lisa claims. Unpublished Assessment Report #060931, Energy, Mines and Resources, Yukon Government.

McFaull, A.J., 1996. Report on 1996 diamond drilling at the Swim Lakes Basin, Faro, Yukon Territory. Unpublished Anvil Range Mining Corporation internal company report.

Mustard, J.W., 1980. Unpublished Assessment Report #090947. Energy, Mines and Resources, Yukon Government.

O'Connor, C.K., 1966. Summary report on exploration for Jaye Explorations Limited on the Bin, Lamb, and Extra mineral claims. Unpublished Assessment Report #018999. Energy, Mines and Resources, Yukon Government.

Ostensoe, L., 1964. Unpublished Assessment Report #091765. Energy, Mines and Resources, Yukon Government.

Payne, C.W., 1982. Unpublished Assessment Report #091449. Energy, Mines and Resources, Yukon Government.

Pigage, L.C., 1985. Geological report on the ski hill area, Anvil District. Unpublished Cyprus Anvil Mining Corporation internal company report.

Pigage, L.C., 1987. Geological report RR claim group. Unpublished Assessment Report #092101, Energy, Mines and Resources, Yukon Government.

Pigage, L.C., 1989. Geological and drilling report northwest of the Faro minesite. Unpublished Assessment Report #092597, Energy, Mines and Resources, Yukon Government.

Pigage, L.C., 1990. Drilling report northwest of the Faro minesite. Unpublished Assessment Report #092872, Energy, Mines and Resources, Yukon Government.

Pigage, L.C. and Jilson, G.A., 1987. Geology maps of Vangorda Plateau and Faro southeast areas. Unpublished Cyprus Anvil Mining Corporation and Curragh Resources Inc. internal company report (1:5000 scale).

Power, M., 1998. A reflection seismic survey over the Grizzly deposit. Unpublished Yukon Geology Program report prepared by Amerok Geosciences Ltd., 8 p.

Reed, C.V., 1988. Winter 1988 Moose Lake area diamond drilling program, geology and diamond drilling report. Unpublished Assessment Report #092520, Energy, Mines and Resources, Yukon Government.

Rees, C.J., 1989. Geology of the Faro northwest area, report on fieldwork 1989. Unpublished Assessment Report #092840, Energy, Mines and Resources, Yukon Government.

Roberts, W.J., 1971. Geologic, geophysical, geochemical and diamond drilling report on the Lorna Group. Unpublished Assessment Report #060714, Energy, Mines and Resources, Yukon Government.

Sevensma, P.H., 1967. Geophysical, geological, geochemical and drilling work to February 14, 1967. Unpublished Assessment Report #017933, Energy, Mines and Resources, Yukon Government.

Simpson, J.G., 1978. Unpublished Assessment Report #091257, Energy, Mines and Resources, Yukon Government.

Spence, R.W., 1979. Report on diamond drilling Vangorda Property. Unpublished Assessment Report #091244, Energy, Mines and Resources, Yukon Government.

Turnbull, I. and Simpson, J.G., 1970. Report on a geochemical survey and diamond drilling program on the Mount Mye property. Unpublished Assessment Report #060975, Energy, Mines and Resources, Yukon Government.

Woolham, R.W., 1996. Report on a combined helicopter-borne electromagnetic and magnetic survey, Faro, Yukon, NTS 105K/2,3,5,6,7. Unpublished Aerodat Inc. company report for Anvil Range Mining Corporation (1:24 000 scale).

Appendix I: Whole rock geochemical analyses

Analytical method: Samples were analysed at Activation Laboratories Ltd. in Ancaster, Ontario. Samples were crushed and then pulverized with a ceramic mill. Major and minor elements were determined by XRF on a fusion sample. Trace elements and REE were analysed by ICP-MS at research detection limits on a fusion sample containing a lithium metaborate/tetraborate flux.

Notes for all tables
* duplicate sample
** duplicate sample pulp
coordinates are UTM Zone 8, NAD83

Detection limits are indicated with negative values.

Abbreviations
L.O.I. . . . . loss on ignition
chl-phy . . . chloritic phyllite
qtz-carb . . . quartz-carbonate
ecl . . . . . eclogite
serp . . . . . serpentinite

Table I-1. *Geochemistry of volcanic rocks of Menzie Creek formation.*

	Sample	98-1010	98-1011	98-1012	98-1015	98-1013	98-1014	99-2001	99-2014	99-2018
	Station	LP98-028	LP98-039	LP98-188	LP98-188*	LP98-048	LP98-197	LP98-174	LP99-110	LP99-234
	rock	flow	flow	flow	flow	flow	flow	breccia	flow	breccia
UTM	East	587606	591904	599970	599970	577696	599996	596941	580259	601084
	North	6905244	6902614	6923193	6923193	6914602	6925270	6924371	6910776	6926587
%	SiO_2	54.38	40.73	47.42	48.29	49.35	40.18	51.21	45.41	51.75
	Al_2O_3	16.38	17.11	13.88	14.37	13.37	15.13	13.97	12.51	12.92
	Fe_2O_3	11.08	15.97	13.41	13.49	11.88	14.08	10.76	9.27	9.92
	MnO	0.03	0.06	0.16	0.17	0.16	0.21	0.17	0.13	0.10
	MgO	6.75	5.90	5.24	5.18	6.77	8.71	5.59	5.61	2.38
	CaO	0.65	5.23	5.46	4.62	8.23	5.19	5.74	11.59	6.66
	Na_2O	4.00	2.87	4.21	5.02	3.89	1.66	3.23	3.10	2.54
	K_2O	0.47	1.17	0.41	0.30	0.75	2.82	1.74	-0.01	2.85
	TiO_2	2.42	3.21	3.18	3.11	2.44	3.34	2.60	2.09	2.86
	P_2O_5	0.39	0.81	0.46	0.42	0.30	0.39	0.28	0.28	0.37
	L.O.I.	4.34	6.99	5.51	4.96	2.78	5.55	3.42	8.81	6.23
	Total	**100.89**	**100.05**	**99.34**	**99.93**	**99.92**	**97.26**	**98.71**	**98.80**	**98.58**
ppm	V	226	115	292	285	255	343	299	245	282
	Cr	-20	-20	36	43	303	133	108	255	68
	Co	29	57	40	39	46	45	31	32	25
	Ni	12	23	61	51	176	79	48	113	33
	Cu	35	64	133	144	104	164	46	102	37
	Zn	64	112	119	133	97	114	47	75	-30
	Ga	26	19	22	22	18	25	18	16	18
	Ge	0.9	0.9	1.5	1.6	1.5	1.1	0.8	1.0	1.1
	As	-5	9	–5	-5	-5	-5	-5	-5	-5
	Rb	9	24	6	6	8	30	28	-2	60
	Sr	62	115	207	202	429	91	147	438	84
	Y	44.0	31.0	36.0	35.0	26.0	32.0	34.1	23.8	33.1
	Zr	340	392	250	244	174	273	222	165	257
	Nb	45.0	79.0	42.0	41.0	28.0	44.0	28.6	19.6	32.6
	Mo	1	-2	1	1	1	1	-2	-2	-2
	Ag	-0.5	-0.5	-0.5	-0.5	-0.5	-0.5	-0.5	-0.5	-0.5
	In	-0.1	-0.1	-0.1	-0.1	-0.1	-0.1	-0.1	-0.1	-0.1
	Sn	3	2	2	2	2	2	2	1	2
	Sb	0.3	0.4	1.0	0.7	0.2	0.3	0.2	0.5	4.0
	Cs	0.3	0.8	5.8	15.0	0.2	1.2	0.8	0.5	5.9
	Ba	409	288	6770	7790	539	6700	1740	77	1220
	La	41.80	52.50	34.10	35.10	20.90	35.90	29.90	16.00	27.50
	Ce	85.1	115.0	71.9	71.6	47.6	75.4	60.2	34.7	58.1
	Pr	10.36	13.26	8.61	8.35	5.89	9.48	7.52	4.61	7.45
	Nd	44.6	55.5	39.6	37.9	27.6	41.5	30.9	19.9	31.9
	Sm	8.98	9.84	8.49	8.23	6.13	8.60	6.99	4.77	7.14
	Eu	2.10	2.48	2.80	2.51	1.77	2.93	2.32	1.82	2.25
	Gd	8.00	8.13	8.18	7.77	5.78	7.76	7.40	5.28	7.45
	Tb	1.35	1.10	1.25	1.21	0.92	1.20	1.27	0.88	1.21
	Dy	7.54	5.57	6.74	6.46	4.95	6.28	6.63	4.68	6.48
	Ho	1.47	0.99	1.21	1.16	0.90	1.16	1.24	0.87	1.20
	Er	4.24	2.69	3.31	3.17	2.40	3.06	3.40	2.33	3.32
	Tm	0.631	0.378	0.439	0.431	0.337	0.412	0.474	0.325	0.463
	Yb	3.75	2.25	2.67	2.54	1.91	2.54	3.00	1.89	2.81
	Lu	0.532	0.295	0.366	0.337	0.252	0.343	0.403	0.268	0.388
	Hf	8.5	8.1	6.0	5.8	4.2	6.7	5.5	4.0	6.3
	Ta	2.9	4.7	2.6	2.6	1.7	2.8	2.2	1.4	2.5
	W	0.3	0.5	0.4	0.4	0.3	0.5	0.4	0.4	0.4
	Tl	0.08	0.11	-0.05	2.16	-0.05	0.24	0.08	0.43	0.37
	Pb	-5	-5	-5	5	-5	-5	-5	-5	-5
	Bi	0.08	0.13	0.06	0.07	-0.06	0.11	-0.06	-0.06	-0.06
	Th	10.90	8.05	3.54	3.44	2.51	4.39	3.83	1.72	3.55
	U	2.49	1.85	0.90	0.87	0.63	1.06	0.94	0.49	0.67

Table I-1 (continued). *Geochemistry of volcanic rocks of Menzie Creek formation.*

	Sample	99-2019	99-2020	99-2021	99-2022	99-2024	99-2025	99-2026	99-2027	99-2003
	Station	LP99-256	LP99-273	LP99-276	LP99-285	LP99-286	LP99-287	LP99-287*	LP99-288	LP99-019
	Rock	flow	flow	flow	breccia	flow	flow	flow	flow	flow
UTM	East	604875	605171	606156	603915	598638	596523	596523	595385	554967
	North	6925090	6926192	6925556	6925622	6930412	6928084	6928084	6925400	6922235
%	SiO_2	44.03	43.93	39.90	56.68	48.34	46.92	47.15	46.04	57.41
	Al_2O_3	14.26	12.96	8.47	12.87	13.87	14.78	14.41	15.07	15.51
	Fe_2O_3	13.34	9.15	15.63	11.66	15.17	13.20	11.91	10.55	6.85
	MnO	0.21	0.15	0.14	0.08	0.16	0.16	0.17	0.09	0.09
	MgO	8.33	7.86	13.64	3.80	5.76	6.88	6.93	5.40	6.41
	CaO	4.94	16.46	12.59	1.78	4.19	6.39	6.20	6.49	2.50
	Na_2O	2.29	0.55	0.15	0.50	3.72	2.94	3.32	4.56	5.70
	K_2O	1.15	2.12	0.10	5.54	1.51	2.76	2.20	1.13	0.27
	TiO_2	3.10	1.46	1.02	3.00	2.94	2.59	2.60	2.56	2.05
	P_2O_5	0.51	0.34	0.28	0.33	0.43	0.33	0.26	0.41	0.36
	L.O.I.	6.76	3.47	7.15	3.98	2.94	3.11	3.36	6.34	1.55
	Total	**98.92**	**98.45**	**99.07**	**100.22**	**99.03**	**100.06**	**98.51**	**98.64**	**98.70**
ppm	V	253	227	146	335	314	320	304	286	153
	Cr	82	237	1020	23	82	122	113	256	-20
	Co	39	20	85	34	15	46	43	47	13
	Ni	55	47	604	-15	25	76	68	112	–15
	Cu	53	69	31	84	-10	114	90	126	–10
	Zn	105	-30	92	82	-30	102	81	64	-30
	Ga	20	13	9	18	12	20	18	18	16
	Ge	1.4	0.9	1.7	1.4	0.0	1.8	1.5	1.0	0.6
	As	-5	-5	75	-5	-5	-5	-5	-5	-5
	Rb	8	27	-2	69	19	73	44	17	9
	Sr	337	394	116	44	177	168	169	191	135
	Y	31.9	23.2	12.3	32.4	36.8	29.7	28.1	28.6	42.0
	Zr	270	148	120	280	264	206	195	221	395
	Nb	41.6	26.5	31.3	40.3	33.1	26.1	24.8	29.7	40.0
	Mo	-2	-2	-2	-2	-2	-2	-2	-2	-2
	Ag	-0.5	-0.5	-0.5	-0.5	-0.5	-0.5	-0.5	-0.5	-0.5
	In	-0.1	-0.1	-0.1	-0.1	-0.1	-0.1	-0.1	-0.1	-0.1
	Sn	1	-1	1	2	-1	1	1	1	–1
	Sb	0.2	6.1	1.9	0.5	-0.2	-0.2	-0.2	-0.2	-0.2
	Cs	1.2	1.2	0.3	1.6	0.8	1.8	0.9	4.9	2.7
	Ba	9200	4400	220	3190	1950	2160	1660	2810	480
	La	36.70	27.80	34.30	27.50	31.70	22.30	21.50	23.70	61.80
	Ce	74.0	58.0	61.5	58.6	66.8	48.9	46.0	51.9	122.0
	Pr	9.15	7.06	6.63	7.32	8.31	6.35	6.03	6.81	14.20
	Nd	38.1	27.3	23.8	30.3	34.1	27.4	25.9	28.7	54.9
	Sm	8.09	5.30	3.90	6.54	7.46	6.28	5.84	6.43	10.20
	Eu	2.89	1.77	1.35	1.93	2.42	2.14	2.08	2.07	2.23
	Gd	8.08	5.04	3.16	6.70	7.73	6.73	6.32	6.81	9.26
	Tb	1.27	0.83	0.47	1.12	1.29	1.10	1.05	1.11	1.47
	Dy	6.43	4.28	2.52	6.02	6.99	5.79	5.53	5.64	7.96
	Ho	1.15	0.80	0.47	1.16	1.34	1.07	1.01	1.07	1.52
	Er	3.01	2.17	1.24	3.30	3.70	2.87	2.77	2.88	4.13
	Tm	0.404	0.288	0.180	0.487	0.517	0.403	0.382	0.395	0.634
	Yb	2.62	1.77	1.18	3.04	3.30	2.42	2.33	2.38	3.72
	Lu	0.349	0.255	0.167	0.411	0.467	0.336	0.318	0.333	0.520
	Hf	6.4	3.4	2.7	6.7	6.4	5.0	4.7	5.4	9.4
	Ta	3.2	2.0	2.3	2.8	2.7	2.0	1.8	2.2	3.1
	W	0.3	1.0	0.5	0.5	0.2	0.2	0.3	0.3	0.3
	Tl	0.06	0.18	-0.05	0.27	-0.05	0.14	0.07	0.16	-0.05
	Pb	-5	-5	-5	-5	-5	-5	-5	-5	-5
	Bi	-0.06	-0.06	-0.06	-0.06	-0.06	-0.06	-0.06	-0.06	-0.06
	Th	4.28	3.80	4.55	4.42	4.39	2.28	2.24	2.79	12.20
	U	1.05	0.86	1.12	1.04	1.07	0.62	0.58	1.03	2.50

Table I-2. *Geochemistry of Ordovician-Silurian gabbro.*

	Sample	98-1006	98-1007	98-1008	98-1017	98-1018	98-1020	98-1021	98-1023	99-2002
	Station	LP98-031	LP98-032	LP98-026	80X-10 76.0m	CNR76-4 49.4m	80X-10 676.6m	81F-01 56.0m	79BC-01 268.0m	LP99-006
	Rock	gabbro	gabbro	gabbro	gabbro	gabbro	gabbro	gabbro	gabbro	gabbro
	Host	COVcs	COVp	COVp	COVp	COVp	COVp	COVp	uPCMMp	COVcs
UTM	East	584016	590085	602288	597035	592658	597035	585471	599447	554017
	North	6915227	6905773	6897684	6900602	6903809	6900602	6908693	6900454	6923307
%	SiO_2	50.12	47.50	46.66	45.84	40.00	44.88	45.24	36.60	47.65
	Al_2O_3	15.10	14.08	15.76	11.82	9.04	15.25	13.34	5.28	16.75
	Fe_2O_3	11.63	9.11	12.04	11.68	10.85	11.02	12.83	9.78	12.84
	MnO	0.17	0.15	0.14	0.16	0.15	0.13	0.17	0.18	0.16
	MgO	6.84	8.86	7.77	11.63	16.11	5.40	6.37	22.04	5.62
	CaO	9.50	9.80	5.03	8.66	9.64	7.26	8.44	7.90	7.82
	Na_2O	2.52	3.20	3.91	3.01	0.02	4.76	2.06	0.03	4.03
	K_2O	1.08	0.05	0.05	0.05	-0.01	0.64	0.19	0.03	1.12
	TiO_2	1.86	1.68	2.45	1.56	1.19	2.07	2.31	0.75	2.54
	P_2O_5	0.29	0.17	0.33	0.19	0.17	0.26	0.28	0.10	0.33
	L.O.I.	1.29	3.10	6.08	5.14	12.20	7.49	7.78	14.90	1.49
	Total	**100.40**	**97.70**	**100.22**	**99.74**	**99.37**	**99.16**	**99.01**	**97.59**	**100.35**
ppm	V	235	214	269	226	155	242	266	102	282
	Cr	37	520	64	831	820	122	150	1640	102
	Co	40	34	36	65	61	36	44	87	40
	Ni	42	142	76	267	620	82	101	1060	65
	Cu	29	85	98	70	63	122	133	64	88
	Zn	120	65	105	96	129	116	126	63	103
	Ga	20	16	20	15	11	20	19	8	18
	Ge	2.0	1.2	1.2	1.6	1.2	1.5	1.3	1.0	1.2
	As	-5	-5	-5	-5	44	15	8	322	-5
	Rb	50	2	1	1	-2	27	3	-2	11
	Sr	295	617	124	600	308	281	208	223	606
	Y	23.0	20.0	28.0	20.0	14.0	24.0	26.0	9.4	28.1
	Zr	151	105	174	105	81	151	165	55	193
	Nb	23.0	21.0	36.0	20.0	17.0	32.0	36.0	9.8	26.5
	Mo	1	-2	1	1	-2	1	1	-2	-2
	Ag	-0.5	-0.5	-0.5	-0.5	-0.5	-0.5	-0.5	-0.5	-0.5
	In	-0.1	-0.1	-0.1	-0.1	-0.1	-0.1	-0.1	-0.1	-0.1
	Sn	2	1	1	1	1	1	1	-1	1
	Sb	0.6	1.2	0.3	1.9	2.9	1.3	1.2	12.3	0.6
	Cs	3.3	0.2	0.2	0.7	0.4	3.1	0.3	0.1	1.0
	Ba	345	43	30	92	22	824	351	5	2850
	La	22.80	16.70	26.90	17.80	12.90	26.10	29.30	7.82	22.50
	Ce	47.0	33.3	53.1	36.1	26.2	51.9	59.3	16.7	47.5
	Pr	5.93	4.18	6.59	4.32	3.03	6.00	7.00	2.03	6.22
	Nd	26.1	18.7	28.4	19.6	13.5	26.0	30.1	9.1	26.5
	Sm	5.28	3.98	5.73	4.13	2.87	5.39	6.04	1.93	6.02
	Eu	1.59	1.35	1.77	1.35	1.01	1.67	1.75	0.60	2.24
	Gd	4.88	3.97	5.67	4.55	3.21	5.38	5.84	1.97	6.51
	Tb	0.75	0.63	0.87	0.64	0.45	0.78	0.89	0.29	1.06
	Dy	4.07	3.46	4.86	3.49	2.42	4.30	4.81	1.57	5.43
	Ho	0.74	0.65	0.90	0.62	0.44	0.77	0.88	0.28	1.02
	Er	2.04	1.73	2.47	1.71	1.24	2.16	2.39	0.80	2.72
	Tm	0.289	0.242	0.351	0.233	0.165	0.295	0.333	0.114	0.372
	Yb	1.68	1.45	2.00	1.32	0.98	1.71	1.93	0.65	2.33
	Lu	0.231	0.194	0.280	0.177	0.138	0.219	0.267	0.087	0.306
	Hf	3.8	2.8	4.3	2.7	2.0	3.6	4.2	1.4	5.0
	Ta	1.4	1.3	2.2	1.2	1.0	2.0	2.2	0.6	2.0
	W	0.7	0.0	0.8	0.3	0.2	0.7	0.7	0.0	0.3
	Tl	0.49	0.00	0.00	0.00	0.00	0.25	0.42	0.15	0.09
	Pb	15	-5	55	8	-5	7	-5	-5	-5
	Bi	0.11	-0.06	0.15	0.05	0.09	0.06	0.06	-0.06	-0.06
	Th	3.93	2.16	3.72	2.01	1.82	3.21	3.48	1.01	2.32
	U	0.83	0.44	0.87	0.45	0.87	0.72	0.75	0.23	0.61

Table I-2 (continued). *Geochemistry of Ordovician-Silurian gabbro.*

	Sample	98-1025	98-1026	98-1027	98-1028	98-1029	98-1030	98-1031	98-1032	98-1033
	Station	80X-10	80VX-01	80X-11	77X-08	77X-08	U142	U144	U151	LP98-033
		495.8m	206.5m	649.0m	535.3m	476.2m	18.4m	48.8m	29.2m	
	Rock	chl phy	chl phy	chl phy	chl phy	chl phy	qtz-carb	qtz-carb	qtz-carb	qtz-carb
	Host	COVp	COVp	COVp	COVp	COVp	COVp	COVp		COVp
UTM	East	597035	593230	597259	597583	597583	592108	592111	592016	592253
	North	6900602	6902872	6901111	6901613	6901613	6905381	6905383	6905383	6905470
%	SiO_2	44.12	51.22	49.13	45.79	48.14	42.29	36.93	40.56	33.10
	Al_2O_3	13.65	14.10	13.66	13.47	13.43	13.61	12.08	12.19	4.40
	Fe_2O_3	10.65	5.85	10.31	9.93	9.37	12.21	9.92	8.50	9.89
	MnO	0.14	0.09	0.11	0.16	0.15	0.14	0.15	0.15	0.14
	MgO	5.96	3.73	5.81	5.87	6.21	4.04	5.42	4.31	14.76
	CaO	8.15	9.15	7.00	8.98	8.16	5.30	10.52	10.93	8.13
	Na_2O	3.67	5.61	2.96	3.36	3.24	0.15	0.25	1.47	0.03
	K_2O	0.15	0.13	0.61	0.05	0.08	1.19	0.63	0.35	0.04
	TiO_2	1.88	0.77	1.56	1.86	1.48	1.92	1.80	1.65	0.67
	P_2O_5	0.27	0.19	0.20	0.25	0.18	0.25	0.21	0.22	0.08
	L.O.I.	10.14	8.72	8.14	10.03	8.92	15.50	21.14	17.59	27.40
	Total	**98.78**	**99.56**	**99.49**	**99.75**	**99.36**	**96.60**	**99.05**	**97.92**	**98.64**
ppm	V	241	85	194	222	185	233	208	194	90
	Cr	160	130	65	28	69	421	291	30	1
	Co	34	16	35	37	35	50	34	39	86
	Ni	121	230	14	31	-15	194	86	17	1190
	Cu	115	19	43	38	28	100	57	36	61
	Zn	53	52	72	99	71	386	130	72	106
	Ga	17	18	16	17	15	19	15	15	7
	Ge	1.5	1.2	2.1	1.5	1.4	10.3	1.6	1.3	3.9
	As	6	-5	42	17	14	264	45	41	751
	Rb	6	3	22	1	4	53	30	16	8
	Sr	199	350	192	288	253	111	199	272	330
	Y	23.0	22.0	18.0	22.0	21.0	20.0	21.0	19.0	9.3
	Zr	133	179	128	152	134	135	127	135	51
	Nb	29.0	17.0	18.0	24.0	17.0	24.0	23.0	22.0	8.5
	Mo	1	1	1	1	1	1	-2	1	-2
	Ag	-0.5	-0.5	-0.5	-0.5	-0.5	-0.5	-0.5	-0.5	-0.5
	In	-0.1	-0.1	-0.1	-0.1	-0.1	-0.1	-0.1	-0.1	-0.1
	Sn	1	1	1	1	1	1	1	1	-1
	Sb	1.2	0.4	1.4	0.6	1.2	11.1	2.0	1.1	94.5
	Cs	0.7	0.4	1.7	0.3	0.4	2.6	1.7	2.8	13.0
	Ba	67	53	383	19	70	10200	587	484	162
	La	21.10	39.20	20.90	23.30	21.30	20.60	19.30	23.20	7.41
	Ce	43.9	80.1	43.2	49.2	44.5	43.8	40.8	49.0	15.6
	Pr	5.14	8.50	5.05	5.91	5.25	5.22	4.94	5.80	1.85
	Nd	22.9	33.9	22.0	25.8	23.0	23.7	22.1	25.5	8.4
	Sm	4.72	5.89	4.34	5.17	4.53	5.01	4.67	4.83	1.78
	Eu	1.28	1.28	1.09	1.53	1.28	2.37	1.40	1.50	0.89
	Gd	4.80	5.03	3.93	4.81	4.13	4.68	4.42	4.58	1.82
	Tb	0.74	0.70	0.62	0.72	0.64	0.70	0.68	0.64	0.27
	Dy	4.18	3.63	3.38	3.97	3.55	3.61	3.74	3.42	1.49
	Ho	0.76	0.65	0.62	0.71	0.67	0.64	0.68	0.61	0.28
	Er	2.10	1.86	1.75	1.96	1.83	1.77	1.88	1.67	0.76
	Tm	0.299	0.283	0.249	0.273	0.262	0.229	0.262	0.235	0.103
	Yb	1.74	1.82	1.45	1.58	1.55	1.43	1.50	1.38	0.58
	Lu	0.240	0.275	0.205	0.216	0.218	0.200	0.214	0.186	0.084
	Hf	3.3	4.6	3.2	3.7	3.2	3.4	3.2	3.4	1.2
	Ta	1.8	1.1	1.1	1.5	1.1	1.5	1.4	1.3	0.5
	W	0.9	0.9	1.1	0.7	0.6	5.4	2.4	0.8	1.5
	Tl	-0.05	-0.05	0.97	-0.05	-0.05	23.70	4.91	1.01	3.45
	Pb	-5	-5	15	7	-5	52	-5	63	12
	Bi	-0.06	-0.06	0.06	0.07	0.11	-0.06	-0.06	0.55	-0.06
	Th	2.80	12.50	3.78	3.26	4.24	2.40	2.37	3.06	0.94
	U	0.63	1.94	0.85	0.76	0.91	0.55	2.59	0.75	0.28

Table I-3. *Geochemistry of chloritic phyllites and eclogites of Yukon-Tanana Terrane.*

	Sample	LP99-055A	LP99-055B*	LP99-056	99-2016	LPAN-6
	Station	LP99-055	LP99-055	LP99-056	LP99-160	LP00-006
	Rock	chl-phy	chl-phy	chl-phy	ecl	ecl
UTM	East	586415	586415	586091	590611	580643
	North	6900559	6900559	6901025	6900040	6907950
%						
	SiO_2	52.90	51.65	44.01	60.01	57.93
	Al_2O_3	15.46	15.42	11.86	11.60	15.81
	Fe_2O_3	10.23	9.82	12.50	9.55	8.88
	MnO	0.232	0.214	0.185	0.19	0.18
	MgO	6.46	7.04	8.75	5.48	3.12
	CaO	4.81	5.35	8.42	5.12	6.42
	Na_2O	4.45	3.81	3.55	2.89	3.40
	K_2O	1.39	1.93	0.04	0.82	1.10
	TiO_2	1.067	1.007	1.956	1.18	1.01
	P_2O_5	0.14	0.12	0.40	0.17	0.22
	L.O.I.	2.39	2.62	7.70	2.04	2.25
	Total	**99.53**	**98.98**	**99.37**	**99.05**	**100.32**
ppm						
	V	203	239	182	247	208
	Cr	87	91	344	86	37
	Co	29	30	59	18	19
	Ni	25	27	253	35	-15
	Cu	45	17	49	37	96
	Zn	93	87	103	-30	97
	Ga	14	14	17	12	19
	Ge	2	2	2	-0.5	1.9
	As	-5	-5	-5	-5	-5
	Rb	48	66	5	15	26
	Sr	124	135	369	100	301
	Y	28	25	22	29.1	35.7
	Zr	82	64	152	105	124
	Nb	6	8	36	3.3	5.2
	Mo	-2	-2	-2	-2	-2
	Ag	-0.5	-0.5	-0.5	-0.5	-0.5
	In	-0.2	-0.2	-0.2	-0.1	-0.1
	Sn	-1	-1	1	-1	1
	Sb	2.2	3.0	0.5	-0.2	0.7
	Cs	1.2	1.7	2.3	0.7	1.2
	Ba	1320	1770	191	628	627
	La	8.1	7.2	27.3	7.91	13.20
	Ce	18.1	16.0	55.6	19.3	29.7
	Pr	2.30	2.04	6.18	2.69	3.74
	Nd	11.3	10.1	27.8	12.6	18.0
	Sm	3.1	2.8	5.8	3.60	4.53
	Eu	1.34	1.27	2.14	1.25	1.46
	Gd	4.3	3.7	6.4	4.61	4.58
	Tb	0.8	0.7	1.0	0.87	0.83
	Dy	5.2	4.4	4.9	5.05	5.06
	Ho	1.1	0.9	0.8	1.07	1.03
	Er	3.5	2.9	2.3	3.21	3.20
	Tm	0.51	0.44	0.28	0.499	0.490
	Yb	3.1	2.7	1.6	3.25	3.26
	Lu	0.50	0.44	0.24	0.466	0.495
	Hf	2.6	2.0	3.8	2.9	3.7
	Ta	0.2	0.3	2.4	0.3	0.4
	W	-1	73	-1	0.3	-0.2
	Tl	0.4	0.5	-0.1	-0.05	0.11
	Pb	-5	-5	5	-5	8
	Bi	-0.4	-0.4	-0.4	-0.06	0.40
	Th	1.4	1.2	3.0	1.19	2.30
	U	0.6	0.5	0.7	0.50	0.88

Table I-4. *Geochemistry of volcanic rock of Faro Peak formation.*

	Sample	99-2009
	Station	LP99-058
	Rock	flow
UTM	East	572110
	North	6912320
%	SiO_2	52.27
	Al_2O_3	14.27
	Fe_2O_3	11.90
	MnO	0.18
	MgO	5.13
	CaO	7.07
	Na_2O	5.42
	K_2O	0.46
	TiO_2	1.71
	P_2O_5	0.16
	L.O.I.	1.70
	Total	**100.27**
ppm	V	335
	Cr	117
	Co	38
	Ni	52
	Cu	91
	Zn	70
	Ga	12
	Ge	1.5
	As	-5
	Rb	12
	Sr	344
	Y	40.5
	Zr	128
	Nb	2.3
	Mo	-2
	Ag	-0.5
	In	-0.1
	Sn	-2
	Sb	0.2
	Cs	1.2
	Ba	2340
	La	4.35
	Ce	12.6
	Pr	2.24
	Nd	11.9
	Sm	4.06
	Eu	1.53
	Gd	5.78
	Tb	1.16
	Dy	6.84
	Ho	1.43
	Er	4.43
	Tm	0.674
	Yb	4.17
	Lu	0.608
	Hf	3.4
	Ta	0.4
	W	-0.2
	Tl	0.23
	Pb	-5
	Bi	-0.06
	Th	0.18
	U	0.10

Table I-5. *Geochemistry of volcanic rocks of Campbell Range formation.*

	Sample	98-1001	98-1002	98-1003	98-1004	98-1005	99-2011	99-2012	99-2013	99-2005
	Station	JA98-021	LP98-001	LP98-112	LP98-075	LP98-112*	LP99-066	LP99-076	LP99-076*	LP99-048
	Rock	flow	flow	flow	flow	flow	flow	flow	flow	flow
UTM	East	593952	595771	567858	575057	567858	574731	572532	572532	568422
	North	6897569	6897253	6915664	6912592	6915664	6912479	6913774	6913774	6914984
%	SiO_2	52.02	50.77	50.50	49.20	50.87	50.78	50.22	51.58	52.49
	Al_2O_3	14.81	14.40	14.24	14.86	14.62	13.08	14.14	14.27	14.74
	Fe_2O_3	10.08	10.89	10.30	10.75	12.01	12.33	9.46	8.84	10.77
	MnO	0.34	0.19	0.20	0.20	0.21	0.19	0.14	0.13	0.16
	MgO	5.11	5.64	6.30	6.36	6.41	6.79	6.50	5.52	5.88
	CaO	7.09	5.10	7.57	9.40	8.12	9.48	8.67	9.94	9.15
	Na_2O	6.09	3.55	4.37	4.42	4.41	4.19	3.45	2.73	3.57
	K_2O	0.28	0.57	0.14	0.11	0.12	0.02	0.06	0.04	0.12
	TiO_2	1.37	1.51	1.63	1.53	1.68	1.42	1.12	1.01	1.37
	P_2O_5	0.24	0.16	0.17	0.15	0.18	0.14	0.11	0.10	0.15
	L.O.I.	2.65	7.58	2.65	3.43	2.12	2.51	4.90	4.93	1.99
	Total	**100.08**	**100.36**	**98.07**	**100.41**	**100.75**	**100.93**	**98.77**	**99.09**	**100.39**
ppm	V	273	273	295	290	306	369	272	248	299
	Cr	114	149	145	157	313	123	129	117	136
	Co	33	38	30	36	37	25	33	29	28
	Ni	63	57	67	62	351	36	49	46	48
	Cu	56	57	49	18	65	60	12	58	44
	Zn	68	79	65	79	91	-30	42	34	37
	Ga	15	15	15	18	17	13	14	14	14
	Ge	1.4	0.6	0.9	1.6	1.2	0.5	1.3	1.4	0.9
	As	-5	-5	-5	-5	-5	-5	-5	30	-5
	Rb	7	19	1	2	1	2	-2	-2	-2
	Sr	83	102	117	170	140	95	115	73	49
	Y	36.0	37.0	40.0	38.0	42.0	30.5	26.0	23.8	34.1
	Zr	98	108	110	112	119	96	80	75	104
	Nb	1.8	1.9	2.3	2.0	6.8	1.7	1.3	1.4	1.8
	Mo	1	-2	-2	-2	-2	-2	-2	-2	-2
	Ag	-0.5	-0.5	-0.5	-0.5	-0.5	-0.5	-0.5	-0.5	-0.5
	In	-0.1	-0.1	-0.1	-0.1	-0.1	-0.1	-0.1	-0.1	-0.1
	Sn	1	1	1	1	1	-1	-1	-1	-1
	Sb	0.2	1.6	0.2	0.2	0.2	-0.2	-0.2	0.2	-0.2
	Cs	0.3	2.4	0.4	1.4	0.4	1.9	2.0	1.5	0.2
	Ba	136	280	281	185	269	177	267	176	701
	La	3.68	3.26	4.07	4.19	4.33	3.91	3.13	3.14	3.84
	Ce	11.0	10.2	12.2	12.2	13.0	11.2	9.0	8.9	11.2
	Pr	1.89	1.79	2.10	2.09	2.25	1.89	1.49	1.45	1.86
	Nd	10.8	10.4	12.0	11.7	12.9	9.7	8.0	7.8	9.9
	Sm	3.48	3.46	3.87	3.81	4.19	3.16	2.64	2.46	3.34
	Eu	1.19	1.08	1.29	1.37	1.39	1.25	1.07	0.97	1.33
	Gd	4.74	4.72	5.33	4.84	5.45	4.36	3.76	3.51	4.89
	Tb	0.88	0.90	1.00	0.96	1.08	0.87	0.76	0.70	0.99
	Dy	5.46	5.70	6.24	5.94	6.59	5.06	4.50	4.07	5.83
	Ho	1.15	1.20	1.32	1.25	1.43	1.10	0.94	0.86	1.25
	Er	3.53	3.70	4.05	3.80	4.34	3.24	2.89	2.64	3.79
	Tm	0.514	0.547	0.584	0.556	0.642	0.515	0.453	0.410	0.577
	Yb	3.41	3.59	3.81	3.71	4.18	3.29	2.89	2.61	3.71
	Lu	0.564	0.571	0.616	0.587	0.665	0.467	0.417	0.367	0.556
	Hf	2.6	2.8	3.0	3.0	3.2	2.5	2.2	2.0	2.8
	Ta	0.1	0.1	0.2	0.2	0.2	-0.1	-0.1	-0.1	0.1
	W	-0.2	-0.2	-0.2	-0.2	-0.2	-0.2	-0.2	-0.2	-0.2
	Tl	0.00	0.10	0.00	0.00	0.00	0.12	0.00	0.38	-0.05
	Pb	-5	5	-5	-5	-5	-5	-5	-5	-5
	Bi	0.07	0.08	0.05	0.05	0.07	-0.06	-0.06	-0.06	-0.06
	Th	0.21	0.21	0.27	0.22	0.27	0.29	0.20	0.19	0.22
	U	0.10	0.19	0.14	0.09	0.15	0.13	0.09	0.08	0.15

Table I-5 (continued). *Geochemistry of volcanic rocks of Campbell Range formation.*

	Sample	99-2015	99-2017	99-2010
	Station	LP99-157	LP99-207	LP99-060
	Rock	flow	flow	flow
UTM	East	588098	569899	572293
	North	6902412	6915163	6912654
%	SiO_2	50.41	50.81	47.13
	Al_2O_3	14.36	14.68	15.26
	Fe_2O_3	11.05	10.25	10.07
	MnO	0.18	0.31	0.16
	MgO	6.28	5.40	6.95
	CaO	8.16	8.40	9.42
	Na_2O	4.56	4.43	4.91
	K_2O	0.14	0.33	0.19
	TiO_2	1.40	1.43	1.09
	P_2O_5	0.14	0.16	0.10
	L.O.I.	3.23	2.78	4.03
	Total	**99.91**	**98.98**	**99.31**
ppm	V	308	295	273
	Cr	141	187	131
	Co	38	35	38
	Ni	49	69	57
	Cu	55	57	71
	Zn	60	84	70
	Ga	14	16	14
	Ge	1.1	2.0	1.4
	As	-5	-5	-5
	Rb	2	7	-2
	Sr	213	94	165
	Y	33.3	37.0	25.4
	Zr	104	124	73
	Nb	1.8	2.1	1.3
	Mo	-2	-2	-2
	Ag	-0.5	-0.5	-0.5
	In	-0.1	-0.1	-0.1
	Sn	-1	1	-1
	Sb	0.2	2.0	-0.2
	Cs	0.3	0.4	0.1
	Ba	100	322	70
	La	3.51	4.77	2.54
	Ce	10.7	13.2	7.6
	Pr	1.86	2.17	1.30
	Nd	9.9	11.4	7.2
	Sm	3.30	3.60	2.46
	Eu	1.31	1.39	1.06
	Gd	4.83	5.08	3.62
	Tb	0.97	1.01	0.74
	Dy	5.72	6.09	4.36
	Ho	1.19	1.32	0.91
	Er	3.61	4.00	2.78
	Tm	0.569	0.622	0.434
	Yb	3.50	3.90	2.81
	Lu	0.523	0.558	0.399
	Hf	2.7	3.1	1.9
	Ta	-0.1	0.1	-0.1
	W	-0.2	-0.2	-0.2
	Tl	-0.05	-0.05	-0.05
	Pb	-5	-5	-5
	Bi	-0.06	0.41	-0.06
	Th	0.18	0.35	0.12
	U	0.16	0.13	0.05

Table I-6. *Geochemistry of Permian mafic and ultramafic intrusive rocks.*

	Sample	99-2004	99-2008	99-2006	99-2028	99-2028
	Station	LP99-047	LP99-052	LP99-050	LP99-046	LP99-046**
	Rock	serp	serp	gabbro	diabase	diabase
UTM	East	568287	566802	567085	568204	568204
	North	6914909	6915357	6915400	6914847	6914847
%	SiO_2	37.98	40.47	46.07	48.06	48.12
	Al_2O_3	1.04	1.95	17.46	14.53	14.45
	Fe_2O_3	8.76	7.02	6.53	6.66	7.37
	MnO	0.15	0.11	0.11	0.12	0.12
	MgO	39.34	39.21	10.02	13.37	13.22
	CaO	0.01	0.97	12.54	11.49	11.43
	Na_2O	0.09	0.06	2.21	1.53	1.55
	K_2O	0.02	0.00	0.21	0.41	0.41
	TiO_2	0.01	0.03	0.49	0.33	0.34
	P_2O_5	0.01	0.00	0.03	0.02	0.02
	L.O.I.	13.18	11.17	3.58	2.87	2.97
	Total	**100.59**	**100.99**	**99.25**	**99.39**	**100.00**
ppm	V	51	59	189	173	166
	Cr	2	2	209	725	696
	Co	114	97	34	41	46
	Ni	1950	1610	204	198	226
	Cu	-10	-10	-10	50	59
	Zn	57	33	33	-30	35
	Ga	-1	2	13	9	9
	Ge	1.0	0.8	1.5	1.6	1.4
	As	-5	-5	-5	-5	-5
	Rb	-2	-2	-2	5	5
	Sr	-2	5	275	266	254
	Y	-0.5	0.9	12.2	10.0	9.6
	Zr	2	2	13	11	10
	Nb	-0.5	-0.5	-0.5	-0.5	-0.5
	Mo	-2	-2	-2	-2	-2
	Ag	-0.5	-0.5	-0.5	-0.5	-0.5
	In	-0.1	-0.1	-0.1	-0.1	-0.1
	Sn	-1	-1	-1	-1	-1
	Sb	-0.2	-0.2	-0.2	0.7	-0.2
	Cs	-0.1	-0.1	0.1	0.3	0.3
	Ba	4	-3	31	99	94
	La	0.13	-0.05	0.90	0.57	0.53
	Ce	0.3	-0.1	2.4	1.7	1.6
	Pr	0.03	-0.02	0.42	0.32	0.29
	Nd	0.1	-0.05	2.4	1.9	1.8
	Sm	0.03	0.02	1.02	0.77	0.74
	Eu	0.01	0.02	0.65	0.43	0.41
	Gd	0.03	0.06	1.65	1.34	1.22
	Tb	0.01	0.02	0.36	0.27	0.26
	Dy	0.05	0.13	2.17	1.70	1.59
	Ho	0.01	0.04	0.47	0.37	0.34
	Er	0.06	0.12	1.40	1.08	1.03
	Tm	0.012	0.022	0.216	0.169	0.160
	Yb	0.08	0.16	1.32	1.10	1.05
	Lu	0.012	0.022	0.193	0.151	0.141
	Hf	-0.1	-0.1	0.5	0.4	0.4
	Ta	-0.1	-0.1	-0.1	-0.1	-0.1
	W	-0.2	-0.2	-0.2	-0.2	-0.2
	Tl	-0.05	-0.05	-0.05	-0.05	-0.05
	Pb	-5	-5	-5	-5	-5
	Bi	-0.06	-0.06	-0.06	-0.06	-0.06
	Th	0.12	-0.05	-0.05	-0.05	-0.05
	U	-0.05	-0.05	-0.05	-0.05	-0.05

Appendix II: Fossil identification

Report No. MJO-1999-3

REPORT ON CONODONTS AND OTHER MICROFOSSILS

TAY RIVER (105K)

4 samples (1 productive) collected by L. Pigage

Yukon Geoscience Office
1998

Paleontologic and biochronologic data contained herein should not be published without prior approval of the responsible paleontologist, generally the author.

Reference to the data should quote the author, report number, and unique GSC locality number of the collection.

M.J. Orchard

25/5/99

C.J. Hickson
Vancouver Subdivision
Geological Survey of Canada

GSC Loc. No: C-304121 **NTS:** Tay River, 105K/3
Fld. No: 98-IG-LP-120

Collector: L. Pigage
GEOGR - Lat./Long.:
UTM: Zone 8; 587731E, 6902228N.
Description: Faro Northwestel repeater site
STRAT - Rock Unit:
Description: Carbonate, within Templeman-Kluit's unit 10 (GSC Bulletin 208), fine grained, silty, dark grey lst. interbanded with black to dark grey, calcareous siltstone; black chert beds (1-10 cm thick) present; med. to light grey weathering
PALEO - Fossils: conodonts
Conodont taxa: **CAI:** 4.5
Epigondolella sp. indet. (6)
ramiform elements (1)
Epigondolella sp. cf. *E. quadrata* Orchard 1991 (1)
AGE - Late Triassic, Early? Norian

---

3 UNPRODUCTIVE COLLECTIONS

GSC Loc. No: C-304122 **NTS:** Tay River, 105K/5
Fld. No: 98-IG-LP-114-1530

Collector: L. Pigage
GEOGR - Lat./Long.:
UTM: Zone 8; 567600E, 6916185N.
Description: near Rose Mountain
STRAT - Rock Unit:
Description: Carbonate, at outcrop elevation of 1530m; within Templeman-Kluit's unit 8a (GSC Bulletin 208), thick, dark grey lst. thinly interbanded with black argillite phyllitic
PALEO - Fossils: barren
AGE - Indeterminate

GSC Loc. No: C-304123 **NTS:** Tay River, 105K/5
Fld. No: 98-IG-LP-114-1490

Collector: L. Pigage
GEOGR - Lat./Long.:
UTM: Zone 8; 567600E, 6916185N.
Description: near Rose Mountain
STRAT - Rock Unit:
Description: Carbonate, at outcrop elevation of 1490m; unit 8a of Templeman-Kluit (GSC Bulletin 208), dark grey lst. thinly interbanded with black argillite and phyllitic
PALEO - Fossils: barren
AGE - Indeterminate

GSC Loc. No: C-304124 **NTS:** Tay River, 105K/5
Fld. No: 98-IG-LP-114-1480

Collector: L. Pigage
GEOGR - Lat./Long.:
UTM: Zone 8; 567600E, 6916185N.
Description: near Rose Mountain
STRAT - Rock Unit:
Description: Carbonate, from several horizons at oucrop elevation of 1480 to 1490m; from unit 8a of Templeman-Kluit (GSC Bulletin 208), composite lst. thinly interbanded with black argillite and phyllitic
PALEO - Fossils: barren
AGE - Indeterminate

Report No. MJO-2000-3

REPORT ON CONODONTS AND OTHER MICROFOSSILS

Tay River (105K)

12 samples (5 productive) collected by L. Pigage
Yukon Geoscience Office

1999

Paleontologic and biochronologic data contained herein should not be published without prior approval of the responsible paleontologist, generally the author.

Reference to the data should quote the author, report number, and unique GSC locality number of the collection.

M.J. Orchard
26/07/00

C.J. Hickson
Vancouver Subdivision
Geological Survey of Canada

GSC Loc Num: C-304782 **NTS: 105K/5 Tay River**

Field Number: 99-IG-LP98-83

Leader:

Collector: Lee Pigage

Geography: **Lat/Long:** ° ' " ° ' "

UTM: 8 578200 6912292

Description:

NAD 83; Rose Mtn area

Stratigraphy: **Rock Units:**

Road River/Rose Mt Earn?

Description:

occurs within unnamed unit structurally above Road R. Gp

maroon & pale green bedded cherts & argillites

Interpretation: **Age:** Indeterminate

Notes:

Paleo: **Fossils:** barren **CAI:** -

GSC Loc Num: C-304783 **NTS: 105K/6 Tay River**

Field Number: 99-IG-LP98-176

Leader:

Collector: Lee Pigage

Geography: **Lat/Long:** ° ' " ° ' "

UTM: 8 597428 6924392

Description:

NAD 83

Stratigraphy: **Rock Units:**

Road River

Description:

occurring within Menzie Ck volcanics; structurally beneath Road R. argillites containing Tetragraptus graptolite (GSC loc C-107902)

Interpretation: discontinuous bands & lenses of limestone

Age: Indeterminate

Paleo: **Notes:**

Fossils: barren **CAI:** -

GSC Loc Num: C-304784 **NTS: 105K/5 Tay River**

Field Number: 99-IG-LP99-29

Leader:

Collector: Lee Pigage

Geography: **Lat/Long:** ° ' " ° ' "

UTM: 8 566674 6916482

Description:

Rose Mtn area, NAD 83

Stratigraphy: **Rock Units:**

Earn Group? Mt Christie Formation?

Description:

within succession consisting of pale tan bedded cherts; ls beds range from 1-10 cm in thickness; ls about 5 m thick & occurs about 22 m above mapped contact (Pigage,98) between black argill overlain by tan bedded cherts

Interpretation: thin-bedded limestone interbanded w black siltstone

Age: Indeterminate

Paleo: **Notes:**

Fossils: barren **CAI:** -

GSC Loc Num: C-304785 **NTS: 105K/5 Tay River**

Leader: **Field Number: 99-IG-LP99-80**

Collector: Lee Pigage

Geography: **Lat/Long:** ° ' " ° ' "

UTM: 8 572029 6914337

Description:

NAD 83

Stratigraphy: **Rock Units:**

Mt. Christie?

Description:

in pale to medium green bedded phyllitic chert

brown weathering, argillaceous limestone

Interpretation: **Age:** Early Carboniferous ?Serpukhovian

Notes:

Paleo: **Fossils:** **CAI:** 6? -

conodont	Gnathodus	sp. cf. G. bilineatus	1

GSC Loc Num: C-304786 **NTS: 105K/5 Tay River**

Leader: **Field Number: 99-IG-LP99-85**

Collector: Lee Pigage

Geography: **Lat/Long:** ° ' " ° ' "

UTM: 8 572610 6914109

Description:

NAD 83

Stratigraphy: **Rock Units:**

Earn Mt. Christie

Description:

occurs generally at contact between underlying Earn Gp & overlying Mt Christie Fm.

tan brown weathering thin limestone w abund quartz grains

Interpretation: **Age:** Early Carboniferous ?Visean

Notes:

Paleo: **Fossils:** **CAI:** 5 -

conodont	Hindeodella	?	segaformis Bischoff 1957	2
conodont	ramiform elements			170
conodont	'Prioniodina'		sp. A	9
conodont	Gnathodus		sp.	1
conodont	Bispathodus		ex gr. stabilis (Branson & Mehl 1934)	15

GSC Loc Num: C-304787 **NTS: 105K/5 Tay River**

Leader: **Field Number: 99-IG-LP99-164A**

Collector: Lee Pigage

Geography: **Lat/Long:** ° ' " ° ' "

UTM: 8 571664 6915306

Description:

NAD 83

Stratigraphy: **Rock Units:**

Rose Mtn Earn

Description:

bed about 45 cm thick (med dk grey when fresh);occurs immed beneath barite horizon in dk to black sity arg & bedded cherts of Rose Mt Earn Gp

Interpretation: dk brown weathering, fine grained, calcareous sandstone

Age: Early Carboniferous

Notes:

Paleo: **Fossils:** **CAI:** 5.5 -

conodont	ramiform elements			25
conodont	Gnathodus		sp.	1 gnathodid recorded but lost

GSC Loc Num: C-304788 **NTS: 105K/5 Tay River**

Field Number: 99-IG-LP99-165

Leader:
Collector: Lee Pigage
Geography: **Lat/Long:** ° ' " ° ' "
UTM: 8 571756 6915420
Description:
NAD 83
Stratigraphy: **Rock Units:**
Rose Mtn Earn
Description:
ls beds range up to 50 cm thick; interval of interbedded ls & arg apprx 13 m thick (ls 50-60% of interval)
fine grained, grey, sandy limestone interbedded w black siliceous argill
Interpretation: **Age:** Indeterminate
Notes:
Paleo: **Fossils:** barren **CAI:** -

GSC Loc Num: C-304789 **NTS: 105K/5 Tay River**

Field Number: 99-IG-LP99-186

Leader:
Collector: Lee Pigage
Geography: **Lat/Long:** ° ' " ° ' "
UTM: 8 570676 6915452
Description:
NAD 83
Stratigraphy: **Rock Units:**
Rose Mtn Mt Christie
Description:
horizon occurs within general sequence of pale green bedded cherts of Rose Mnt Mt Christie Fm.
Carbonate lenses & concretions within dk grey silic arg
Interpretation: **Age:** Indeterminate
Notes:
Paleo: **Fossils:** barren **CAI:** -

GSC Loc Num: C-304790 **NTS: 105K/6 Tay River**

Field Number: 99-IG-LP99-236

Leader:
Collector: Lee Pigage
Geography: **Lat/Long:** ° ' " ° ' "
UTM: 8 601177 6926701
Description:
NAD 83; Menzie Ck volcanics NE of Anvil Batholith
Stratigraphy: **Rock Units:**
Description:
volcanics occur structurally above section of Black Rd River argillites
pale tan weathering dolostone forming thin bed canics
Interpretation: **Age:** Indeterminate
Notes:
Paleo: **Fossils:** barren **CAI:** -

GSC Loc Num: C-304791 **NTS: 105K/6 Tay River**

Field Number: 99-IG-LP99-246A

Leader:
Collector: Lee Pigage
Geography: **Lat/Long:** ° ' " ° ' "
UTM: 8 597809 6928877
Description:
NAD 83
Stratigraphy: **Rock Units:**
Road River Menzie Creek
Description:
within massive volcanics flows of Menzie Ck Fm.
grey limestone bed
Interpretation: **Age:** Early Ordovician
Notes:
Paleo: **Fossils:** **CAI:** 5.5 -

conodont	Panderodus	?	sp.	1
conodont	'Scolopodus'		sp.	1
conodont	Protopanderodus		sp.	3

GSC Loc Num: C-304792 **NTS: 105K/6 Tay River**

Field Number: 99-IG-LP99-246B

Leader:
Collector: Lee Pigage
Geography: **Lat/Long:** ° ' " ° ' "
UTM: 8 597809 6928877
Description:
NAD 83
Stratigraphy: **Rock Units:**
Road River Menzie Creek
Description:
occurring as calcareous sequence within massive flows of Menzie Ck. Fm.
orange weathered dolostone
Interpretation: **Age:** Ordovician
Notes:
Paleo: **Fossils:** **CAI:** -

conodont	Staufferella	?	sp.	1

GSC Loc Num: C-304793 **NTS: 105K/7 Tay River**

Field Number: 99-IG-LP99-291

Leader:
Collector: Lee Pigage
Geography: **Lat/Long:** ° ' " ° ' "
UTM: 8 606405 6919435
Description:
NAD 83
Stratigraphy: **Rock Units:**
Road River
Description:
occurs within sequence of black argillites mapped as Road River Gp
tan-grey to grey weathering, thinly laminated dolostone
Interpretation: **Age:** Indeterminate
Notes:
Paleo: **Fossils:** barren **CAI:** -

REPORT ON RADIOLARIANS
No. FC2000-GSC-4

Fieldwork 1999
2 samples (chert)
by Lee Pigage

Chemical processing, picking,
and radiolarian micropaleontology
by Cordey

To: Steve Irwin, curator
Geological Survey of Canada
101 - 605 Robson Street,
Vancouver, B.C., V6B 5J3

Fabrice Cordey

April 2000

SAMPLE No: LP-99-84	COLLECTOR: Pigage	NTS: 105K/5 UTM: 571 593 E 6 914 404 N
GEOLOGICAL UNIT: chert package beneath massive dark green basalts of the Anvil Range Group		LITHOLOGY: Red bedded chert
OCCURRENCE OF RADIOLARIANS: confirmed		PRESERVATION: poor
RADIOLARIAN TAXA: *Entactinia* sp.		
OTHER: quartz crystals, clays, silica fragments		
AGE: possibly Paleozoic		

SAMPLE No: LP-99-180	COLLECTOR: Pigage	NTS: 105K/5 UTM: 570 756 E 6 914 888 N
GEOLOGICAL UNIT: chert package within basalts of the Anvil Range Group		LITHOLOGY: red bedded chert
OCCURRENCE OF RADIOLARIANS: confirmed		PRESERVATION: moderate
RADIOLARIAN TAXA: *Entactinia* sp. *Pseudoalbaillella bulbosa* Ishiga *Pseudoalbaillella U-forma* Ormiston and Babcock *Pseudoalbaillella* sp. cf. *Ps. simplex* Ishiga and Imoto *Pseudoalbaillella* sp. cf. *Ps.* sp. in Kuwahara 1992, Pl. 2, fig. 8		
OTHER: clays, silica fragments (matrix), rare sponge spicules		
AGE: Early Permian (Asselian-Sakmarian) based on common age range of occurring morphotypes.		

REPORT ON CONODONTS AND OTHER MICROFOSSILS

Tay River (105K)

1 sample (1 productive) collected by L. Pigage (2000)

Paleontologic and biochronologic data contained herein should not be published without prior approval of the responsible paleontologist, generally the author.

Reference to the data should quote the author, report number, and unique GSC locality number of the collection.

M.J. Orchard

18/02/02

L.C. Struik
Vancouver Subdivision
Geological Survey of Canada

GSC Loc Num: C-305665 **NTS:** 105K/6 **Mount Mye**

Leader: **Field Number:** 00-IG-LPA-5

Collector: Pigage, L.

Geography:
Lat/Long: ° ' " ° ' "
UTM: 8 580995 6909886
Description:
NAD83

Stratigraphy:
Rock Units:
Description:
outcrop about 1.5 - 2 m thick & occurs above a mapped contact w underlying Menzie Ck volcanics (Ordov)
thin-bedded, dark grey limestone w beds ranging from 1-5 cm thickness; contains minor small crinoid stems

Interpretation:
Age: Middle Devonian
Notes: Very distorted fauna.

Paleo: **Fossils:** **CAI:** 5 - 5.5

conodont	ramiform elements			30
conodont	Panderodus		sp.	2
conodont	Polygnathus	?	parawebbi Chatterton 1978	4
conodont	Polygnathus		linguiformis linguiformis Hinde 1879	6

Appendix III: Isotopic age dating

^{40}AR/^{39}AR ANALYTICAL PROTOCOL:

^{40}Ar/^{39}Ar samples were analyzed by splitting the samples into 2-3 aliquots. Initially, each aliquot of a sample is treated as a separate step-heated analysis. If two aliquots give identical plateau ages (within error), the data is combined and treated as a single step-heated analysis for data reduction. Ages are referenced to a Fish Canyon Tuff Sanidine (FCT-SAN) standard with an assumed age of 28.03 Ma (Renne at al., 1994). It should be noted that any refinement or change in the accepted age of FCT-SAN will affect the absolute age (i.e., the age when used in comparison to age data produced by other laboratories or methods) but will not affect any age differential between the samples analyzed herein.

In gas release diagrams, multiple step-heating analyses are combined to form a single result, whereby the fraction of ^{39}Ar released relative to the sum total of ^{39}Ar released for all analyses forms the x-axis. Thus, the apparent ^{40}Ar/^{39}Ar age of each heating step is plotted against the amount of ^{39}Ar released from the sample. Because of the use of replicate analyses (aliquots), gas release plots presented here differ from conventional ^{40}Ar/^{39}Ar spectra in that data from each aliquot is displayed in adjacent, alternately shaded regions of a gas release spectra. Upon ascertaining reproducibility of individual spectra and plateau regions between aliquots, data was combined by integrating plateau portions (marked by line above steps) weighted by analytical error. Alternatively, data may be presented on inverse isochron diagrams which essentially provide a graphical display of mixtures of pure atmospheric (^{36}Ar/^{40}Ar, marked by the y-intercept) and pure radiogenic Ar (^{39}Ar/^{40}Ar marked by the x-intercept). In this case, relationship between temperature of heating and apparent age are lost, but the most radiogenic steps are considered to give the best estimate of the age. Age and errors for each gas fraction were calculated using formulae detailed in Roddick (1988). Analytical uncertainties for individual steps are reported at the 2σ level and do not include uncertainty in irradiation calibration of the amount of ^{39}K converted to ^{39}Ar (J factor). The error limit in the final age determination includes uncertainty in the J parameter, typically 0.5% (1σ).

U/Pb Isotopic Dating

Methodology

Zircons were separated from 15-20 kg samples using conventional crushing, grinding, Wilfley table, heavy liquids and Frantz magnetic separation techniques. U-Pb analyses were done at the Pacific Centre for Isotopic and Geochemical Research at the University of British Columbia. The methodology for zircon grain selection, abrasion, dissolution, geochemical preparation and mass spectrometry are described by Mortensen et al. (1995). Procedural blanks for Pb and U were 2 and 1 pg, respectively. Analytical data are listed in Table III-1 and are shown on conventional U-Pb concordia plots in Figures 72 and 73. Errors attached to individual analyses were calculated using the numerical error propagation method of Roddick (1987). Decay constants used are those recommended by Steiger and Jäger (1975), and compositions for initial common Pb were taken from the model of Stacey and Kramer (1975). All errors are given at the 2 sigma level.

Sample AR-4

The sample yielded a moderate amount of stubby to elongate, prismatic zircons, most of which contained obvious cloudy inherited cores. Abundant monazite was also recovered; it comprised clear, pale yellow, multifaceted, tabular grains. Three fractions of monazite were analyzed (Table III-1). All three analyses are concordant, and the total range of $^{207}Pb/^{235}U$ ages of 95.3±1.3 Ma is taken as the best estimate for the crystallization age of the sample.

Sample GAR-1

Zircons and monazite recovered from this sample are similar in appearance to those in the previous sample. Four fractions of monazite were analyzed (Table III-1). All of them lie slightly above Concordia, indicating the presence of a minor component of excess ^{206}Pb (due to the high Th/U of the monazite). Three of the analyses yield overlapping the $^{207}Pb/^{235}U$ ages with a total range of 109.3±1.2 Ma, which is interpreted to be the best estimate for the crystallization age of the sample. The fourth analysis (M2) yields slightly younger Pb/U ages, indicating that this fraction suffered minor post-crystallization Pb-loss.

Sample GAR-2

Three fractions of monazite were analyzed (Table III-1). All of them lie on or slightly above concordia, indicating the presence of a minor component of excess ^{206}Pb in some fractions. The total range of $^{207}Pb/^{235}U$ ages for the three analyses is 103.9±1.5 Ma, which is interpreted to be the crystallization age of the sample.

Sample A-098

The sample yielded a moderate amount of clear, stubby to elongate, prismatic, pale yellow zircons. A small proportion of the grains contained obvious cloudy inherited cores. Four fractions of unabraded, very high quality zircon were analyzed (Table III-1). Fraction B yields a concordant analysis with a $^{206}Pb/^{238}U$ age of 98.6±0.2 Ma, which is interpreted as the crystallization age of the sample. The other three analyses yield much older Pb/U and Pb/Pb ages, indicating the presence of inherited zircon cores in some or all of the grains in these fractions. The four analyses together define a linear array with a calculated upper intercept age of 1.60 Ga, which represents an average age for the inherited zircon component present in the sample.

Sample LP98-22

Seven fractions of moderately to strongly abraded zircons were analyzed (Table III-1). All of the zircons contained abundant clear rod- or bubble-shaped inclusions, that contributed to relatively high common Pb contents and resulting low measured $^{206}Pb/^{204}Pb$ ratios. Four of the fractions yield overlapping, concordant analyses with a total range of $^{206}Pb/^{238}U$ ages of 53.8±0.2 Ma, which gives the crystallization age of the sample. Three other fractions yield slightly older Pb/U ages, indicating the presence of a small inherited component.

Sample LP99-228

Five fractions of strongly abraded zircons were analyzed (Table III-1). The analyses are all concordant, but yield a small range of $^{206}Pb/^{238}U$ ages. Fractions A2 and B2 yield overlapping, concordant analyses with a total range of $^{206}Pb/^{238}U$ ages of 55.8±0.1 Ma, which gives the crystallization age of the sample. Three other fractions yield slightly younger Pb/U ages, indicating the effects of minor post-crystallization Pb-loss that were not completely removed by abrasion.

Table III-1. *U-Pb analytical data for plutonic rocks from the Anvil District.*

Sample description[1]	Wt (mg)	U (ppm)	Pb[2] (ppm)	$^{206}Pb/^{204}Pb$ (meas.)[3]	total common Pb (pg)	% ^{208}Pb[2]	$^{206}Pb/^{238}U$[4] (±%1σ)	$^{207}Pb/^{235}U$[4] (±%1σ)	$^{207}Pb/^{206}Pb$[4] (±%1σ)	$^{206}Pb/^{238}U$ age (Ma; ±%2σ)	$^{207}Pb/^{206}Pb$ age (Ma; ±%2σ)
Sample AR-4											
M1	0.019	2620	176	872	53	80.0	0.01486(0.10)	0.09796(0.91)	0.04780(0.86)	95.1(0.2)	89.5(40.7)
M2	0.130	4253	246	5069	102	76.7	0.01483(0.16)	0.09796(0.17)	0.04790(0.04)	94.9(0.3)	94.1(1.8)
M4	0.018	3863	205	1474	43	74.7	0.01476(0.12)	0.09749(0.26)	0.05792(0.18)	94.4(0.2)	95.5(8.7)
Sample GAR-1											
M1	0.010	19678	1373	1869	111	77.8	0.01707(0.14)	0.11285(0.27)	0.04795(0.17)	109.1(0.3)	96.7(8.2)
M2	0.050	2542	166	777	163	78.0	0.01587(0.15)	0.10466(0.29)	0.04783(0.28)	101.5(0.3)	90.9(13.4)
M3	0.020	3135	237	2688	25	79.3	0.01721(0.13)	0.11441(0.22)	0.04823(0.14)	110.0(0.3)	110.5(6.4)
M4	0.016	5032	322	1167	59	80.6	0.01708(0.14)	0.11385(0.29)	0.04834(0.20)	109.2(0.3)	115.8(9.3)
Sample GAR-2											
M1	0.045	7662	400	3634	105	72.0	0.01612(0.16)0.0162	0.10674(0.24)	0.04803(0.12)	103.1(0.3)	100.8(5.5)
M2	0.048	5452	267	3290	84	70.0	0(0.09)	0.10720(0.12)	0.04799(0.07)	103.6(0.2)	98.7(3.2)
M3	0.013	6340	337	2817	30	72.0	0.01639(0.15)	0.10864(0.34)	0.04807(0.28)	104.8(0.3)	102.8(13.1)
Sample A-098											
A: N5,+105	0.080	304	17.5	8560	10	10.8	0.05505(0.09)	0.6589(0.10)	0.08680(0.03)	345.5(0.6)	1356.1(1.2)
B: N5,+105	0.044	387	6.3	1470	11	14.8	0.01542(0.11)	0.1020(0.16)	0.04796(0.12)	98.6(0.2)	97.2(5.6)
C: N5,74-105	0.097	295	5.3	529	58	16.6	0.01656(0.13)	0.1204(0.29)	0.05274(0.22)	105.9(0.3)	317.7(10.0)
D: N5,+105,c	0.037	589	14.8	246	151	9.2	0.02490(0.25)	0.2326(0.54)	0.06776(0.41)	158.5(0.8)	861.2(17.2)
LP98-22											
A: N2,+105	0.077	1376	12.1	210	281	14.3	0.00835(0.31)	0.05438(4.67)	0.04721(4.49)	53.6(0.3)	59.8(218.5)
B: N2,+105	0.097	1271	11.1	764	84	13.4	0.00837(0.12)	0.05452(0.84)	0.04725(0.79)	53.7(0.1)	61.6(37.5)
C: N2,+105	0.067	1564	13.6	1012	53	13.7	0.00834(0.26)	0.05380(1.04)	0.04678(0.95)	53.5(0.3)	38.1(45.2)
D: N2,+105	0.073	1375	12.2	513	105	13.8	0.00850(0.15)	0.05593(0.45)	0.04775(0.35)	54.5(0.2)	86.9(16.5)
E: N2,+105	0.098	1285	11.8	2300	30	13.2	0.00882(0.13)	0.05777(0.22)	0.04752(0.12)	56.6(0.2)	75.4(5.9)
F: N2,+105	0.088	1362	11.8	310	211	13.1	0.00839(0.32)	0.05386(0.91)	0.04655(0.73)	53.9(0.3)	26.3(35.2)
G: N2,+105	0.125	1759	16.0	528	228	14.2	0.00865(0.15)	0.05689(0.46)	0.04771(0.36)	55.5(0.2)	84.8(17.1)
LP99-228											
A: N2,+105	0.043	12974	114	4777	62	12.7	0.00853(0.16)	0.05549(0.31)	0.04716(0.23)	54.8(0.2)	57.5(11.1)
B: N2,+105	0.033	10862	95.0	4463	42	13.3	0.00841(0.16)	0.05479(0.32)	0.04724(0.25)	54.0(0.2)	61.2(11.9)
A2: N2,+105	0.023	9338	94.1	7459	15	13.0	0.00869(0.10)	0.05648(0.22)	0.04715(0.16)	55.8(0.1)	56.6(7.8)
B2: N2,+105	0.035	12023	118	6376	35	20.0	0.00868(0.10)	0.05644(0.24)	0.04716(0.18)	55.7(0.1)	57.3(8.7)
C2: N2,+105	0.138	8756	77.4	1743	366	13.4	0.00850(0.20)	0.05519(0.58)	0.04711(0.51)	54.5(0.2)	54.8(24.4)

[1]N1,N2 = non-magnetic at n degrees side slope on Frantz magnetic separator; grain size given in microns; c = contains visible cores.

[2]radiogenic Pb; corrected for blank, initial common Pb, and spike

[3]corrected for spike and fractionation

[4]corrected for blank Pb and U, and common Pb

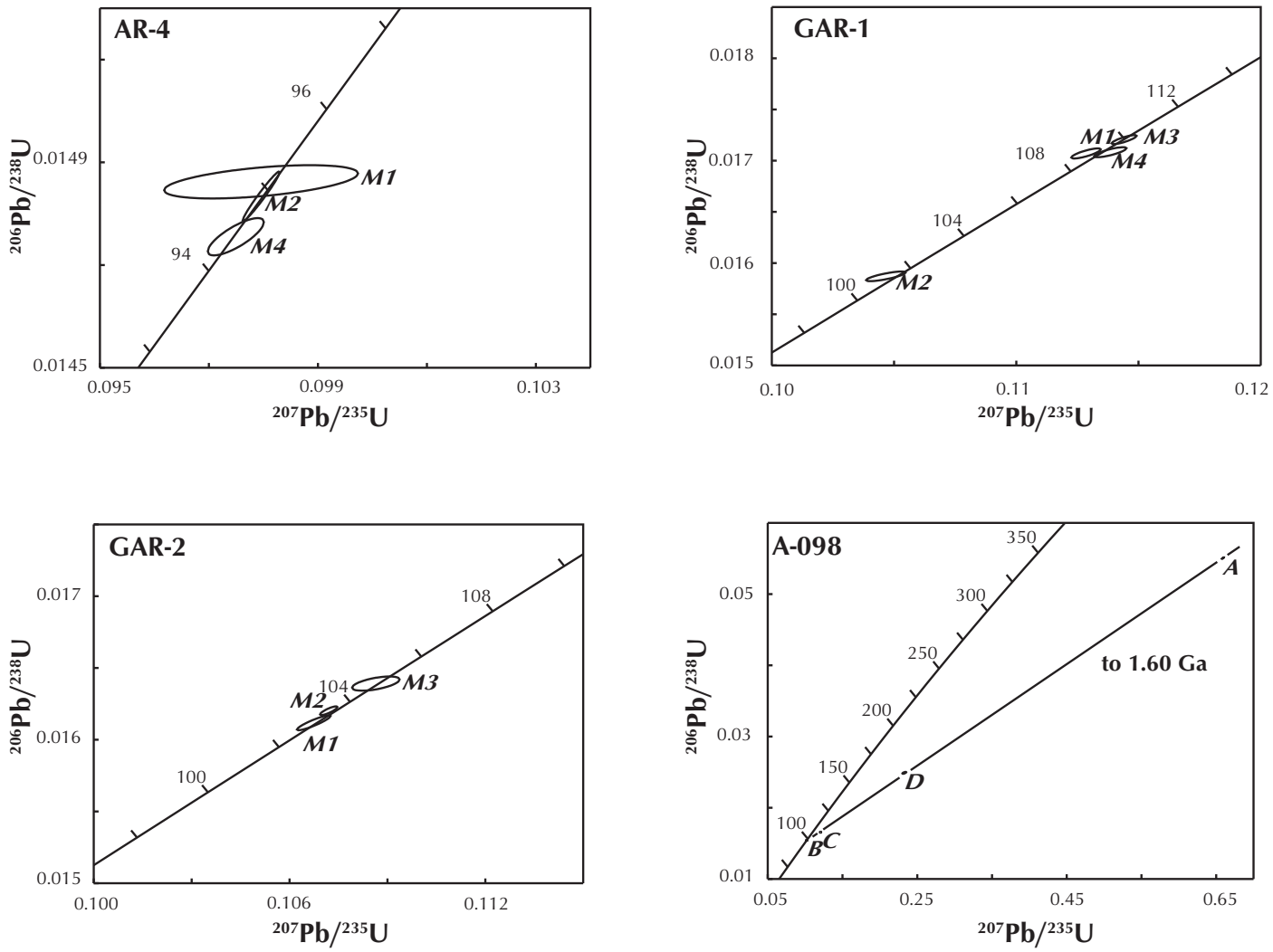

Figure 72. *Concordia diagrams for Cretaceous granitic samples, Anvil District.*

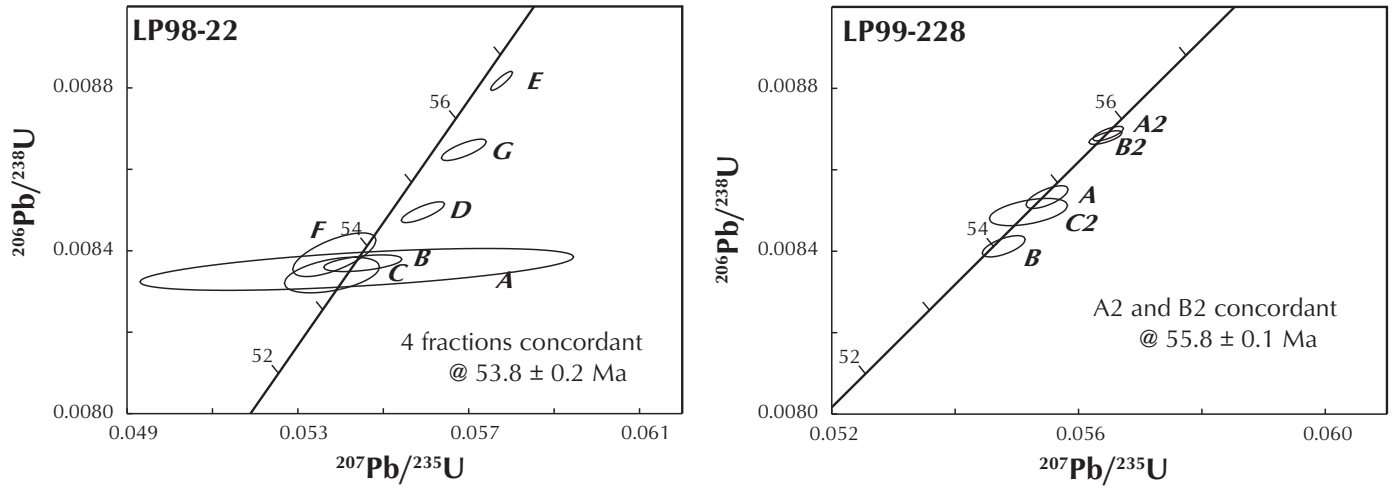

Figure 73. *Concordia diagrams for Eocene porphyry samples, Anvil District.*